Preferred citation: B. Norman and D. Söderberg. Overview of Forming Literature, 1990-2000. In **The science of papermaking**, *Trans. of the XIIth Fund. Res. Symp. Oxford, 2001*, (C.F. Baker, ed.), pp 431–558, FRC, Manchester, 2018. DOI: 10.15376/frc.2001.1.431.

OVERVIEW OF FORMING LITERATURE, 1990–2000

Bo Norman, KTH /STFI
Daniel Söderberg, STFI

ABSTRACT

Paper structure characterisation has been extended to include 2-D formation and periodic marks as well as wavelet techniques. Local fibre orientation anisotropy and misalignment angle analysis, in combination with tape-splitting layering and image analysis have improved the understanding of the relationship between paper structure and properties as well as increased the possibilities to trace the forming history from final paper structure.

The Crowding Factor has been introduced, to describe the tendency of fibre suspensions to form fibre flocs. It gives an improved predictability in comparison with fibre concentration, by also taking fibre slenderness into account. The dynamic characterisation of de-flocculating and re-flocculating mechanisms is getting increased attention, partly due to the potential of CCD-cameras and image analysis techniques. It is the opinion of the authors that floc stretching is a more promising way of de-flocculating than turbulent shear. It is doubtful whether turbulence in simple fluids can aim as a model for the flow irregularities in fibre suspensions, due to the damping effects of fibres and flocs.

For headbox CD-profile control, dilution water injection has been introduced. Since this makes slice lip deformations unneeded, it has the potential to uncouple control of grammage and misalignment angle profiles and also to improve CD-control resolution.

The importance of headbox nozzle design for fibre orientation

anisotropy is now appreciated. A high nozzle contraction ratio will increase anisotropy and also introduce some deflocculation through floc stretching. Vane insertion helps to decrease fibre orientation anisotropy and is also applied for multi-layer forming. Although applied in tissue forming and in linerboard forming, further improvements have to be made for printing paper applications.

In twin-wire forming, the roll-blade principle has been accepted by the main machine manufacturers. Since its introduction in the STFI-Former in 1991, the blade section design with stationary blades on one side and loadable blades on the opposite side is the main design for printing paper applications, and also increasingly used for different board qualities.

TABLE OF CONTENTS

1 BACKGROUND

The present overview can be considered as a continuation of the corresponding review twelve years ago at the 9th Fundamental Research Symposium in Cambridge, 1989 [1]. It is the intention here to give a comprehensive picture of what R&D has taken place within the paper forming area since that time.

The developments since 1989 within the following areas will be discussed:

- Paper structure characterisation.
- Fibre suspensions.
- Headboxes.
- Wire section designs.
- Web forming.
- Dewatering processes.
- Laboratory forming.
- Forming, structure and properties.

At the 1989 Symposium, there was a separate overview dealing with paper chemistry in forming, [2] but this will not be the case at the 2001 Symposium. Even so, paper chemistry aspects on retention and flocculation will generally not be included in this overview. With few exceptions, there will be no references to forming work published before 1990. However, if a reference was included in the 1989 overview, quotation may be made to the list of 143 literature citations included at that time [1].

Firstly, some terms, which often cause misunderstandings, are defined:

There is some confusion around the terms used to describe the process to form a paper web as opposed to the small-scale basis weight variability in the final product. Unfortunately, the term formation is frequently used in both these senses. To avoid misunderstandings, it is necessary to use two distinctly different terms. In this overview, the term **forming** denotes the overall process of generating a paper web, while the term **formation** exclusively refers to small-scale local basis weight variations in the final paper web.

A similar type of terminology dilemma exists regarding the term **fibre flocculation**, which could mean either the state of flocculation or the process of fibres entangling into a floc. At this time, we do however not suggest different words for these two cases, which means that fibre flocculation will still be an ambiguous expression. Hopefully, this will not cause too much misunderstanding in the following text.

The term **mix** will be used to denote the diluted thick stock, with a **fibre concentration** low enough to avoid excessive flocculation. The term "consistency" will be avoided, since it alludes to the rather imprecise evaluation of concentration traditionally performed by different kinds of "consistency" meters – characterized by the fact that they never actually intend to directly measure concentration.

The degree of **fibre orientation anisotropy** and **fibre orientation misalignment** is increasingly important. Regarding terminology, **fibre orientation** to many seems to specifically denote the misalignment angle. It is recommended that **anisotropy** or **misalignment** respectively be added to avoid misunderstandings.

What used to be a **wire** now increasingly is denoted a **forming fabric**. This is to emphasize that what was originally a two-shaft bronze material weave is now a much more sophisticated design based on polymer threads. Correspondingly, what used to be a **felt** is nowadays a **press fabric**. In this overview the old, simpler terms will still be used to some extent. Thus, e.g., **twin-wire**, **wire section**, **wire mark** and **felt mark** will be the preferred terms. In this context it does not seem quite compatible that a fabric generates a wire mark. On the other hand, it could not generate a fabric mark, since a press fabric might equally well have generated that.

The term **roll-blade** former will often be used for all designs where a roll is followed by some kind of blade arrangement. In principle, this term could thus also include the **roll-adjustable blade** design, in which the forming roll is followed by a combination of fixed and movable blades on the two sides of the wires.

The use of different material mixtures on different levels in a product as now is increasingly applied to different products can be achieved using two basically different principles. The tradition is to manufacture board in several **plies**, while e.g., tissue products are increasingly formed in different **layers**. The **multi-layer** products are formed using a single headbox, with different component mixtures in different headbox layers, while a **multi-ply** product consists of plies formed from separate headboxes.

For readers, not familiar with the basics of forming, it could be advisable to initially study a textbook covering the area, such as *Papermaking Part 1, Stock Preparation and Wet End* in the new book series *Papermaking Science and Technology* [3].

2 PAPER STRUCTURE CHARACTERISATION

Variations in paper structure occur in a very wide range of scales. Different mechanisms or different parts of the process are responsible for the initiation of variations in the different scale ranges.

- **Micro scale** denotes the variations in a scale smaller than 0.1 mm. On this scale particle size, micro flow, and colloidal interactions are important.

- **Small scale** covers the range of 0.1 to 40 mm, in which range fibre flocculation and hydrodynamic conditions during forming are the main causes for irregularity.
- **Medium scale** covers the range of 40 mm to 10 m and is affected mainly by instabilities in headbox flow (partly generated in the approach flow system) and wire section dewatering.
- **Macro scale** variations are those in excess of 10 m and are caused mainly by the variability in the incoming thick stock. The variations are then mainly in the machine direction. Such variations will not be treated in this overview.

2.1 Power spectra

To quantify the variations at different scales in a stochastic signal, the **power spectrum** is often applied. Already during the 1930s, the **autocorrelation** and its Fourier transform, the **frequency power spectrum**, were introduced, initially to characterize the energy content within different frequency bands for electrical signals. The power spectral density describes how the variance (square of standard deviation) of a signal is distributed on different frequency ranges.

The frequency power spectrum has since been applied to characterize the structure of turbulence for more than 60 years. The frequency power spectrum has also long been used to characterize variations of basis weight and moisture at the dry end of the paper machine. An analysis of the distribution of variance on different frequency ranges is a useful tool to trace the origin of the variations.

Turbulence, flocculation, and formation represent stochastic variations in local flow velocity, local fibre suspension concentration, and local basis weight in the small-scale range, respectively. To describe such variations, it is useful to use geometrical scale instead of frequency for the characterization. This method is also applicable to medium and macro scale variations. Knowledge of geometrical size often simplifies the tracing of the origins for variations, such as wire lengths, felt lengths, and cylinder circumferences. The frequency spectrum is therefore transformed into a **wavelength spectrum**. The wavelength is calculated as the scanning speed (or flow velocity) divided by the frequency. Since one complete sine wave can be interpreted as one negative and one positive floc, floc size will be half a wavelength. To conserve the basic property of the power spectrum, i.e., to describe the distribution of variance, also the frequency spectral density has to be transformed, into the **wavelength spectral density** [1].

It is a common misunderstanding that the power spectrum is the Fourier transform of the sample variations. This is incorrect, since it is instead a generalised Fourier transform, with principally different properties. In practical terms, the difference between evaluation of a Fourier spectrum and a Power spectrum respectively at a certain frequency could thus be described as follows (the mathematics involved are much more complex).

- To evaluate the Fourier spectral density at one specific frequency, the complete sample curve is correlated with an equally long sine curve and this correlation is integrated while the sine curve is moved one wavelength along the sample curve length.
- To evaluate the Power Spectral density, one sine wave period of a specific frequency is correlated with the sample curve and this correlation is integrated while the sine wave is moved along the whole sample curve length.

This is illustrated in Figure 1.

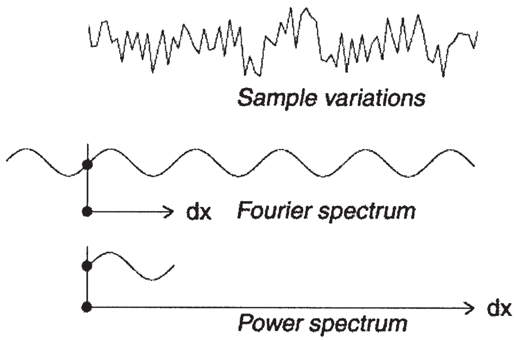

Figure 1 1-D sample variations (top), hypothetical waveform and wave displacement for evaluation of Fourier spectrum (middle) and Power spectrum (bottom).

While the Fourier analysis primarily quantifies variations, which are periodic (and thus in phase) over the whole sample length, the power spectrum analysis quantifies the total amount of sample variations of a certain frequency, even if they do not occur in phase.

2-D power spectrum analysis is becoming increasingly used, often based on optical quantification of variations using CCD-techniques. One example is periodic wire marking, see further below.

Sometimes the absolute values of variations of a property are difficult to evaluate due to calibration difficulties, such as in optical formation or fibre suspension flocculation measurements, aiming to evaluate local basis weight or local fibre concentration variations respectively. Scale information can however still be obtained, by dividing the power spectrum area into two equal parts by a vertical line at the mean wavelength. Mean floc size will then amount to half that mean wavelength; see e.g., [4].

For practical reasons, the wavelength power spectrum is often presented using logarithmic scales on the spectral density axis (and sometimes also on the wavelength axis). When two spectra are compared, a certain vertical difference between the spectra then corresponds to a specified ratio between the spectral densities, independently of the absolute level.

2.2 Specific perimeter

One method to evaluate mean scale information from a two-dimensional field of variations is to calculate the **specific perimeter**. Using image analysis, the variation field is transformed into a two-dimensional grey-scale field, and a cut is made at 50% of the mean grey scale intensity. At this grey scale level, two-dimensional flocs of different sizes will be defined, and the specific perimeter is defined as the sum of the circumferences of all the flocs divided by the total image area. The dimension of the specific perimeter will be inverted length scale.

2.3 Wavelets

Wavelet methods give a more complete description of local variations in comparison with power spectra. While the power spectrum gives an average of variations of different scales over the whole sample area, wavelets also specify the location of specific variations. In the power spectrum, variations are described based on comparisons with sine wave shaped curves, while with the wavelet technique the choice of curve shape is free (even if some mathematical restrictions exist). Two examples are given in Figure 2.

An application of wavelet technology (Morlet) is demonstrated for the

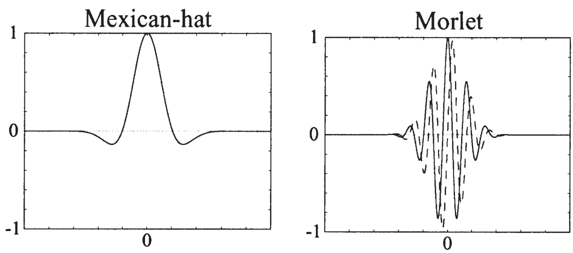

Figure 2 Left: Mexican-hat wavelet, Right: Morlet wavelet (sinusoidal signal weighted with a Gaussian distribution), real part (solid line) and imaginary part (dashed line).

signal $\sin(x^2)$ as function of distance x, see Figure 3a. The power spectrum of this curve is shown in Figure 3b, and demonstrates high spectral density at short wavelengths, and a gradual decrease towards longer wavelengths.

In the image map from the wavelet analysis, Figure 3c, the wavelength is plotted as a function of distance, and it is apparent that the wavelength decreases towards longer distances. This information is not available in a power spectrum.

In Figure 3d the same result is presented using contour lines.

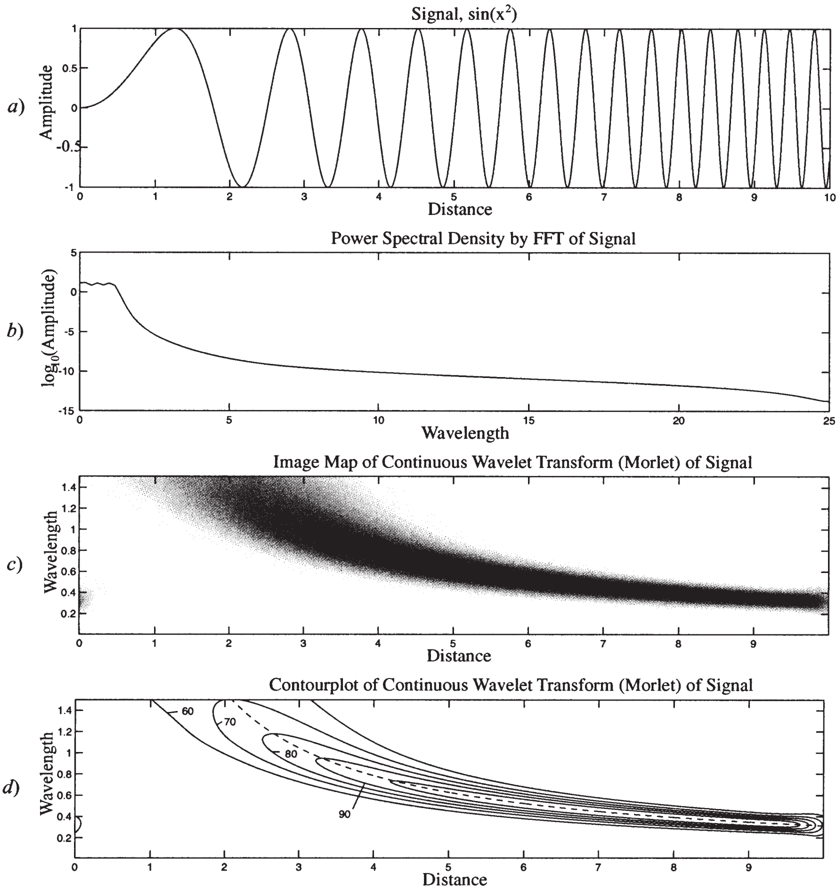

Figure 3 a) $\sin(x^2)$ signal, b) Power spectral density, c) Image map of wavelet (Morlet) transform and d) Contour plot of wavelet transform with exact wavelength variation (dashed line) [7].

Use of wavelet techniques has been discussed by Keller et al. [5,6] and applied by Söderberg [7] (see further below).

2.4 Formation

The formation of a paper sheet, i.e., the local grammage variations up to about 40 mm wavelength, is determined by the fibre distribution in the plane of the sheet and has a great influence on many sheet properties; it is therefore desirable to be able to quantify this distribution. The geometrical resolution of the basis weight measurement is of decisive importance for the amount of variations recorded. The smaller the measurement area is, the more small-scale variations can be detected and the larger the total variations recorded. In industry, formation evaluation is often done using light transmission methods. Besides local grammage variations, this method is however also sensitive to other parameters, primarily variations in local light scattering coefficient. Beta radiation is a good alternative to be used in evaluating grammage variations.

Beta ray transmission

In the **STFI method**, based on beta radiography, which has been used since the early 1970s, an X-ray film in contact with the paper sample is exposed to transmitted beta particles from a C-14 radiation source with a size of 100×150 mm^2 [1]. The scanning of the exposed and developed X-ray film has later been modified, and the radiographs are now analysed using a desk-top scanner, giving a 300 dpi resolution (which corresponds to ≈0.08 mm resolution) grey-scale map. Based on calibration areas along the radiograph edge, the grey-scale map can be transformed into a basis weight map. Thus a two-dimensional map of actual sample basis weight can be generated [8].

Video-beta radiography was applied by Cresson and Luner to evaluate paper formation [9]. They described the texture of basis weight variations using co-occurrence matrices to evaluate parameters like floc size and shape [10,11 and 12].

Dodson et al. have later used beta radiography with a CCD camera for radiograph analysis [13].

The **Ambertec meter** [14], directly records beta ray transmission within local areas of 1×1 mm^2. The measuring point is moved automatically using an x-y table, and 400 measuring points are collected on a paper sample size of 70×70 mm^2. This method is commercially available, and widely used.

A similar principle was later applied at IPST, using a sample size of 80×80 mm^2 [15].

Luner et al. compared four imaging techniques [16]:

- β-radiography;
- electrography;
- light transmission; and
- soft X-radiography.

Keller studied electron beam transmission imaging to quantify formation [17].

Formation characterisation

The **Formation number *F*** is often used to denote the coefficient of variation of local basis weight, that is, standard deviation divided by mean basis weight and it is often expressed as a percentage [1]. One exception was the use by Dodson of the same term to denote the variance of local grammage of a paper sample, normalised with that of a sheet with random fibre distribution [18]. Although physically sound, this use of the term is unpractical, since knowledge of the corresponding random fibre distribution is usually missing. It would require complete knowledge of dimension and coarseness values for all the individual fibres.

Normalisation with the formation of a standard laboratory sheet made from the same furnish has also been used be several researchers, e.g., Lloyd [19].

Regarding normalising the formation values for differing mean grammage, a method based on statistical means has been used [1]:

$$F_{norm} = F\sqrt{w_m/w_n} \tag{1}$$

where w_n = normalization basis weight and w_m = sample basis weight.

Normalization according to Equation 1 assumes that all layers in paper samples of different basis weights have similar fibre distributions and are independent. This will generally not be strictly true, when basis weight is changed on a paper machine. At constant forming concentration, e.g., the total structure will often improve with increasing basis weight due to a self-healing effect during dewatering of additional sheet layers [1] (see further discussion below). 60 g/m^2 was chosen for normalization basis weight in the STFI Formation method.

Equation (1) was later also promoted by Dodson [18].

A useful description of formation, should quantify the amount of local variations, but also give some scale information. A change in forming conditions sometimes can reduce the number of large flocs by breaking them apart, and thus move them to a smaller floc size range. This may not always show up in a single formation number.

In the STFI method, formation is described by its wavelength spectrum. The information in a complete formation spectrum can be simplified by integration within different scale ranges. In the STFI method, a small-scale wavelength range of 0.3 to 3 mm and a large-scale range of 3 to 30 mm are used, and together they make up the total formation number F.

In the Ambertec meter, the limited sample size sometimes requires measurements on several samples to give accurate values of the standard deviation. The normalized Ambertec formation value with dimension "$(g/m^2)^{0.5}$" (not easy to understand) can actually be interpreted as the dimensionless normalized formation number F according to Equation 1, using a normalization basis weight of 1 g/m^2. It is thus possible to compare an Ambertec to a STFI value by multiplication with $60^{0.5} \approx 7.7$. It should however be remembered that the Ambertec meter suppresses all variations smaller than 1 mm, so its formation value mainly correlates with the STFI large-scale value.

Dodson et al. used the variance against zone size to characterise the scale distribution in basis weight variations [20]. This is defined as the integral of the wavelength spectrum from the specified zone size to some upper limit. This makes it hard to evaluate differences in small-scale variations between two samples, since the influence of the dominating variance at larger zone sizes will always dominate.

An alternative method of evaluating formation scale is by the specific perimeter as promoted by Jordan et al. [21].

Using wavelets to characterise formation, it is possible to describe the distribution of floc sizes within different parts of a paper sample, not only give the average over the whole area. This method has been applied by Keller et al. [5].

Periodic marking

While formation measures mainly quantify the degree of fibre flocculation in a paper sample, different kinds of periodic marking is also of interest. Such marking is mainly generated by wire patterns, but sometimes also by the felts. In a one-dimensional formation spectrum, wire marks will show up as peaks in the spectrum. It will then be possible to rank samples depending on the magnitude of such peaks.

A more complete way of describing periodic marks is to first calculate the two-dimensional frequency power spectrum, in which periodic variations will show up as a pattern of individual points of higher intensity than the surrounding; see Figure 4.

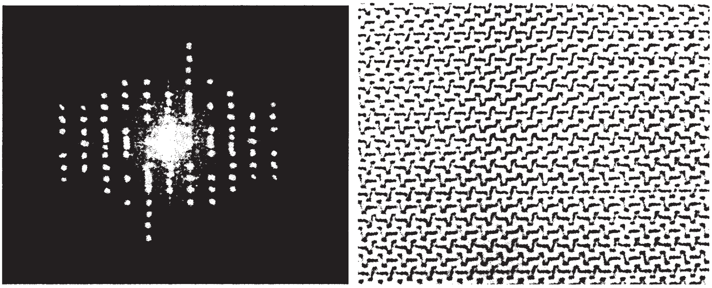

Figure 4 Two-dimensional frequency spectrum (left) and corresponding geometrical pattern for wire mark (right) [22].

These points can then be inversely transformed back into the original x-y plane, where the geometric pattern of the generating wire and/or felt will show up, see e.g., [22,23].

Optical measurements

The term "formation index" is reserved for **optical formation meters**. Such meters have the drawback that they do not give absolute values of basis weight variations, due to their sensitivity to variations in light scattering coefficient.

This has been demonstrated repeatedly, recently by Duffy et al. [24]. Two light transmission meters were compared with the Ambertec and STFI methods (beta ray transmission). The light transmission methods gave reverse results from the beta ray methods when e.g., grammage was changed in laboratory forming.

Luner et al. [16] concluded that for newsprint samples, electrography gave higher spatial resolution, shorter exposure time and wider basis weight range than β-radiography. Light transmission gave the poorest spatial resolution and correlation with mass. Soft X-radiography gave the highest spatial resolution but the poorest contrast.

Bernié and Douglas [25] compared light transmission and beta ray transmission and came to the conclusion that light transmission can be used to measure formation. This was however based on absolute calibrations and was applied to laboratory sheets only. For practical purposes, this is of less interest.

Bouydain et al. used uncalibrated light transmission images in combination with wavelet analysis to study paper formation [26].

However, optical methods due to their simplicity can still be valuable, for instance to follow changes on a specific machine at constant furnish, basis weight and calendaring conditions. Absolute comparisons between paper samples from different machines should be avoided.

Two of the more commonly used optical formation testers in North America are the NUI (Non Uniformity Index) meter [27] and the M/K-meter [28]. The NUI-meter analyses light transmitted through a rotating paper sample, and a total variation number is given as a formation index. With the M/K-meter, on the other hand, a high value corresponds to good formation. Recently also the Kajaani optical formation tester has been introduced and, like in the M/K-meter, the formation index is higher for a more even paper sample.

If the aim of an optical formation meter is to resemble perceived look-through formation the wavelength distribution of the light analysed should be matched with the colour response of the human eye [29].

Lloyd [19,30] introduced the parameter "surface ply variation", SPV, to characterise the final mixing in paper samples manufactured from a three-ply headbox. A light blue colour was added to the middle ply, to make it possible to optically evaluate the degree of mixing between centre and outer layers. 87×174 mm^2 samples were analysed using a colour scanner at a resolution of 300 dpi. The cyan part of the image was separated. This image was inverted, i.e., a negative taken, because the cyan represented an absence of the white surface layer, and it was the absence of the surface layer that was of most interest. The resulting image was a grey-scale TIFF image. The image was analysed with a procedure similar to that used for the evaluation of the small-scale and large-scale STFI formation values; see further below.

On-line measurements

Today optical CCD-techniques can be applied to both laboratory and on-line evaluation. One example is the formation meter developed at CTP [31]. Using a CCD camera a sample size of 120×120 mm^2 is scanned with 0.25 mm resolution. From this a total formation index can be evaluated as well as flocs in the size classes 1, 2, 3, 6, 10 and 16 mm. It is also possible to evaluate shape (MD/CD) as well as angle of orientation of flocs, see Figure 5. Means are also provided to filter out and present periodic wire markings. In on-line

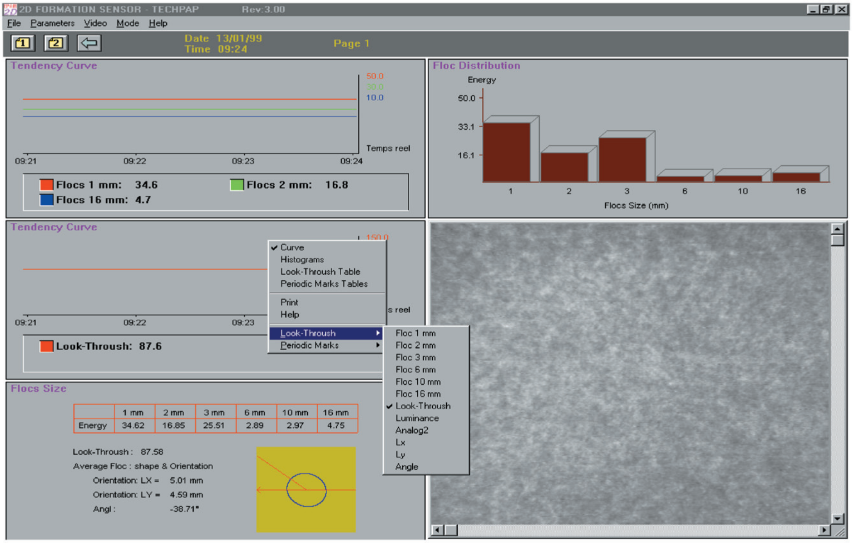

Figure 5 Presentation of results from the CTP on-line formation analyser [31].

applications a stroboscope is used for incident light, while ordinary light sources are enough for laboratory evaluations.

A more simple on-line formation analysis can also be made using the ABB Hyperscan System; see the following section.

2.5 Medium-scale variations

Maps of the two-dimensional basis weight distribution in the scale above the formation range, that is, around 40 mm, up to about 10 m, give good pictures of the medium-scale variations in basis weight and is an important tool for tracing the origin of different basis weight defects. Equipment for handling full size paper rolls, and methods for measuring basis weight measurements using beta ray absorption techniques in a laboratory scale has been developed by STORA [32]. Figure 6 shows an example of such a basis weight map.

Two-dimensional maps of light transmission are recorded on-line with the ABB Hyper-scan system [33,34]. Even though only light transmission variations are recorded, some calibration against actual basis weight variation is possible by comparison with the basis weight signal from the conventional scanning beta meter at the dry end. A resolution of 1 mm^2 is obtained, and it

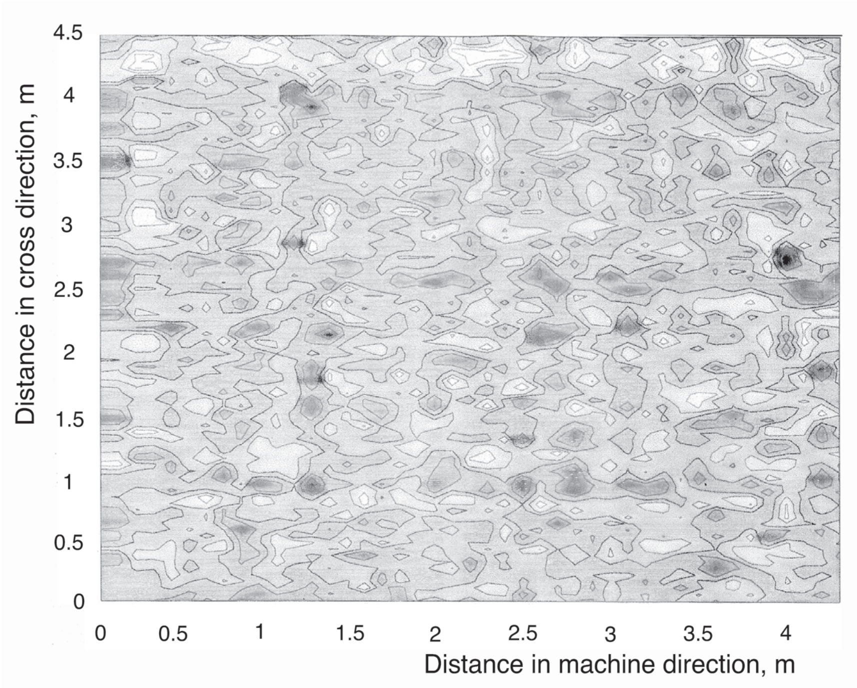

Figure 6 Grey-scale picture (original in colour) of basis weight of full width paper web. Newsprint quality, with each level curve indicating a deviation of 1 g/m^2 [32] (Courtesy STORA, original in colour).

is even possible to on-line follow the patterns of the narrow wire shower marks using this technique.

Honeywell-Measurex developed a method for detecting water weight in the wire section, aiming at following the CD and MD dewatering profiles [35]. Non-scanning sensor technology was used, based on the measurement of effective electrical properties of water between sensor elements mounted below the wire. It is yet uncertain if it will develop into commercial equipment.

2.6 Fibre orientation

An overview of fibre orientation in paper was made by Niskanen [36].

During the last decade, the details of fibre anisotropy have received increased interest, much depending on the easy recording of angular distribution of paper elastic modulus using automated ultrasonic techniques [37,38]. Special emphasis has been given to fibre orientation misalignment, but fibre orientation anisotropy has also become more important.

Laboratory evaluation

Hasuike et al. [39] analysed fibre orientation anisotropy after splitting a sample into eight layers using adhesive tape; see Figure 7. Fibre orientation

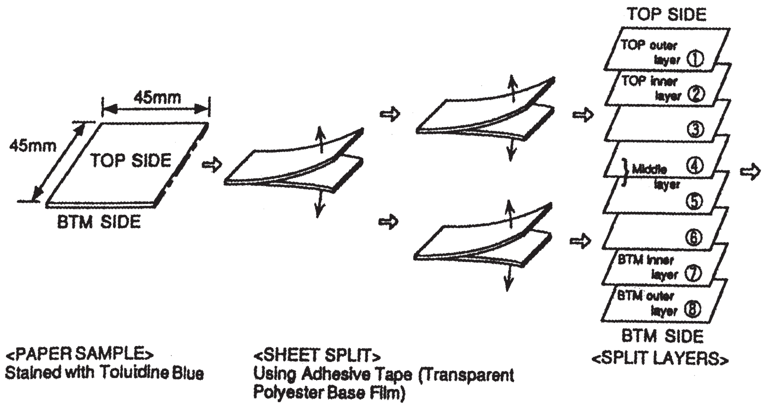

Figure 7 Principles for sample splitting into eight layers [39].

anisotropy in the layered samples was evaluated from manual counting of the number of fibre crossings with a 5 mm-long MD and CD test line respectively, within sample areas of 30 × 30 mm^2.

They further analysed the three-dimensional structure of paper samples [40,41]. Fibre entanglement in the thickness direction was evaluated by embedding a sample in epoxy resin, cutting it into 4μm thick sections (2 mm wide) and following the positions in the thickness direction of individual fibres along its length, through 150 sections.

Hasuike et al. [42] also studied 3-D floc structure in 45 × 95 mm^2 paper samples using tape-layering techniques. Floc distribution in each layer was evaluated optically, and the correlation between floc positions in adjacent layers was utilised to quantify floc dimensions in the thickness direction. A limitation of this method is that tape delamination does not strictly split the paper samples into even layers, since some flocs tend to resist splitting.

Erkkilä et al. also used a method based on tape splitting [43]. A 60 g/m^2 sample was split into ca 6–8 layers, on which 30×30 mm^2 samples were analysed in transmitted light using a CCD-camera with a resolution of 640×640 pixels. An image analysis program was developed to evaluate the orientation distribution of fibre segments in the images. The results were presented in polar diagrams where the orientation distribution has an elliptic-like shape. Anisotropy was evaluated from the eccentricity b/a, and misalignment angle as the deviation of the main axis from MD; see Figure 8.

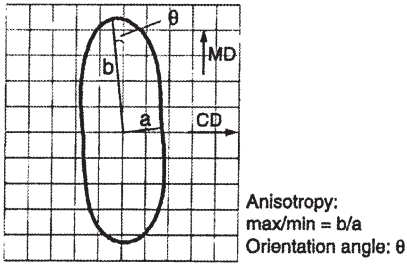

Figure 8 Orientation distribution and parameter definition [43].

Local fibre layer orientation was also studied, on sub areas of 3×3 mm^2, and presented in vector form.

$$Anisotropy = b/a \approx \; MD/CD \tag{2}$$

Jansson [44] used another tape quality, and separated an 80 g/m^2 sample into 20 layers, which he imaged using a desktop scanner with a resolution of 600×600 dpi. He analysed the images of the size 40×40 mm^2 using the program developed by Erkkilä.

Lloyd and Chalmers used similar techniques to study the effects of sheet structure on paper curl and cockle [45].

Scharcanski and Dodson [46] demonstrated an image gradient evaluation technique to quantify anisotropy from a beta-radiograph or a light transmission image.

Thorpe [47] used a "new method" to split a copy paper into 13 layers. The black coloured layers were mounted in 35 mm slide frames and imaged with a CCD camera attached to a microscope. Fibre orientating data were evaluated using the Hough transform. He analysed samples of size 20×25 mm^2, and each picture was divided into 5 × 5 mm^2 segments for local orientation analysis. He could evaluate the occurrence of orientation streaks on the wire side of fourdrinier formed paper.

Parker et al. [48] studied local fibre orientation at different levels in the thickness direction using confocal laser scanning microscopy and application of the Hough transform. The thickness resolution was ≈ 3μm and the depth was limited to 80μm. The scanning area for each sample was limited to 650 × 650 μm^2.

3 FIBRE SUSPENSIONS

It should be pointed out that the physical flocculation of papermaking fibres is the main reason for small-scale unevenness in the final paper product. A deeper understanding of how fibre flocs are generated and how they can be dispersed is therefore of vital importance, if the evenness of paper products is to be improved.

It is well established that fibre flocs are generated by mechanical fibre entanglement [1]. Once a floc is formed, the fibres have to be disentangled. This can be obtained by a high degree of fluid turbulence (see further in section *Headboxes*). One main problem is, however, that when the fluid motion is dissipated, fibre flocs will form again.

It was first demonstrated by Kao and Mason [49] that dispersion of flocs by extensional flow is much more effective than by simple shear, since shear flow mainly generates rotational movements of flocs.

Duffy and Norman [50] showed experimentally that fibre flocs can actually be broken apart through the stretching effect in an elongational flow.

As will be discussed further below, it therefore does not seem to be possible to avoid fibre flocculation based on turbulent shear effects, but rather by applying floc stretching.

The behaviour of fibres and fibre flocs in flowing fibre suspensions is a formidable two-phase problem, and its modelling is only in the initial stages. However, experimental studies of fibre suspensions have been undertaken to a considerable extent, and modern techniques open new possibilities in this field.

3.1 Fibre suspension modelling

Steen [51] modelled fibre flocculation in turbulent flow, introducing the rate of both rupture and aggregation of fibre flocs. The model was applied to pipe flow at different Reynolds number as well as to a pipe with a step diffuser. In the latter case, minimum flocculation intensity was predicted a certain distance downstream of the step, which is close to observations reported in literature.

Kerekes and Schell [52] introduced the concept of **Crowding Factor N** for the number of fibres of length L and diameter d at a volume concentration of c_v, within a given reference volume. The reference volume was chosen as the volume of a sphere of diameter L, i.e., the sphere created by a freely rotating fibre of length L. The following relation-ship is then valid for the crowding factor N:

$$N = \frac{2}{3} c_v \left(\frac{L}{d}\right)^2 \tag{3}$$

Table 1 is a summary of the findings using the turbulence decay cell described above. In standard hand sheet forming, the crowding factor approximately equals unity.

Table 1 Fibre contacts at different crowding factor levels.

Crowding factor N	Concentration	Type of fibre contact
N < 1	Dilute	Rare collisions
1 < N < 60	Semi-concentrated	Frequent collisions
60 < N	Concentrated	Continuous contact

Since the density of cellulose is approximately 1.5, it would be expected that the volume concentration of fibres is lower than the weight concentration. However, because of the swelling of the fibre wall, the lumen volume etc., the average volume concentration can be as high as twice the weight concentration.

The crowding factor is a better indicator than the fibre concentration of the flocculation tendency of a fibre suspension, and it is increasingly used to characterise the mix conditions during forming, see Kiviranta and Dodson [53].

Kerekes made an analysis of fibre flocculation in relation to paper forming [54]. Besides the crowding factor, he then introduced two additional dimensionless numbers: a **fibre Reynolds number** to reflect the ability of a fibre to follow fluid streamlines, and a **force factor** to account for hydrodynamic crowding forces in relation to fibre contact forces resisting crowding.

Basic studies of fibre network properties have been made by Andersson, Wikström et al. [55,56] with the main aim of improving pulp processing, which generally means concentration ranges higher than those in paper-making. It was e.g., suggested that fibre network yield stress was a better measure than fibre concentration for designing pulp lines [57]. Experimental studies of fibre-fibre friction were combined with fibre force models to predict fibre network properties [58,59].

Experiments by Bennington [60] , based on modelling of chemical reactivity indicated that in a 3% fibre suspension, 95% of the energy dissipation takes place by direct friction between the fibres and thus only 5% in the fluid itself.

Huhtanen [62] studied the non-Newtonian properties of fibre suspensions, without taking fibre flocculation specifically into account. He made rheological measurements to analyse shear viscosity of pulp suspensions at moderate shear rates and small deformations. He also applied a commercial code to describe the non-Newtonian effects on pipe flow of pulp suspensions.

Klingenberg et al. have an extensive program to study flowing suspensions of rigid and flexible fibres, modelled as chains of prolate spheroids connected through elastic ball and socket joints [63]. Attractive forces between fibres can form flocs, but the properties of such flocs are different from flocs formed from elastic interlocking and inter-fiber friction. Simulations suggest that fibre shape is important and that effective formation aids in paper-making should reduce inter-fibre friction under normal force loadings of 1–10mN [61,64,65]. Examples of the influence of friction coefficient on the flocculation in shear flow shown in Figure 9.

Shah et al. [66] studied the flow patterns generated by a half Δ-wing in a water tunnel, specifically the fluid stress fields. Applying these fields on fibre suspension models, they came to the conclusion that the local stresses were large enough to break apart fibre flocs.

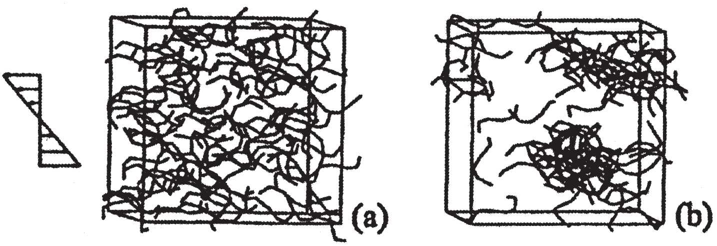

Figure 9 Simulations of shear in a 0.125 vol% suspension of helical-shaped fibres. Static friction coefficient a: 0 and b: 20 [61].

3.2 Fibre flocculation evaluation

Qualitative studies of fibre flocculation in flowing fibre suspensions are possible using different optical set-ups, but quantitative description of local concentration variations is extremely difficult, due to secondary light-scattering effects. Several investigations have recorded transmitted light through a flat channel. For thicker channels or pipes, light reflection measurements have a potential of better geometrical resolution, while limiting the measurements to the surface of the suspension. Evaluations have been carried out in turbulent flows as well as in decaying turbulence fields.

Kaji et al. [67] used a rectangular flow channel with a cross section of 60×3.5 mm^2. Both transmission of a laser beam and imaging using a CCD camera were used for flocculation evaluation.

Among other means they also applied fractal analysis to characterise the geometry of floc periphery for different pulp suspensions. They found that as floc forming proceeds, the shape of flocs tends to be simpler, while as dispersion proceeds, the shape of flocs tend to be more complicated

Kerekes and Schell [52] , experimentally studied the effect of different parameters on fibre flocculation using a vertical, transparent cell of 23×342 mm^2 cross section, and closed at the bottom; see Figure 10. A grid was pushed

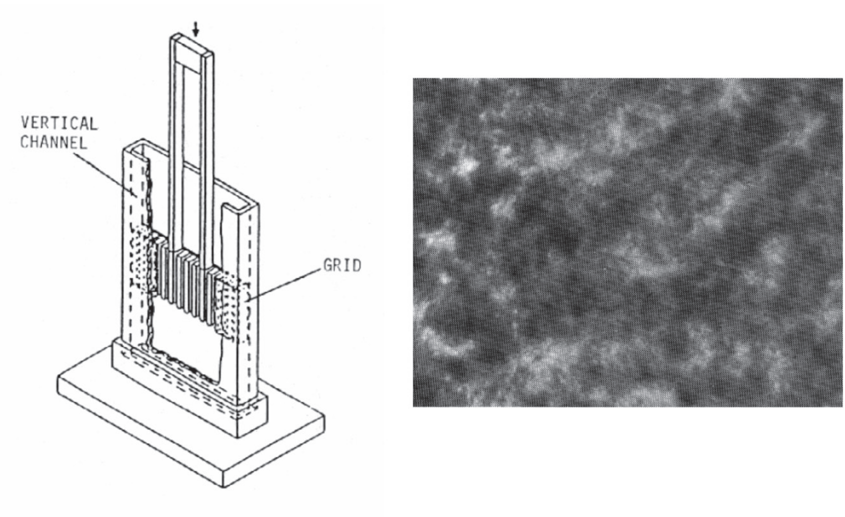

Figure 10 Left: Concept for grid pulled through a vertical, narrow channel. Right: State of flocculation for Douglas fir, 0.5% , Crowding Factor $N = 75$ [52].

down through the fibre suspension in the cell. After turbulence decay (app. 15s) a flocculation image was photographically recorded in transmitted light. From this image, contrast intensity and floc scale was evaluated.

Kallmes et al. [68] demonstrated equipment for on-line analysis of mix flocculation. Mix was extracted from the headbox into a 13 mm-wide channel. The light transmission variations of a narrow light beam directed through the fibre suspension gave a flocculation value. A comparison was made with the inherent flocculation tendency of the mix, as recorded after the passage of a dispersing 90° flow elbow, as well as with a formation index recorded with an on-line, light beam transmission meter. Preliminary test on different paper machines showed promising correlations between flocculation and formation values in response to e.g., changes in chemicals addition.

Zhao and Kerekes [69] used the above-mentioned cell with decaying turbulence to study fibre flocculation at different suspending liquid viscosities. One way of presenting the results is to find the "critical crowding factor", below which no flocculation can be detected. In pure water (viscosity 1 mPas) the critical crowding factor for long fibre pulp is around 10, but increases linearly to 70 when sugar is added to increase liquid viscosity to 20 mPas. This is explained by reduced turbulent motion, decreased initial turbulence and faster turbulence decay, and higher shear forces on the fibres.

Duffy et al. [70] made a study of pipe flow of fibres suspended in liquids of different viscosities. The numerous flow regimes normally observed for friction loss curves in pipe flow were not present for viscous suspensions. Drag reduction is also observed in viscous suspensions but it onsets at higher velocities. Increasing viscosity leads to reduced floc size in pipe flow. Overall, it is suggested that increasing viscosity has the same effect as decreasing fibre concentration.

Giro et al. studied the effects of adding CMC dispersants to high concentration pulp slurries (≈ 30%) [71]. The torque requirement in a bowl mixer was used as a measure of pulp dispersibility. It was concluded that increasing CMC molecular weight had a positive effect, and pulp dispersion was more closely related to the amount of CMC adsorbed than to the amount in solution. This indicates that at this high concentration level, fibre friction seems to be the determining factor, and not fluid viscosity.

Kerekes and Schell [72] , also used the decaying turbulence cell to study the effects of fibre length and coarseness on flocculation. Their main findings are:

- Fibre length exerts its influence on nonuniformity through the number of contacts per fibre and floc size.
- Coarseness exerts its influence on nonuniformity through the number of contacts per fibre, floc size and mobility.

- Mixtures of short and long fibres of a given length-weighted average length gave the same nonuniformity as homogenous fractions of the same fibre length.

They point out that the definition of the crowding factor assumes identical fibres. Normally, a rather wide distribution of fibre lengths will be found in a practical situation. This means that the crowding factor concept has to be used with caution in such cases.

Beghello [4,73] used a 15 mm; wide transparent channel with turbulence generating constrictions at the entrance; see Figure 11. A digital camera was used and pictures were taken in reflected light of an area sized 80 × 120 mm^2. To minimize reflection from the channel bottom wall, a black surface was placed below it. Absolute concentration variations were not possible to evaluate. Instead the power spectrum was evaluated up to 32 mm wavelength, and the mean floc size was calculated from the wavelength dividing the area below the spectrum into two equal parts. The studies aimed at three main areas:

- How the physical and mechanical aspects of suspended fibres influence the flocculation process prior to the addition of wet end chemicals.
- How the chemical and physical environments in the fibre suspension influence and/or contribute to the flocculation process.

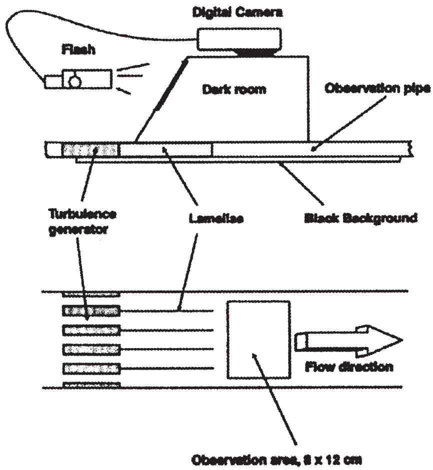

Figure 11 Drawing of the turbulence generator and camera system for the floc-measuring device (not to scale). Turbulence generator channel widths 15 mm and length 80 mm. Lamellae length 270 mm and thickness 1 mm [73]

- How changes in the surface chemistry of suspended fibres influence the flocculation process.

Raghem-Moayed [74,75] studied fibre flocculation in a decaying turbulence field in a transparent flow channel with the cross section 11 × 152 mm^2.

Turbulence introducing contractions were provided at the inlet. Diffuse ingoing light was recorded in transmission over an area of 20 × 23 mm^2 on the opposite side using a CCD video camera. Calibration indicated a linear relationship between light absorbance and local concentration for hardwood fibres in the range 0.4–0.7%. Flocculation index was evaluated as the square of the coefficient of variation of local concentration. Due to statistical effects, this can result in a decreasing index with increasing fibre concentration, which was also the result of the evaluations. At increased flow velocity, flocculation index decreased. No spectral analysis was applied to evaluate floc scale.

Wågberg had earlier made studies of chemical-induced fibre flocculation using laser beam optics [1]. In a new investigation he applied a CCD video camera to detect flocculation in a flow channel of cross section 3 × 170 mm^2 using light transmission [76]. He determined flocculation index and mean floc size, both values calculated from the increase in flocculation when chemicals are added. Regarding the nature of flocculation effects for the chemicals used, it was concluded that further tests should be made at very short contact times to improve the understanding of the mechanisms.

Pierre [77] also used CCD-techniques to study flocculation in flowing fibre suspensions; see Figure 12. The camera observed 60 × 60 mm^2 of a transparent channel with a thickness of 3–5 mm. He was particularly interested in analysing suspension samples taken from industrial paper machines producing filler containing fine paper, to be able to predict final paper formation.

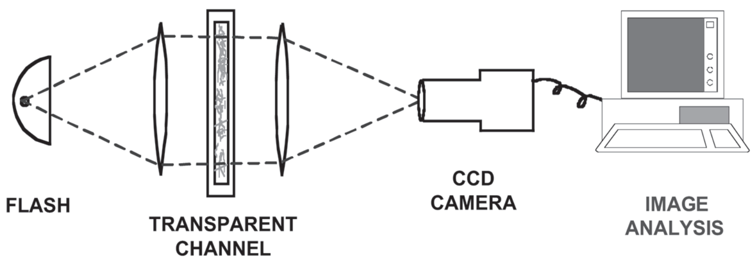

Figure 12 Observation of flocculated suspension according to Pierre [77].

One main objective therefore was to evaluate flocculation in the presence of considerable amounts of highly light scattering filler particles.

Since absolute calibration of transmitted light against fibre concentration is difficult, especially at the presence of filler, he instead evaluated floc sizes. He evaluated flocculation as the floc area in six different size ranges from 0.7 to 13 mm but also summarised the results as a flocculation index. Effects of refining and retention chemical addition on flocculation were studied.

Swerin applied oscillatory shear to fibre suspensions, and studied their rheological properties [78]. A mathematical scaling was found to express the elastic shear modulus as a function of the fibre concentration in excess of the threshold concentration (below which no floc strength can exist). He also studied the effects of chemical additives. It was suggested that the effect of polymeric flocculants on the network strength is due to more fibres being active in the network and to an increase in the bonding strength in the fibre-fibre contacts.

What is known as MC-technology within pulp processing usually involves fibre concentrations above 6%. Gullichsen et al. have studied floc disruption in that concentration range for more than ten years, aiming at paper forming processes [79,80]. Fibre floc disruption takes place in the narrow gaps between wings on a rotor and stationary ribs; see Figure 13. Experiments to form paper using the same geometry have been reported, but no products with acceptable paper properties have been demonstrated [81].

Björkman [82] has performed a considerable amount of experimental studies and interpretations of the flow of flocculated fibres. A shearing cube demonstrated the behaviour of fibre suspensions under deformation in

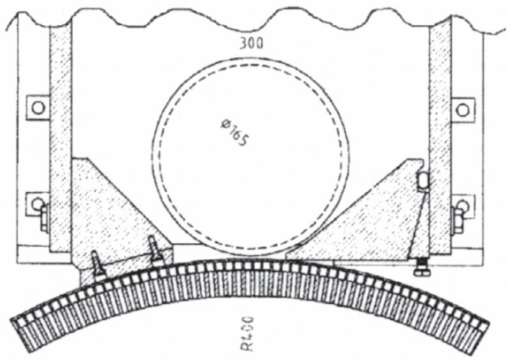

Figure 13 Fluidisation chamber for high concentration forming [81].

compression and extension respectively. The main equipment developed for his studies was a viscometer with independently computer-controlled rotation of inner bob and outer cylinder, with a 20 mm gap width in between. Fibre floc splitting and sizing under different shearing conditions were studied for different fibre types and concentrations. The occurrence of Taylor vortices was observed, as well as fibre orientation anisotropy streaks generated under such conditions; see Figure 14. Such effects are of great importance for the generation of fibre orientation anisotropy streaks in headbox flows.

Helmer et al. [83] studied the concentric mixing of thick stock (central pipe) and water (surrounding pipe). By suspension sampling they measured the concentration profile over the pipe diameter at different locations downstream. The way of sampling at different radial positions resulted in a considerable averaging in the flow direction. The results were largely consistent with those reported in an earlier study [1]. However, it also indicated that fibre concentration at pipe centre could remain at a higher than average level for a considerable distance, which was not possible to reveal in the previous, qualitative, visual study. The pipe dimensions in the new study were comparable to those of the old, i.e., small compared to industrial conditions. This

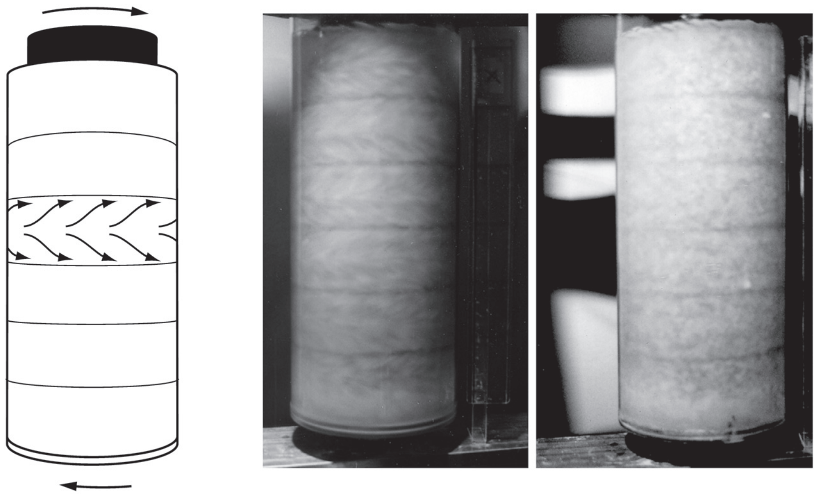

Figure 14 Taylor vortices in fibre suspension of about 0.5% concentration. Left: Schematic view with principal motions of one vortex pair. Photographs: The same vortices photographed with photo lamp to display the motion (middle) and with flash to display the flocs (right), channel thickness 20 mm [82].

means that there is still uncertainty whether or not the higher Reynolds number at realistic dimensions will generate better mixing.

Ringnér and Rasmuson [84] applied X-ray tomography to study 3D fibre distribution under stationary conditions. Their main interest was to investigate inter and intra floc concentrations in a range above 3%, to improve the understanding of pulp treatment processes.

Kellomäki et al. [85] used a fast CCD-camera to detect light transmission through a 30×40 mm^2 cross sectional rectangular channel. They compensated for unevenness in the background illumination and relied on the Lambert-Beer law to calculate fibre concentration as a function on the amount of transmitted light. They evaluated floc size at a grey scale level of average intensity, so that 50% of the image was always interpreted as fibre flocs. They assumed cylindrically shaped flocs, and calculated the effective dimensionless floc volume V_f* from the equation

$$V_f^* = \frac{L_{mx} L_{my}^2}{l_f^3}, \tag{4}$$

where L_{mx} is the mean floc size in the flow direction, L_{my} is the mean floc size in the cross direction and l_f is the mean fibre length.

Karema et al. [86] studied the transient fluidisation of fibre suspensions after a step diffuser, using an optical flocculation analysis method described above. They evaluated the dimensionless floc volume V_f* (see Equation 4) as a function of distance/time after the step at different levels of expansion head loss, which was obtained by different flow velocities; see Figure 15.

Short fibre and long fibre pulps were used. The results indicate that the growth of the dimensionless floc volume V_f* during re-flocculation follows a common power law with respect to time for the pulp types studied. At later times, floc size saturates at a constant value.

3.3 Velocity and turbulence measurements

Particle Image Velocimetry (PIV)

This technique has been applied to flowing fibre suspensions, mainly for flow inside headboxes or for the free jet leaving the headbox. It will be treated in section *Headboxes*.

Ultrasound

Karema et al. used ultrasound to measure fibre turbulence in the thickness direction of a 30 mm thick, plane channel [86]. The instantaneous fibre phase

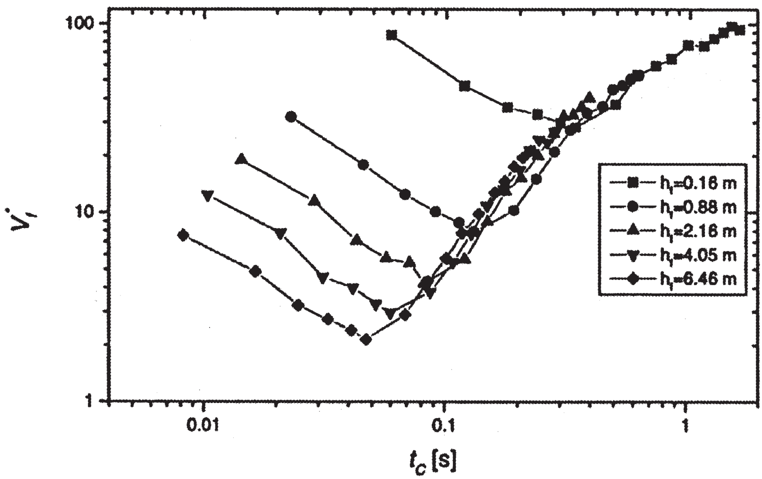

Figure 15. Dimensionless floc volume V_f^* as a function of time t_c elapsed from step expansion at different head loss h_f during expansion [86].

velocities were recorded with a pulsed Doppler ultrasound anemometer, exploiting a single transducer for emitting and receiving ultrasound pulses. The instantaneous beam-wise velocity component at a location on the path of the ultrasound beam is obtained from the Doppler shift frequency of the echoed pulse induced by moving fibres. Velocities at multiple locations along the beam were achieved by detecting the signal with specific time delays after emission. The distance travelled by the pulse was then obtained by multiplying with the speed of sound in the fluid. An example of turbulence measurement is shown in Figure 16.

NMR tomography

Fibre suspension flow was studied by Li et al. using NMR imaging techniques. Pipe flow profiles at flow velocities up to 1 m/s were studied [87]. Various flow patterns from plug flow to complex flow were observed for hardwood suspensions of ca 0.5% fibre concentration. Only plug flow was observed at 0.9% for a softwood pulp suspension. Studies were also made of pulp flow through an abrupt contraction [88], both with water flow and pulp suspension flow. For the pulp suspension, they observed plug flow in the regions both far upstream and far downstream of the contraction. Just

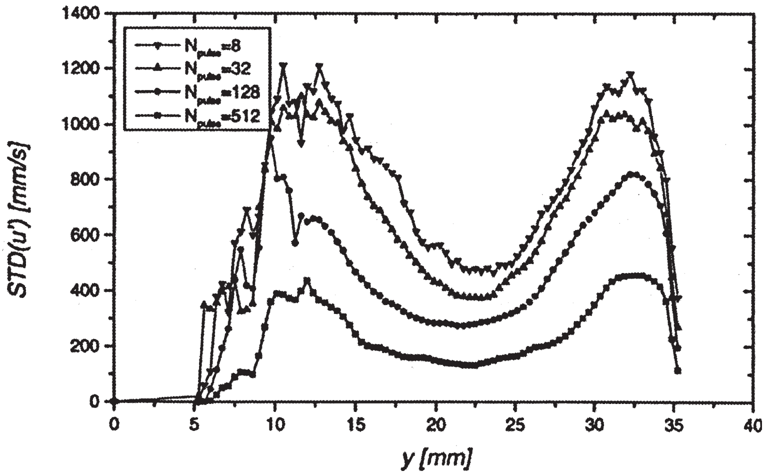

Figure 16 Standard deviation of vertical velocity component of fibres across a horizontal channel. Data collected from 500 velocity profiles at some distance downstream of an expansion. N_{pulse} denotes the number of pulses emitted and echoes received for each profile. The upper and lower walls of the channel are located approximately at $y = 5$ mm and at $y = 35$ mm [86].

upstream of the contraction, off-centred maximum velocities were observed. The extensional flow near the sudden contraction appeared to be highly disruptive to the fibre network. Downstream, the plug in the central core of the tube gradually re-established.

Pipe flow mechanisms with a 0.5–0.9% concentration short fibre suspensions at velocities up to 3 m/s were studied in a 26 mm diameter pipe [89]. The whole range from fully turbulent to mixed flow with a steady plug core was observed. The volume fraction of the fluidised pulp suspension correlated linearly to the mean bulk flow rate. They also studied the influence of retention aids addition on the flow behaviour of fibre suspensions [90]. It was demonstrated that, at low flow rate, adding a polymeric flocculant to a dilute hardwood fibre suspension could introduce a slip velocity between the dense fibre aggregates and the remainder of the suspension. Introducing retention aids at fully turbulent flow resulted in the forming of plug flow immediately after the addition. The disruption of fibre networks flocculated by retention aids was also monitored as a function of the shearing time at constant flow rate.

4 HEADBOXES

A main issue in modern paper machines is to optimise paper structure with respect to the important paper properties of a specific product, and at the same time minimize the MD and CD variations in grammage, fibre orientation anisotropy and misalignment as well as two-sidedness. The headbox design is critical in this perspective and it is obvious that in-depth studies of fibre suspension flow in the headbox are needed in order to achieve higher production rates and improved products.

In principle, the headbox consists of three parts:

- CD distribution, usually a tapered header;
- tube bank(s), to distribute the mix more evenly;
- headbox nozzle, to generate a high quality jet.

A recent overview of headbox flow considerations was given by Houvila et al. [91], and a discussion of the future by Pantaleo [92].

4.1 Tapered header and CD control

The geometry of the tapered inlet header is primarily affecting the paper properties on a CD scale that is the width scale of the paper machine. Historically the manifold shape has been designed to give a constant static pressure across the machine width.

One disadvantage with the tapered header is its sensitivity to changes in flow rate. The shape of the tapered header has together with the slice-lip actuators been the two parameters used to control CD variations. The slice lip has then been used to control the variations on a small scale, down to ca 100 mm. However, when the slice lip opening varies across the width of the machine, cross-flows (CD velocity components) are generated both inside the headbox nozzle and in the jet, which cause fibre orientation misalignment streaks.

A somewhat different design is the BTF distributor by Schultz [93,94]; see Figure 17, which replaces the tapered header. The stock enters the central distributor from the bottom. The central distributor itself is a chamber with an air pad at the top and the stock is distributed through radial, flexible hoses equally spaced around the periphery of the tank. The hoses are connected to the back of the headbox, and all are of the same length in order to have an equal pressure drop. This design allows a good CD distribution of the flow to the headbox, regardless of the incoming flow rate.

To also overcome the problem with fibre misalignment due to slice lip variations, Shultz presented the idea of adding dilution water at the radial

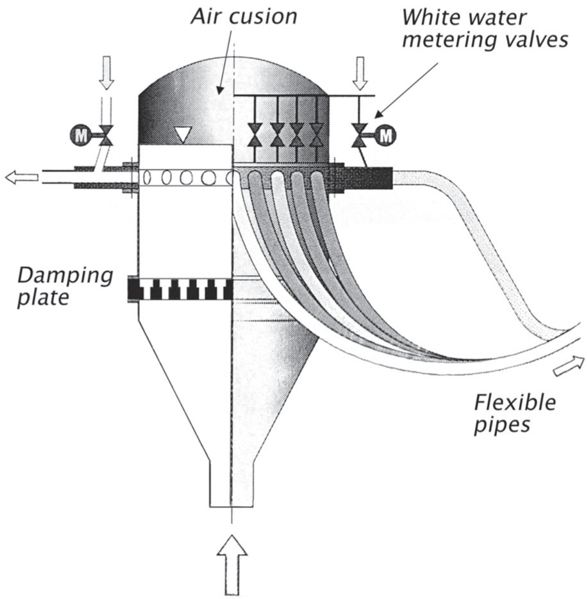

Figure 17 Radial CD-distributor according to Schultz, including BTF dilution control system.

distributor. The water is led into the fittings where the flow leaves the tank. By this local CD addition of water, the local mix concentration can be controlled. Since the basis weight is changed already inside the headbox it is no longer necessary to use the slice lip to control the grammage profile. Hence fibre orientation misalignment due to the induced cross-flow can be avoided and grammage control is de-coupled from fibre orientation misalignment. The BTF dilution control system has also been designed to be retrofitted on existing paper machine headboxes; see Knoller et al. [95].

The concept of dilution control is today also applied in standard headbox designs, where the stock is supplied to the headbox by a tapered header. The first implementation was a Voith-Sulzer Module Jet headbox in Munkedal, which was put into operation in January 1994 [96,97,98]. The dilution control concept has been widely adapted and there are several technical solutions used to add the extra water.

In Figure 18 (top) the addition of dilution water in the Voith-Sulzer Module Jet headbox can be seen [97]. Mix and white water is fed to the headbox.

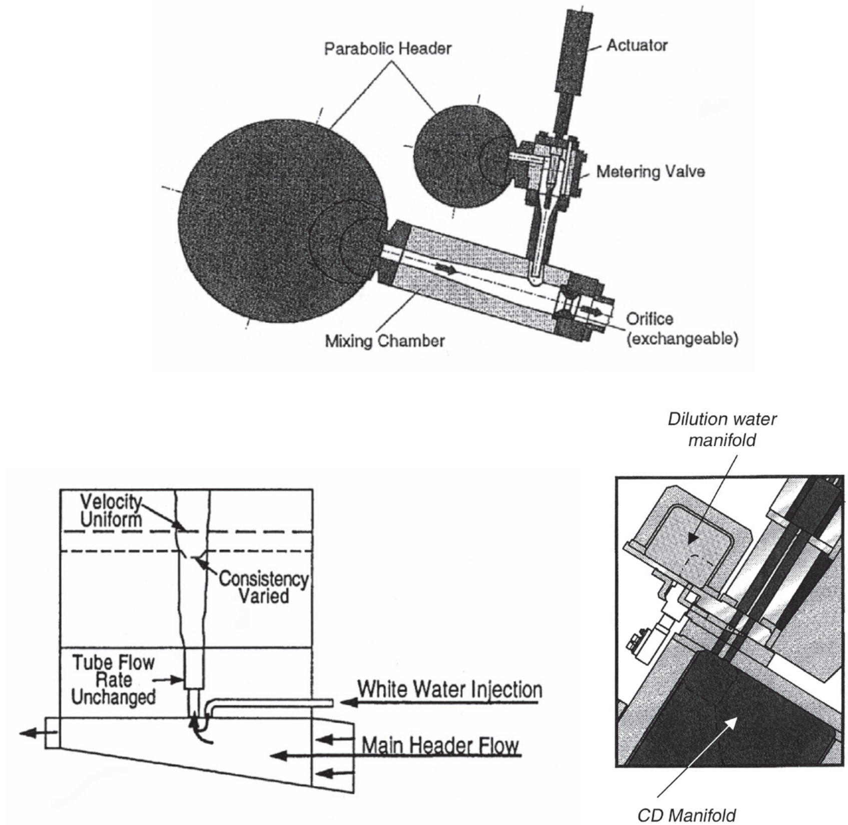

Figure 18 Three different concepts of dilution control. Top: Voith [97] , Bottom, left: Beloit [99]. Bottom, right: Valmet [91].

Motorised valves control the addition of white water, which is blended with the mix in a mixing chamber located in a first, single-row tube bank. An orifice is located after the mixing chamber and the unit (valve, mixing chamber and orifice) is designed so that the volume flow through the orifice (mix + dilution water) is kept constant when the amount of dilution is changed. A good blending of the additional white water and mix is obtained by injecting the dilution water at a specific angle into the mixing chamber.

Figure 18 (bottom, left) shows the technique used by Beloit in the Concept IV-MH headbox [99,100]. The white water is added already in the tapered header. Since it is added before the entrance into the tubes the flow rate into the tubes is only given by the pressure distribution in the tapered header. Hence it remains practically unaffected by the addition of extra water. The direction of the added water into the manifold assures a good mixing.

In Valmet's Sym-Flo D headbox, there are two tube banks separated by a stilling chamber and the additional water is injected directly into the tubes in the first tube bank, at a step change in pipe diameter; see Figure 18 (bottom, right). The constant pressure in the stilling chamber then assures a constant flow rate across the headbox nozzle; see Nyberg and Malashenko [101].

Dilution control is a powerful technology to obtain good CD control of grammage and fibre orientation misalignment, and represents a leap forward in paper process technology. It is widely used on paper machines throughout the world. Many investigations have been made to study the application of dilution control systems in different applications [102,103,104,105,106,107].

Lee and Pantaleo [108] performed CFD simulations aimed at investigating the influence of headbox flow features on fibre orientation.

In order to achieve the most uniform grammage and fibre orientation CD-profiles, Hämäläinen and Tarvainen [109] introduced optimisation methods coupling numerical simulations (CFD) of headbox flow and paper properties such as grammage and fibre orientation misalignment. They illustrated the method by two industrially applicable examples. These were the shape of the tapered header and grammage control both by slice bar position and dilution. In order to perform an optimisation, a cost function had to be defined. For the case of the tapered header the cost function should capture the departure from a uniform flow velocity CD profile. This can be i.e., the standard deviation of the flow velocity in CD. For the case of slice and dilution control the cost function could be based on grammage and/or alignment non-uniformity. The solution to the problem was obtained by standard optimisation techniques.

4.2 Tube bank

The main purpose of the tube bank is to produce a pressure drop that promotes a more uniform CD flow profile. The pulp suspension enters the tube bank through holes, which usually have an open area of about 10%. In modern tube banks, each flow channel has a step-diffuser design, which results in a well predictable separation of the flow and assures a controlled and elevated pressure drop. The step diffusers are also believed to play an important role for floc dispersion through the strong flow gradients created by the separated flow and associated turbulence generation [1].

Fortier [110] tested different tube designs regarding pressure drop using water and also studied the flow conditions in the tubes with particle visualisation.

The results can be seen in Figure 19 where the pressure drop can be seen as a function of velocity through the tubes. The different geometries are included in the figure. As can be seen the highest obtained pressure drop is four times as high as the lowest.

Hauptmann et al. [111] discussed the effect of turbulence generation by backward facing steps and wakes, and made experiments using hot-film anemometry in water. They looked at the generation and decay of turbulence and the turbulent length-scales. Comparisons of the results were made with visualisations of the flow behaviour of the jet and the conditions on the forming table.

Shariati et al. [112] numerically solved the flow through a manifold, tube bank, contraction and slice. The tubes in the tube bank had a somewhat older design with a tapered diffuser instead of a step diffuser. The results clearly showed the effect of re-circulation, which was generated by flow separation in the diffuser. Since the complete flow was solved, the effect of non-uniform flow conditions showed a strong influence in the behaviour of the flow inside the tubes depending on their position in the headbox.

Due to the rapid re-direction of the flow when it enters the tube from the manifold, flow separation is also likely to occur at the inlet end on the upstream side of the tube, immediately after the tube entrance. Since the

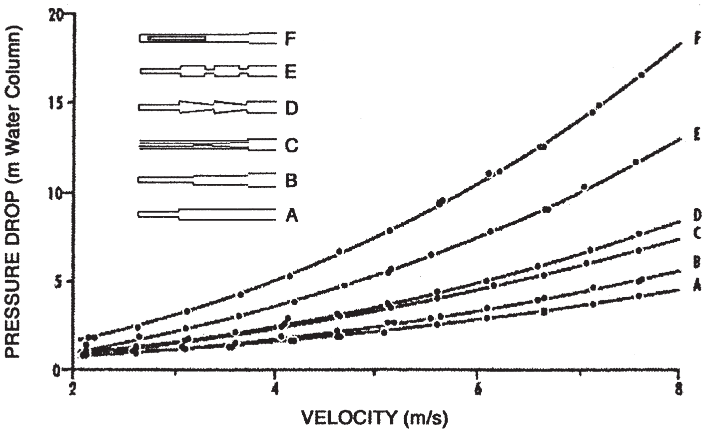

Figure 19 Tube pressure drop as function of inlet velocity for six different tube designs [110].

step-wise increase in area with its associated large-scale separation and re-circulation will generate turbulence, it will have an influence on the dispersion on fibre flocs. Also, the strong acceleration of the entrance flow into the tubes can possibly contribute to the dispersion of flocs as well as to aligning fibres in the flow direction.

However, the strong turbulence generation in the step diffuser will eventually also re-generate flocs through the strong mixing.

Karema et al. [86] presented results regarding the effect of transient fluidisation in channel flow due to a step increase in area, which is closely related to the effect of step diffusers in the tube package. Their experiments are described in section *Fibre suspensions*. The results show a flocculation minimum some distance downstream of the steps, after which the flocculation increases; see Figure 15.

In a typical design, the manifold flow towards an individual hole is not perfectly symmetrical, which can generate a strong swirl into the tube. With the flow rates used in paper manufacturing this could give a considerable effect and create strong vortices in a tube bank. Even if this can occur generically, the effect has been applied wilfully, by generating strong swirls inside the tubes in order to promote isotropy in the final paper sheet, Aidun [113]. This has been later patented [114] and is discussed further below; see Figure 23.

4.3 Headbox nozzle

In the headbox nozzle, the mix flow from the tube package is accelerated to the desired jet velocity. This will impose a pressure drop on the flow, which will even out the CD flow profile and reduce the degree of turbulence. The higher the nozzle contraction (inlet height divided by jet thickness), the better the potential jet quality.

Fibre orientation effects

A surprising effect of large headbox nozzle contraction on fibre orientation anisotropy in the paper produced was found in twin-wire roll forming experiments with TMP in the FEX machine by Nordström [115]. Twin-wire roll forming was used to evaluate headbox effects on paper properties, since it introduces the least amount of fibre rearrangement in the wire section, due to the gradual changes in dewatering pressure (however, there is not a constant pressure level as traditionally assumed; see further below). The studies were made at different mix-to-wire speed differences, but to avoid changes in headbox flow characteristics, headbox flow was kept constant and only wire speed was changed. Zero mix-to-wire speed difference was defined at the wire speed giving minimum fibre orientation anisotropy. Due to the minimum amount of shear introduced during these dewatering conditions, fibre orientation anisotropy in the paper produced should be a good approximation to that already existing in the jet.

At low and medium headbox nozzle contraction ratios (traditional for hydraulic headboxes), fibre orientation anisotropy in the paper produced behaved in the traditional way, with some increase of anisotropy at the minimum point, at increased contraction ratio; see Figure 20. At high nozzle contraction, however, very high fibre orientation anisotropy values were obtained even at zero speed difference. This indicates that fibre orientation anisotropy was high already in the jet. The logical reason for this is the strongly elongational nozzle flow. It was also found that paper formation was improved with higher nozzle contraction ratio, which indicates that fibre flocs were broken apart in the elongational flow – see further in a later section.

As stated above, headbox jet quality improves with increasing nozzle contraction ratio. It would then be a natural choice to use a high nozzle contraction ratio in all headboxes. However, since most paper and board products require a low fibre orientation anisotropy, a high contraction ratio can only be utilised for products allowing a high MD/CD ratio, such as printing papers containing mechanical pulp.

Ullmar [118,119] studied the fibre orientation anisotropy effects in a transparent headbox nozzle. A flat channel extended the slice, to facilitate optical

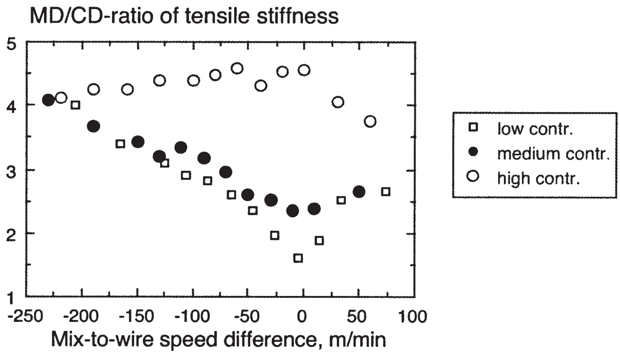

Figure 20 MD/CD-ratio of tensile stiffness for three different headbox contraction ratios during forming of TMP at different mix-to-wire speed differences [116,117].

measurements on the emerging jet; see Figure 21. A stroboscope and a video camera were used to record the fibres in the jet, and image analysis was applied to analyse fibre orientation characteristics.

Nozzle contraction ratio was varied within the range 17–50. Due to the opaqueness of fibre suspensions, it was not possible to view individual fibres more than a few mm inside of the jet surface. Therefore the majority of the experiments were performed at very low fibre concentrations. Coloured polymer fibres (comparatively straight) as well as cellulose fibres (more curly) were used. Some of the conclusions are listed below:

- For dilute suspensions the fibre orientation anisotropy is highly dependent on contraction ratio and moderately sensitivity to flow velocity level.
- At higher fibre concentration lower anisotropy is obtained compared to low concentration and higher flow velocities gives higher anisotropy.
- The effect of fibre dimensions is that stiffer fibres are more oriented than flexible fibres and longer fibres are more oriented than short fibres. Also, straight fibres are more oriented than curled fibres.

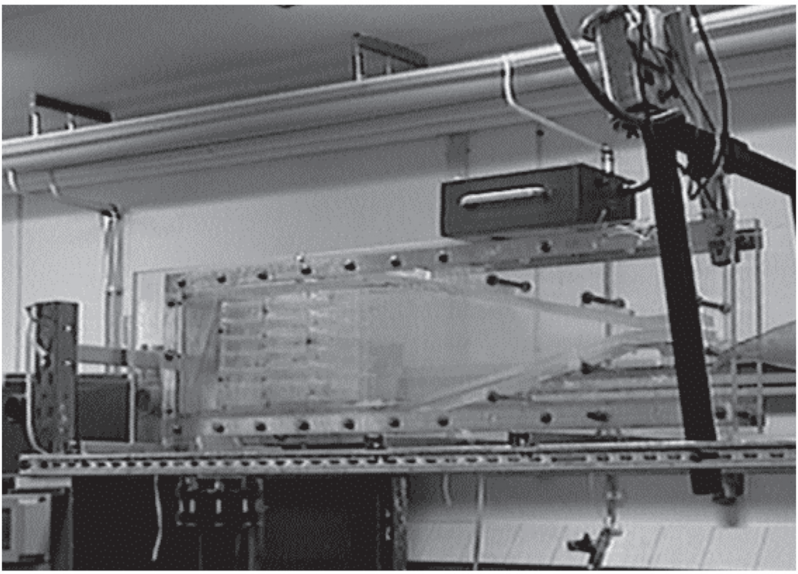

Figure 21 Transparent headbox for fibre orientation studies in the headbox jet; to the upper right: video camera and stroboscope [118].

Table 2 shows the effects when two different contraction ratios, *CR*, and two different nozzle lengths, *L*, are applied. It is assumed that the flow velocity at the slice is constant, which also means that the volumetric flow rate is constant.

Given a large contraction ratio and a short nozzle the acceleration is highest, which would give the strongest strain on the suspension. The opposite would be a small contraction ratio with a long nozzle, which would give a low acceleration and weak strain. However, the longest time is spent in the elongational flow field for the long nozzle with a large contraction ratio and the shortest for the short nozzle with a small contraction ratio. Hence, if the time spent in the contraction is of importance for the final paper sheet it is really a two-parameter problem.

Asplund [120] used the headbox in Figure 21 to study the fibre orientation anisotropy at different levels in the jet. Instead of a stroboscope, a ca 1 mm thick laser light sheet was used as a light source. In Figure 22, results are shown with a centrally inserted vane in the nozzle, ending 30 mm upstream of the nozzle end. Fibre orientation anisotropy is significantly lower in the upper lip boundary layer than outside of it. The thin vane produces approximately the same decrease in anisotropy at jet centre as the boundary layer effect, while the thicker vanes generate further disperging fluid motions.

Aidun [114] suggested a method to decrease fibre orientation anisotropy after the tube package feeding the headbox nozzle; see Figure 23. The left illustration shows an insert, which is mounted inside each tube in the tube bank. This insert will generate a strong and controlled swirl. The swirls that are generated by the different tubes are not all rotating in the same direction. The amount of tubes generating clockwise vortices is the same as the number that generates counter-clockwise vortices and the two types of tubes are arranged in specially designed patterns. An example can be seen in the right illustration where a staggered pattern is used. To obtain an overall design so that all swirls cancel each other before leaving the headbox nozzle will be a delicate task.

Table 2 Effect of headbox nozzle contraction geometries on flow parameters.

Contraction Ratio *CR*	Contraction Length *L*	Flow acceleration	Time in contraction
Large	Long	Intermediate	Long
Large	Short	High	Intermediate
Small	Long	Low	Intermediate
Small	Short	Intermediate	Short

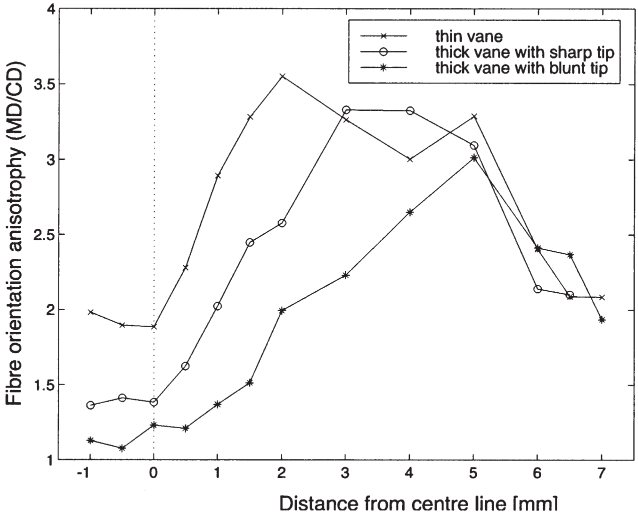

Figure 22 Fibre orientation anisotropy in the upper half of a 15 mm-thick jet. Three alternative vanes inserted: thin, thick with pointed tip and thick with blunt tip [120].

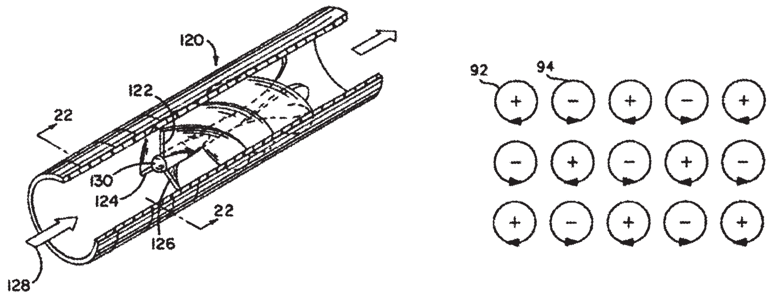

Figure 23 Swirl generation in feed pipes (Left) and rotation directions in adjacent feed pipes (Right) according to patent by Aidun [114].

Flow properties of nozzle flow

The flow through a contraction is basically given by the preservation of mass flow and since the area is decreasing the flow velocity is increasing inversely proportional to the area, i.e., an inviscid flow. The mean flow in the headbox can, with a high degree of accuracy, be described as inviscid, i.e., neither viscosity nor turbulence has any larger influence. However, even though it is not important for the mean flow, the presence of turbulence is still believed to play an essential role for individual fibres and flocs in the headbox nozzle.

In the early 1980s, Chuang studied turbulence (Laser Doppler Velocimeter, LDV) and flocculation (0.5 μs flash and Polaroid camera) in headbox nozzles [121]. He compared a plain nozzle, a triangular bump insertion and a double plate insertion; see Figures 24 a–c.

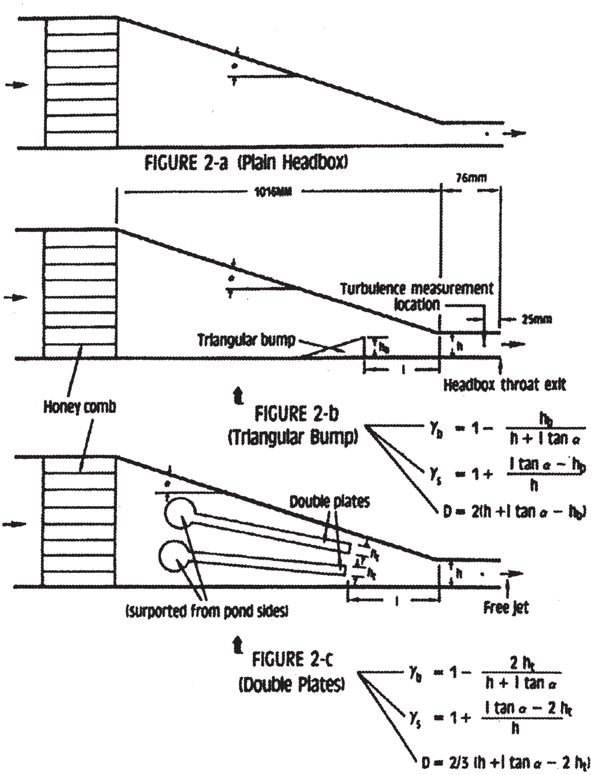

Figure 24 Turbulence generators (triangular bump and double plates) in plain headbox nozzle, and their geometrical parameters, Chuang [121].

His main results can be summarised as follows:

- turbulence level decreased with nozzle angle and flow velocity;
- turbulence level decreased with increasing suspension concentration;
- small-scale turbulence highest for plain nozzle and lowest with bump insertion;
- large-scale turbulence highest with bump inserted and lowest for plain nozzle.

Flocculation scale was largest with bump insertion and smallest with plates insertion. Shands [122] demonstrated the effect of vanes, which have been used in Beloit Converflo headbox nozzles for several decades. By landing the jet on a fourdrinier wire and recording mix surface irregularities, it was clear that vane presence was positive, i.e., they gave a reduction in surface irregularities. This is due to the damping of the large-scale flow irregularities; see Figure 25.

Farrington [123] performed simulations of the headbox nozzle flow using a commercial CFD-package. The simulations were three-dimensional (3-D) and used the standard k-ε turbulence model. One part of the investigation was to compare 2-D and 3-D simulations. He showed that the result of a 2-D simulation could differ significantly from a 3-D simulation, which is to be expected given the nature of the numerical methods. For the 2-D case, conditions have to be specified at the inlet to the headbox nozzle (exit from tube bank) regarding velocity, turbulent kinetic energy and turbulent dissipation. These values have to be estimated and averaged in MD for the 2-D case. For the 3-D case, values have to be estimated at the individual tube exits. Between the tubes conditions are given by the presence of solid surfaces. Hence

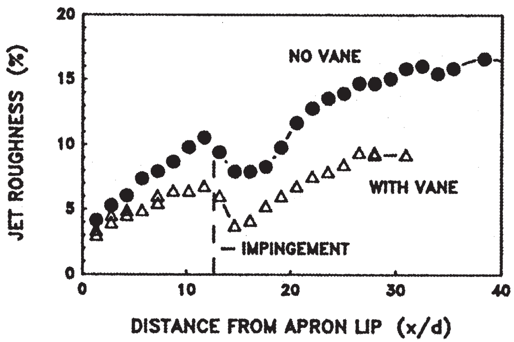

Figure 25 Mix surface roughness profiles with and without headbox nozzle vane [122].

the inlet conditions for the 3-D case are much more physically relevant. The result of the 3-D simulations was in good agreement with experiments regarding the behaviour in the contracting nozzle. However, by comparison of different figures in the article regarding the behaviour of turbulent kinetic energy, it is clear that a comparison with experimental results was not performed for the end of the nozzle contraction, where large differences are to be expected. This is discussed below.

Farrington also investigated the effect of vanes in a nozzle; see Figure 26. The graph shows the behaviour of turbulent kinetic energy and turbulent macro scale with and without vane. The kinetic energy behaves similarly in the two cases throughout the nozzle until the position where the vane ends, where a strong increase is noticed. The vane tip generates turbulence, which however decays before nozzle outlet. The vane clearly has a restricting effect on the turbulence macro scale.

Hua et al. [124] numerically solved the complete flow in a generic headbox using the standard k-ε model. The result showed clear structures after the tube bank. These gradually disappeared towards the slice. Also investigations

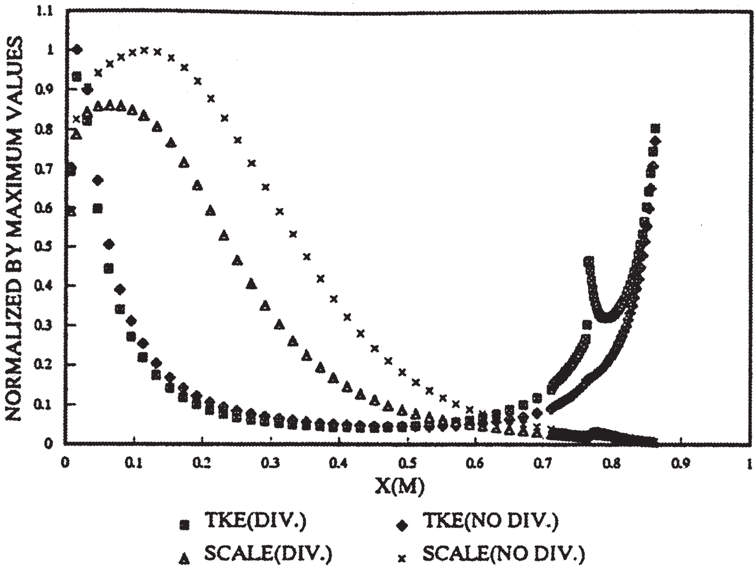

Figure 26 CFD calculations of flow characteristics with and without vanes (DIV/NO DIV) in headbox nozzle; effects on turbulence scale (SCALE) and turbulent kinetic energy (TKE) along the nozzle, X(M) [123].

aimed at a more detailed description of the behaviour of turbulence (water flow) in headboxes have been carried out [125,113,112].

Parsheh and Dahlkild [126] presented numerical and experimental results regarding the behaviour of turbulence for the case of a pure Newtonian fluid. The experiments were performed with hot-wire anemometry and air in a wind tunnel. Their results showed that the strong acceleration of the flow is of major importance and that low-order turbulence models, e.g., the k-ε model, cannot predict the turbulence in a contracting channel.

They showed that the problem originated from the underlying assumptions in the k-ε model, which is based on an isotropic turbulence assumption, i.e., turbulence is the same in all directions. The flow in a contraction is, however, accelerating and the turbulence is not at all isotropic.

This can be seen in Figure 27, which shows a graph containing both theoretical, numerical as well as experimental results. The horizontal axis represents the MD direction along the headbox contraction, given by the local mean velocity divided by the value at the beginning of the contraction. The vertical axis represents the magnitude of the fluctuation of streamwise

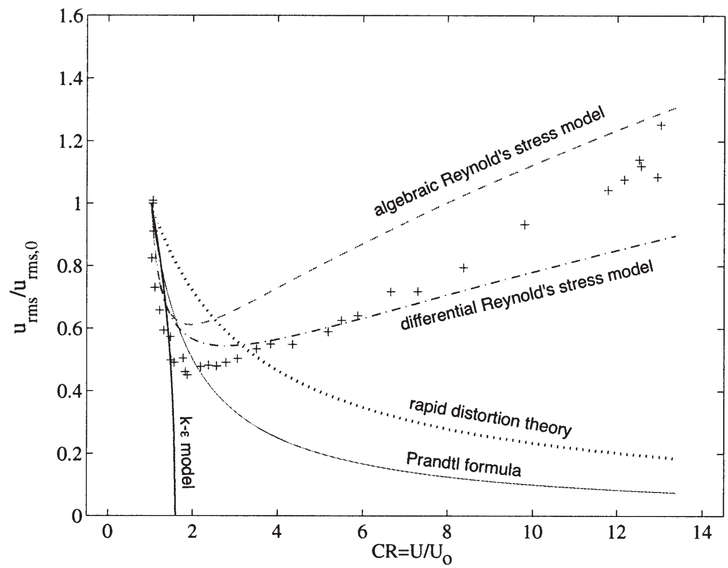

Figure 27 A comparison between theoretical and numerical models and experimental results regarding the behaviour of streamwise velocity fluctuations, normalised with inlet conditions, along a contracting nozzle; legends on the different curves are explained in Table 3 [126].

velocity, i.e., U_{rms}, normalised with the value at the beginning of the contraction. Table 3 explains the different plots.

Table 3 Explanations to Figure 27.

Designation	Method
k-ε model	Numerical
Prandtl formula	Theoretical
Rapid distortion theory	Theoretical
Differential Reynold's stress model	Numerical
Algebraic Reynold's stress model	Numerical
"+ signs"	Experimental

Boundary layer behaviour in contraction flows, e.g., effect of turbulence level and contraction ratio, has also been investigated by Parsheh [127].

Vanes and stratification

Flexible headbox vanes are often mounted in modern paper machine headboxes. These are usually present to give a more isotropic paper sheet but could also be used for stratification (layering). Layering is not uncommon for tissue grades, and is also used in linerboard production. There are strong incentives to also use it in printing paper applications.

The simulations performed by Farrington [123], see previous section, included one headbox design with flexible separation vanes, and the result was a strong effect on turbulence behaviour after the tips of these vanes. It is advisable to handle the results, i.e., regarding the mixing behaviour, with care since the turbulence model that was used cannot properly predict turbulence behaviour of the accelerating flow.

Baker et al. [128] performed experiments with headboxes aimed at stratified forming. The results clearly showed that the vanes initiated strong secondary flows. It was argued that the strong streak-creation, which could be visualised by individual colouring if the layers, is a result of three-dimensional flows after the vanes.

Lloyd and Norman performed experimental pilot machine trials aimed at stratified forming on the EuroFEX at STFI. The experiments were conducted by forming a paper sheet with a 3-layer headbox, see Figure 28a. All three layers consisted of the same stock, but the middle layer was coloured blue to visualise the layer mixing. They introduced the parameter Surface Ply Variation or SPV, see section *Paper Structure Characterisation*. Small-scale

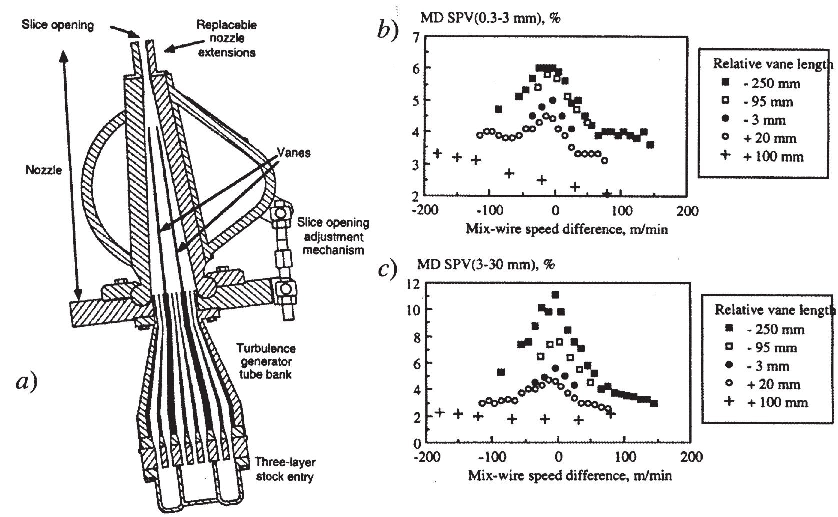

Figure 28 a) 3-layer headbox; effects of relative vane length and mix-to-wire speed on SPV (MD), b) small scale and c) large scale [129].

variations and large-scale variations were evaluated. Since these are spatial variations, the direction in which they are measured is of importance (MD or CD).

The effects of relative vane length and mix-to-wire speed difference on SPV are shown in Figures 28b (small scale) and c (large scale). Relative vane length is the distance from the vane tip to the slice, with a negative value when the vane ends inside the nozzle. Longer vanes seem to give lower SPV values both for the small and the large scales. However, tape splitting of the sheets showed that for the two longest vanes (+ 20mm and + 100mm) the flocs in all of the layers consisted of a mixture of white and blue fibres. For the vanes that ended inside the nozzle (primarily –95mm and –250mm) there was instead a clear differentiation between blue and white flocs. Hence, by changing the vane length, an optimum can be identified where the tip of the vane ends right before the slice lip, where SPV has the lowest value, without "total" mixing.

Three headbox slice geometries in combination with different vane lengths were also tested [30]. A parrot's beak slice lip was compared to a linearly converging slice lip and a plane channel slice lip. With the vanes ending inside the nozzle, the parrot's beak appeared to reduce layer mixing, while the parallel channel appeared to increase it. However, the type of slice lip had little effect on layer mixing if the vanes ended outside of the headbox; vane tip vortices then seemed to be the dominating source of mixing. The parrot's beak also improved the small-scale formation.

Finally, Lloyd and Norman also studied the effect of vane shape [130]. In one set of experiments, a 5 mm-thick vane was followed by a 0.5 mm thin-vane of different lengths, 10–40 mm. The step height was thus 2.25 mm. In another set of experiments, the steps were varied from 0.5 to 1.75 mm. The aim of the steps was to break down the boundary layers formed upstream along the vanes, and thus reduce downstream vortex generation. However, the turbulence introduced by the steps increased the layer mixing, both at floc and fibre level. This turbulence gave lower fibre orientation anisotropy, worsened small-scale formation and Z-toughness, but improved fracture toughness of the formed sheets.

Lloyd summarised the work on layering in a Tekn.lic. thesis [19].

Using flow simulations Parsheh and Dahlkild [131] numerically studied the mixing behind vanes with different tip shapes and positions. The simulations were performed with the k-ε turbulence model. The geometry was similar to that of Lloyd and Norman [129]. In the simulations, which were two-dimensional, the mixing was studied by adding a passive scalar into one of the layers. The spreading of this scalar was then studied. The shortest vane gave the lowest mixing at a relevant distance downstream in the jet. Also, hot-wire studies of mixing behind a vane in a contraction were performed by Parsheh [127].

The vanes in the headbox are not straight but will deform as a function of the flow field and the bending stiffness of the vanes. Parsheh and Dahlkild [126] modelled this problem. They developed a quasi one-dimensional model describing the position and shape of the vane as a function of bending stiffness, vane and nozzle lengths and flow conditions at the inlet. The model was compared with direct simulations using the commercial software CFX to model the flow and the position and shape of the vanes. This was performed using an iterative technique.

Söderberg [7] performed a pilot machine study of the effect of contraction on headbox jet flow, a study not specifically aimed at stratified forming. In the study the same stratified headbox as that of Lloyd and Norman (Figure 28) was used. The length of the nozzle and vane was kept constant and the inlet area was varied. Each layer in the headbox was given an individual colour. The top layer was white, the middle layer was blue and the bottom layer was red, and the headbox was mounted at the fourdrinier position in the EuroFEX pilot machine. The headbox jet was visualised at several MD positions after the slice and these visualisations were compared to the paper produced, which was scanned using an ordinary desktop scanner.

The influence of headbox contraction ratio can be seen in Figure 30. The top row is scanned paper sheets where the blue colour (centre layer) has been coded as black. The bottom row contains images showing the headbox jet at the three different contraction ratios. It is clear that the characteristics of the jet are reflected in the structure of the paper sheet. The low contraction case gives a strong mixing of the different layers, as does the high contraction case. However, the dynamics behind the mixing seem to be very different, which is obvious from the images of the jet.

Li et al. [132] studied stratified 3-layer headbox flow by an experimental technique where salt was added to the centre layer and the conductivity profile was measured across the jet thickness. In Figure 31 the left illustration shows the principle, where the central layer has a higher conductivity. Due to layer mixing there is a spreading (relaxation) of the conductivity profile downstream. The overall mixing was summarised in a single mixing parameter I_{MH}. The right part of the illustration shows some conductivity profiles along the jet. They investigated the effect of slice opening, jet speed and vane tip position on the degree of mixing. Mixing was reduced at higher slice opening and flow velocity.

Li et al. [133] also studied the mixing phenomena in a 2-layer headbox, using the same technique. In principle, the results obtained agreed with those

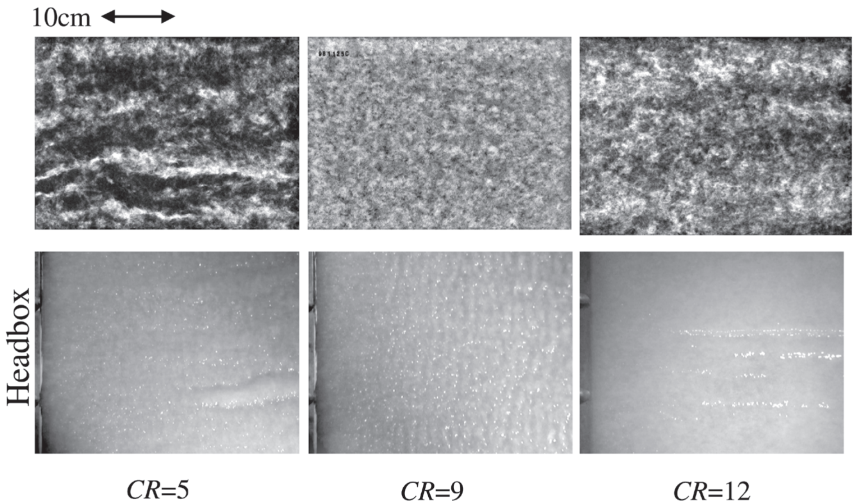

Figure 30 The effect of headbox contraction ratio (*CR*) on jet behaviour and layer mixing. Scanned paper sheets (top) and images from the headbox jet (bottom).

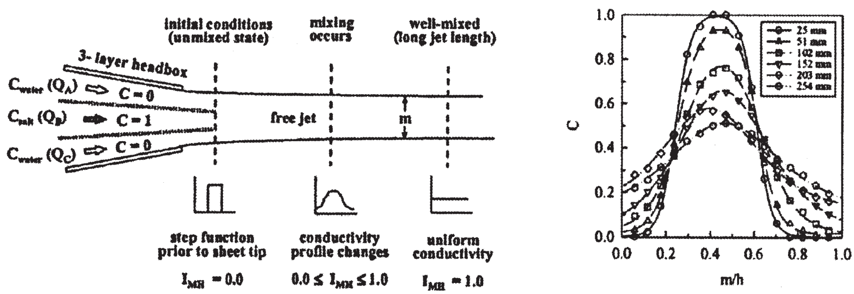

Figure 31 Conductivity analysis of a jet from a 3-layer headbox (Left) and jet conductivity profiles at 25 to 254 mm from slice opening (Right) [132].

for the 3-layer headbox. They also performed visualisations of the mixing in a 3-layered headbox using coloured water. After a comparison with the layering in the paper produced it was concluded that the main part of mixing takes place in headbox and jet, and not during dewatering.

4.4 Headbox jet and streaks

The origin of streaks in the final paper is the flow conditions in the headbox and jet; see e.g., Norman [134]. MD aligned streaks can be coherent variations in grammage, formation and fibre orientation. In the case of layered forming, it can also be streaks in layer mixing. By considering the hydrodynamics of Newtonian fluid flows, possible origins of the streamwise streaks in a liquid jet can be identified.

Four streak-generating mechanisms are illustrated in Figure 32. These are:

1. Vortex stretching, which is a result of the accelerating flow, will give vortices aligned in the streamwise direction. This is a well-known mechanism and the origin of vorticity can, for example, be the upstream conditions in the nozzle or at the exit from the tube bank, see Hauptmann et al. [111].
2. Centrifugal instabilities (vortices) in the flow, which are caused by streamline curvature, see e.g., Matsson and Alfredsson [135]. These could be so-called Dean or Görtler vortices. Robertson and Mason first proposed the existence of centrifugal instabilities in the headbox flow.
3. Streaky structures, which grow inside shear flows due to hydrodynamic instabilities could also occur at solid surfaces in the headbox, see e.g., Alfredsson and Matsubara [136].

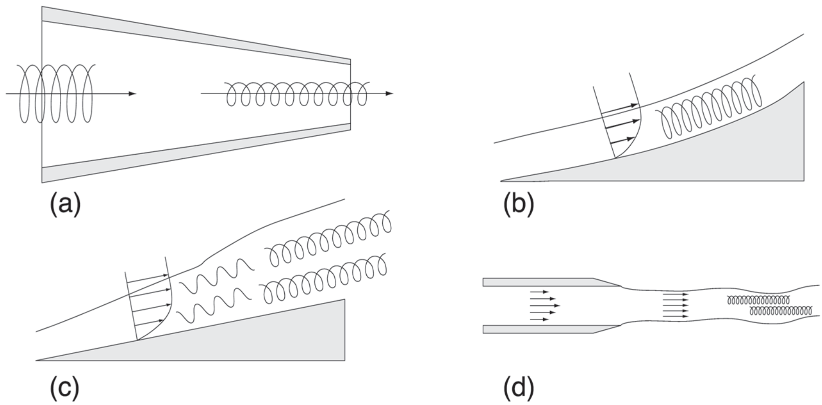

Figure 32 Streak creation mechanisms, which possibly could be present in headbox flow. a) Vortex stretching, b) centrifugal instability, c) boundary layer transition and d) wave instability [138].

4. Instability waves, which originate from velocity profile relaxation in the jet, Söderberg and Alfredsson [137]. Coupled to these waves is a break-up of the jet, which generates dominating streamwise streaks. The waves are found both for a plane water jet at low Reynolds numbers and in headbox flow Söderberg [7].

Typically the width and/or height of streaks are of the order of the shear layer thickness or the smallest size of the geometry perpendicular to the flow direction. Hence, in wall-bounded flows the origin of streaks is usually closely connected to the shear layer and thus has a size similar to its thickness. For the case of a boundary layer flow the streaks typically will have a size comparable to the boundary layer thickness and for the case of fully developed channel flows, i.e., the shear field covers the height of the channel, they will have a size comparable to the channel height.

If the origin of the streaks is not coupled to shear fields, but instead inviscid mechanisms such as vortex stretching, the flow geometry itself will set the size of the streaks. One example of this could be the flow in a nozzle (headbox), where the final vortex diameter will be of the same size as the slice thickness.

Söremark et al. [139] eliminated streaks on a paper machine by inserting a small triangular bump on the bottom wall of the headbox contraction. This small step would disrupt flow patterns (streaks) closest to the wall and due to the small height of the bump it most probably altered the flow inside the boundary layer. This method of streak prevention was earlier proposed by Chuang [121] and can be seen in Figure 24 (centre), which shows a bump mounted on the bottom nozzle wall.

Aidun and Kovacs [140] numerically simulated the flow of water inside a headbox and identified the junctions between the converging nozzle walls and the sidewalls as a source of secondary flow patterns, e.g., streaks.

A detailed experimental investigation of streaks generated by secondary flow behind vanes was performed by Baker et al. [128]. They visualised the flow patterns with Laser Induced Fluorescence and the images obtained clearly showed MD streaks as well as CD structures/streaks.

In order to investigate the behaviour of the headbox jet at elevated speeds (40 m/s) Schlupp et al. [141] performed visualisations of high-speed headbox jets. These visualisations clearly showed streaks in the jet and the images representing the jet surface were quantified regarding surface roughness scales as a function of jet speed. This only showed a weak dependence of jet speed. Experiments regarding streak generation by perforated plates, vanes and slice-lip configuration were also performed; see Schlupp [142].

Lindqvist [143] made experiments concerning the creation of streaks using water in a model headbox. The experiments were performed with Laser Doppler Velocimetry and different visualisation methods. The visualisations clearly showed the presence of large-scale structures in the flow, i.e., vortices, which were generated by the tube bank. The measurements were performed with water and showed the development of the boundary layer in the converging headbox nozzle.

In order to understand how the flow from the headbox affects the jet it is necessary to perform experiments as well as to make numerical simulations of the jet flow. For the case of free jet flows, the simulations are a challenging task since the location of the jet surfaces are not known, but are obtained as a result of the simulation.

Li et al. [144] performed 2D simulations of the jet flow from a converging nozzle.

In order to understand the behaviour of the streaks on the forming table Aidun [145] modelled the flow from the slice and onto the forming table. This included the flow of the jet. Also, the flow was quantified using high-speed imaging and image processing methods, Aidun [146]. An example can be found in Figure 33. The image is a spatio-temporal representation of the mix on the wire. The vertical axis is the same as the CD and the horizontal axis represents the time. The image clearly shows streaks in the mix surface.

In order to quantify flow visualisations of a headbox jet Söderberg [7] used image processing methods, i.e., wavelets, to capture the behaviour of the jet

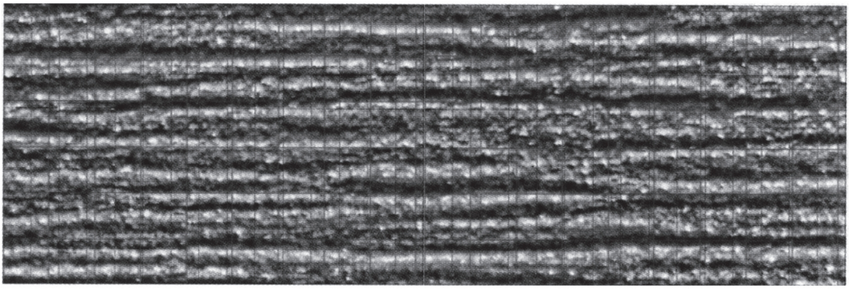

Figure 33 Spatio-temporal representation of the jet surface. The vertical axis represents CD and the horizontal represents the time.

and mix on the wire. These visualisations were performed with transmitted light as well as light reflected from the surface. The transmitted light visualisations were also used to obtain velocity distributions in CD/MD plane using the so-called PIV technique. These showed streaks also in the velocity distribution. Similar methods were used by Ono et al. [147] with the difference that they used light reflected from the suspension surface.

Söderberg and Alfredsson [138] have shown that streaks are not only originating from inside the headbox nozzle, but can be created inside the jet itself. This can be seen in Figure 34. The figure shows the flow of a plane water jet at low Reynolds numbers visualised with the so-called shadowgraph method. The velocity profile inside the jet gives rise to a hydrodynamic instability (wave instability), which can be seen directly after the nozzle exit; Figure 34a.

In Figure 34b, the velocity of the jet has been increased and the waves are present only closest to the nozzle exit. After this short region of waves, the jet experiences a breakup which partly causes a disintegration of the jet and also gives rise to MD aligned structures. These have a CD spacing larger than the waves and much larger than the jet thickness. The difference is one order of magnitude.

Figure 34c shows a close-up of the break-up and the streak generation inside the jet, which is visualised using reflective particles seeded into the water. These particles are flat and thus they tend to orient with the shear in the flow. Before the break-up the particles cannot be seen at all. This indicates that there is no strong orienting shear before the break-up. After the break-up clear white streaks can be seen, oriented in the MD direction and thus implying an onset of strong shear, i.e., streaks.

Figure 34d shows a particle visualisation at the same jet thickness and speed as in Figures 34bc. However, the nozzle is in this case formed as a slit and the flow can be described as inviscid. The viscosity is then negligible and boundary layers are not present.

The MD streaks seen in this image originate from within the nozzle and are an effect of the vortex stretching mechanism, and the strong acceleration tends to increase the strength of this vorticity and thus creates MD vortices.

This wave instability has also been shown to be present in full-scale headbox flow, with water as well as with pulp suspensions; Söderberg [7]. In this investigation, images taken of the jet were evaluated using a Morlet wavelet transform; see Figure 35.

The transform is applied in MD. For one individual image (left) the wavelet map is processed along 0.5 mm-wide MD-strips. The wavelet maps are then averaged over all strips, which gives a spatial mean wavelet map. Further, in this map all peaks along the wave number axis were recorded to form a peak

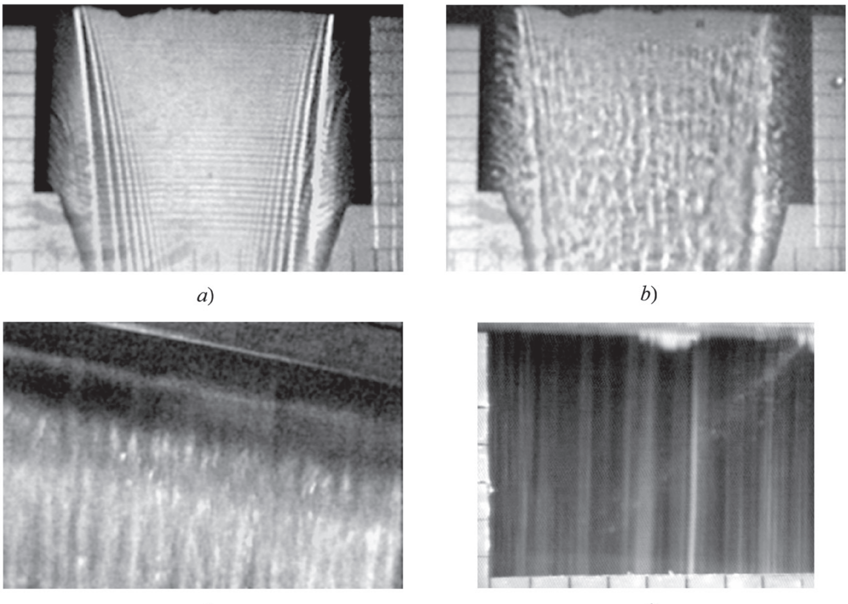

a) *b*) *c*) *d*)

Figure 34 Visualisations of a 1 mm-thick plane water jet. a) Shadowgraph, channel jet at 1.5 m/s, b) shadowgraph, channel jet at 2.0 m/s, c) particles, close-up, channel jet at 2.0 m/s and d) particles, slit jet at 8.0 m/s.

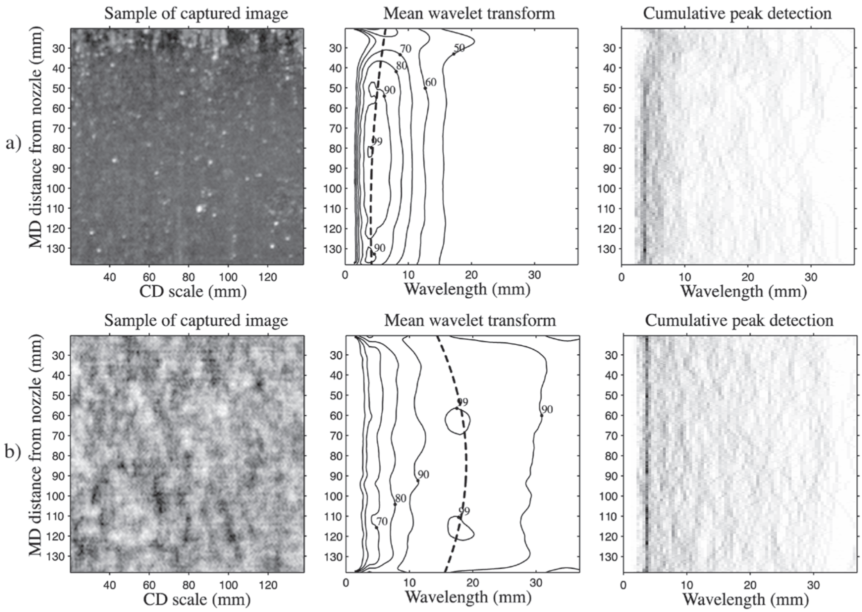

Figure 35 Left to right: Images at 5 m/s using reflected light, mean wavelet transform and cumulative peak detection; a) water jet and b) mix jet with 0.35% softwood fibres.

event map. Finally, for both wavelet transform and peak event map averaging was made from a sequence of 50 images.

The mean wavelet transform map (centre) gives an indication of the dominant structures, while the cumulative peak detection map (right) shows sub-dominant behaviour with high probability (could also be called peak probability map).

The result, which can be seen in Figure 35, represents a jet velocity of 5m/s and the top and bottom graphs are given by water and pulp suspension respectively. The visualisation in this case is aimed at larger structures in the flow; hence the image of water jet (top) does not show any presence of waves. The top of the image is at a MD distance of 20 mm from the headbox and the jet break-up can be seen. The white dots in the image are a result of this jet break-up. If velocity is increased more dots will be visible.

The dots were, by visual inspection, found to be drops leaving the jet surface as a consequence of the strength of the break-up. A ridge in the mean wavelet map with a maximum at ~4 mm can be clearly seen, which can be a result of both the waves and the drops. It is also present in the cumulative peak detection map.

The three graphs in Figure 35b show the flow of a fibre suspension at the same parameters. In the image of the jet the fibre suspension (flocs) can be clearly seen. Waves are present in this image, but are very hard to observe. However, at higher velocity they could be clearly seen. The contour plot shows a maximum at a wavelength of ~20 mm, which is given by fibre flocculation and in the peak map a maximum is found for wavelengths ~4 mm, which is a result of the surface waves.

A short note on turbulence and the flow properties of a fibre suspension

The rheology of a fibre suspension is extremely complicated. For low pipe flow velocities, pulp flows as a plug. When the flow rate is increased the shear at the walls causes disruption of the network close to the walls into network fragments (flocs) and/or fibres. This state is often referred to as turbulent, but in order to prevent confusion with turbulence in an ordinary fluid, fluidised could be a better term. The fluidisation can be both at floc level and at fibre level. The centre plug is gradually broken up as the pipe flow velocity is increased, and finally the flow could be completely fluidised.

This does not necessarily mean that turbulence appears in the same manner as for single-phase linear (Newtonian) fluids. For these, turbulence is characterised by a continuous spectrum of scales in the flow, ranging from the most energetic large scales to the smallest micro scales where energy is dissipated into heat by viscosity. If fibres are added, non-linear effects start to appear and the apparent viscosity will depend on the flow conditions. Due to the fibres and flocs the available scales are fewer and the spectrum is not continuous. The smallest scales are most probably of the same size as the fibres, since the presence of the fibre will suppress scales in the flow, which are smaller than the fibre size. Fibre flocs will also limit the scales, since the flow within a fibre floc will probably not be turbulent (due to the small velocity difference between the floc and fluid).

The dissipation of turbulent kinetic energy within the fibre suspension will also differ from the case of a single-phase fluid. It has been demonstrated that strong agitation of a fibre suspension generates network strength. Hence energy is transferred from the larger scales into the fibre network, where some energy will dissipate through fibre-fibre friction. The discussion of the flow in a headbox can be performed using the word turbulence, if turbulence only implies a non-deterministic, i.e., chaotic, behaviour of the fluctuations. Due to the presence of fibres and fibre flocs, this turbulence will however not have the same characteristics as turbulence in a Newtonian liquid.

A "true" Reynolds number $Re = ud/v$ cannot be calculated for a fibre suspension flow since viscosity is not well defined. An approximation can always be made using a suitable apparent viscosity. Such an estimate will give a viscosity of the fibre suspension, which easily is one order of magnitude higher than the viscosity of water. Therefore, results obtained at low Reynolds numbers using Newtonian fluids can also be relevant for flows of fibre suspensions at higher velocities. If, for example, pure water is considered to be the fluid in the paper manufacturing process $Re \sim 10^5$ but for the model experiments performed by e.g., Söderberg and Alfredsson [138,148] $Re \sim 10^3$. The effect of Reynolds number may still be a second order phenomenon when compared to the presence of fibres and fibre flocs, which will have a strong influence on the liquid behaviour.

As already mentioned in the section *Fibre suspensions*, the break-up of fibre flocs has historically been considered to be promoted by turbulence. It is, however, more likely that the best way to disperse fibre flocs is by elongational flows. Duffy and Norman [50] proposed this and performed experiments with different types of contractions in a cylindrical geometry. The result showed floc break-up for TMP pulps but not for chemical pulps. Corresponding results were obtained in the PhD thesis by Nordström [115]. Using an increased elongational headbox nozzle flow, the formation of twin-wire roll formed paper was significantly improved for TMP pulp, but not for chemical pulp.

5 WIRE SECTION DESIGNS

5.1 Roll-blade dewatering

During the late 1980s, partial roll forming followed by suction shoes had been introduced for new printing paper machines. Together with the opposite alternative, initial suction shoe or blade dewatering followed by roll dewatering, these were expected to dominate newsprint machines in the US during the 1990s [149].

During the 1980s, Dörries had developed a new twin-wire design for board making, with fixed blades on one side, and adjustable blades on the other side of the wires [150]. Voith, who bought Dörries, continued to apply the design to different board machines as the D-former. Ahlström later produced an identical design in their Alform MB former. Although this was a clear patent infringement, Voith did not object, although they later declared that this has been a mistake. Two backgrounds made an influence: Firstly, it was initially not their own design; secondly, the basic principle for dewatering with this former was not well understood at the time. Eventually Valmet acquired Ahlström, and their former became the "Valmet SymFormer MB" unit.

The D-former was initially considered to generate a gradually thinning space between the wires, through a gradually increasing force applied to the bottom blades along the forming zone. This was supposed to make it possible to gradually increase the dewatering pressure along the fabrics. In a presentation at the1989 Cambridge Symposium [1] it was explained for the first time that instead of the gradually increased dewatering pressure suggested by Dörries, a pulsating pressure was instead generated, by a zigzag movement of the wires between top and bottom blades.

It was further suggested that the Dörries principle could have broader applications:

> The new principle has been applied to board making. It seems to have a large potential also for high-speed papermaking. [1].

This basic principle of pulsating dewatering according to Figure 36 was adapted in combination with roll dewatering in the STFI-Former. This was initially presented at the PIRA Conference *New technologies in multiply and*

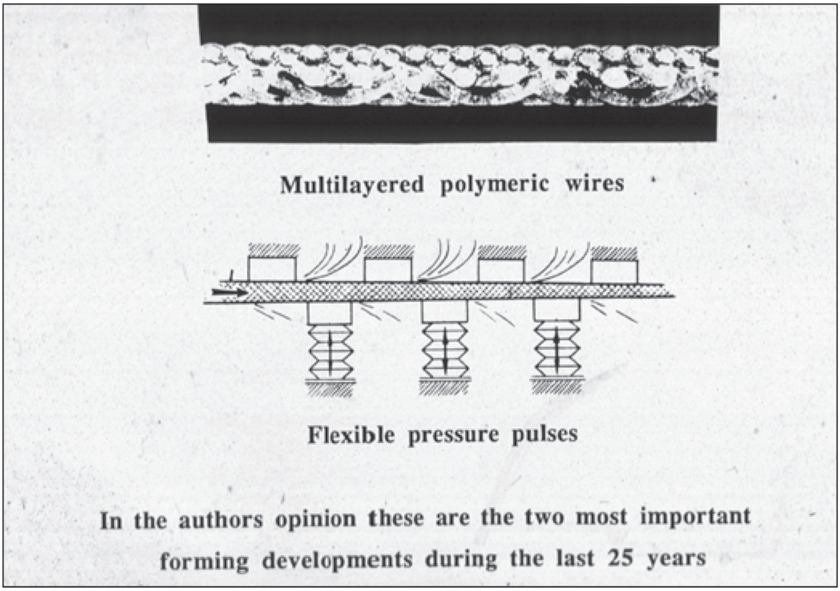

Figure 36 Concluding slide from 1989 Cambridge Symposium [1].

multilayer structures, one week before the start-up of the STFI-Former on the EuroFEX pilot machine in June 1991 [151]. After some initial roll dewatering, the fabrics were guided vertically upwards. Fixed blades were mounted along the vertical tangent to the forming roll, against which the inner fabric was run. On the opposite side, adjustable blades were mounted in a zigzag manner; see Figure 37 [152].

In twin-wire forming, it is important to arrange the dewatering in a way allowing automatic fabric position adjustment at changes in fabric separation (stock quality or production changes) without significant changes in dewatering pressure events. Therefore, the adjustable blades were mounted against the movable outer fabric, and not against the inner fabric, the position of which is initially defined by the forming roll surface.

One of the important development aims for the STFI-Former was three-layer forming, and the idea was to form the outer layers during gentle dewatering over the forming roll. This was followed by formation improving pressure pulses that could break apart fibre flocs still remaining in the middle layer.

It is important that all stages of dewatering are symmetrical, which is the case when a suitable vacuum is applied at the roll surface and when the blades are mounted symmetrically on both sides of the fabrics. The amount of roll dewatering could be controlled by an adjustable cover angle along the

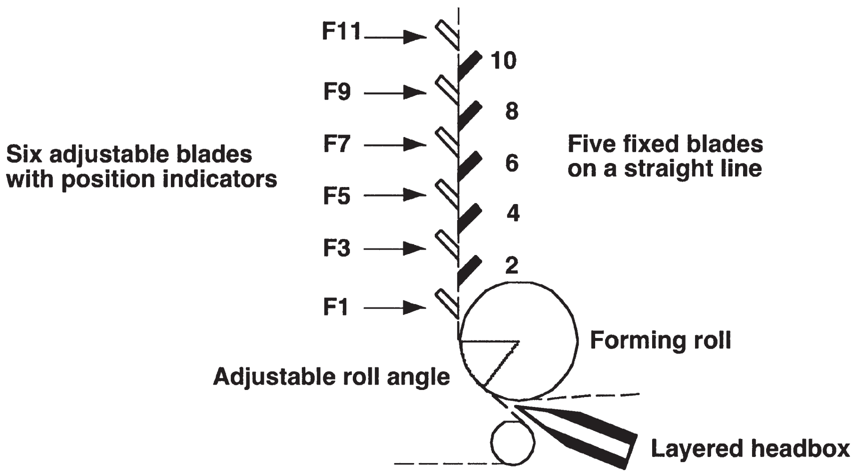

Figure 37 The STFI-Former with symmetrical roll dewatering followed by symmetrical blade dewatering with adjustable blade forces $F_{1–11}$.

forming roll, and the individual blade pressure pulses could be controlled by blade force adjustments.

One principal difference between pure roll dewatering and roll-blade dewatering is the situation when the fabrics leave the roll. In roll-blade dewatering, contrary to what is the case in pure roll forming, there is still mix left between the two partially formed webs when the fabrics separate from the roll surface, and the dewatering pressure disappears. This pressure drop will cause an increase in mix velocity [153], see Figure 38.

At the same time, a critical table roll suction pulse will be generated when the wires leave the roll surface. This may create a local velocity pulse as indicated in Figure 38. If this pulse is strong, and the grammage of the web on the inside of each wire is too low, sheet damage may arise. This mechanism limits how small cover angle on the forming roll that can be used in practice.

It should be pointed out that in reality, the mix velocity during the roll dewatering phase will not be generated by the long, constant amplitude pressure pulse indicated in Figure 38, since the pressure build-up along the roll is much more gradual; see further below.

Influence of gravity will mean that the mix velocity along the vertical section at an average speed of 1200 m/min will decrease by nearly 60 m/min for 2 m increase in height level.

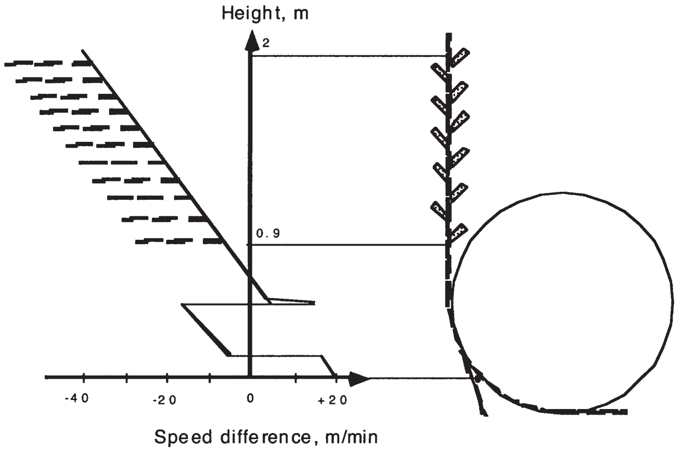

Figure 38 Example of the variations in speed difference between mix and wires when viscous effects are restricted to thin boundary layers. Broken lines indicate blade pulses. Wire speed 1180 m/min, jet speed 1200 m/min, wire tension 6 kN/m, roll radius 0.8 m.

Voith developments

When the new Voith pilot machine in Heidenheim was started up in 1990 [154], it was set up for twin-wire blade forming, a technique which was promoted by Voith at the time [155]. At the same time the development of the STFI-Former was taking place, and thinking along the same lines, based on the Dörries patent, also started at Voith. In a patent application from August 1989 [156], a roll-blade former is one of the alternative designs; see Figure 39. However, in the patent there is no discussion of blade pressure pulses, and the wires are described to gradually converge along the D-zone (marked II in Figure 39).

Late in 1991, about one year after the start-up of the new pilot machine, a rebuild was started to what eventually became the Douformer CFD unit ("D" from Dörries) [157]; see Figure 40.

Besides the 45-degree angle against a vertical direction of the wire package leaving the forming roll, there is one major difference from the STFI-Former.

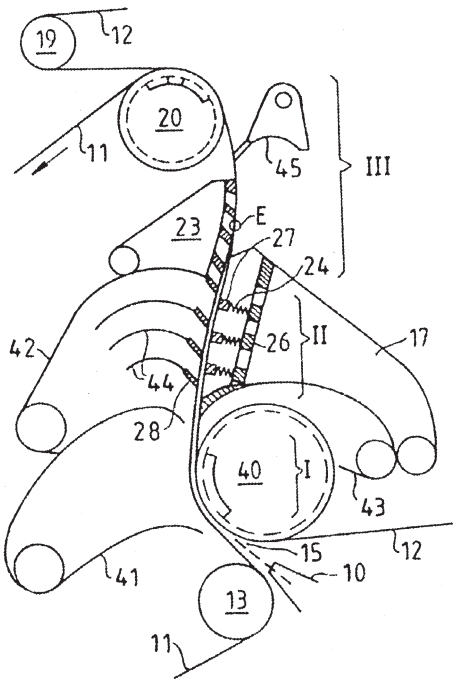

Figure 39 Voith patent of roll blade former including adjustable blades [156].

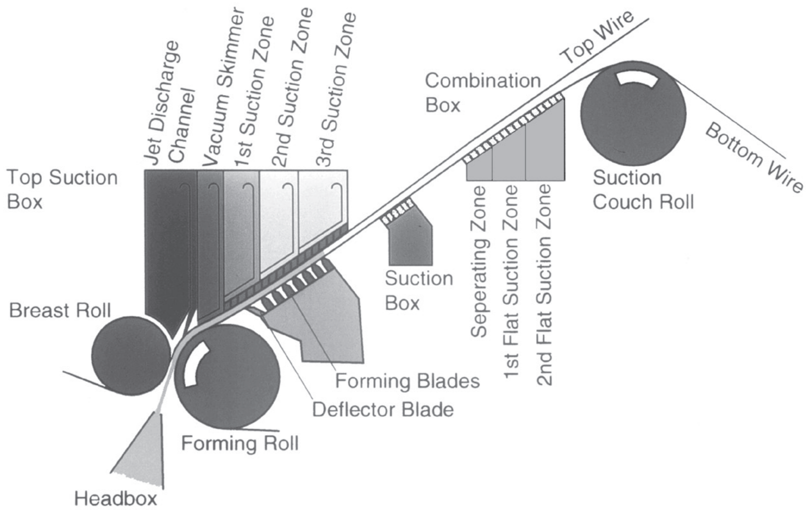

Figure 40 Roll-blade Douformer CFD forming unit by Voith with loadable blades against inner wire.

The fixed dewatering blades in the suction shoes are mounted against the outer wire.

This means that the front-end position of the first shoe should be adjusted depending on the wire separation distance, leaving the roll, if the same initial pressure pulse should be obtained. However, the shoe position is not adjusted, once the suction shoe has initially been installed according to instructions.

Application of the Duoformer CFD to printing papers indicated improved formation and retention in comparison to previous designs [158,159].

The Duoformer CFD was later modified to DuoFormer TQ (Total Quality). A main objective was to increase web dryness entering the press section, which was obtained by increasing the wrap angle of the top (outer) wire around the couch roll, and by the introduction of an extra suction box after the couch roll [160,161]. A further development is the DuoFormer TQv, where “v” indicates a vertical wire run, leaving the forming roll [162,163].

Early 2001, Moser [164] described the main Voith twin-wire forming designs, together with a discussion of important paper properties. A total number of 190 DouFormer D units were reported to have been delivered at the time.

Voith also suggested a simplified version of roll-blade forming by positioning some adjustable blades against the outer wire on a roll former; see Figure

41. This design was tested on an industrial roll former producing newsprint. A clear improvement in large-scale formation was obtained, like that with blades placed after the roll.

However, this concept breaks a fundamental rule of twin wire forming: "Never physically control the positions of both wires at any location along the dewatering section". What happened with time was a gradual increase of grammage streaks.

This was caused by the slight friction wear of the blade surfaces, which in turn generated local changes in roll-to-blade distance across the CD and thus also changes in local wire separation across the machine, causing grammage streaks. When a blade is applied against one of the wires, the opposite wire should be able to automatically adjust its position to compensate local blade surface deviations.

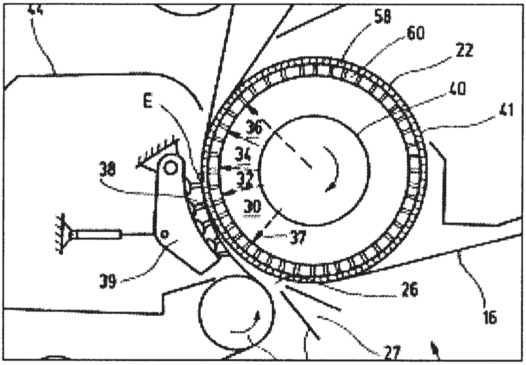

Figure 41 Adjustable blades mounted against forming roll outer wire. Voith patent [165].

Valmet developments

Valmet considered the application of the Sym-Former MB unit with adjustable blades, after some initial roll forming, and a patent was applied for in May 1989 [166]; see Figure 42.

The blade section was designed according to the Alform MB principle for Fourdrinier machine rebuilds, which Valmet had inherited in the acquirement of Ahlström. In the patent there is, however, no disclosure of pressure pulses generated by the adjustable blades; wire convergence in the zone between the stationary and the adjustable blades is described as "mainly linear".

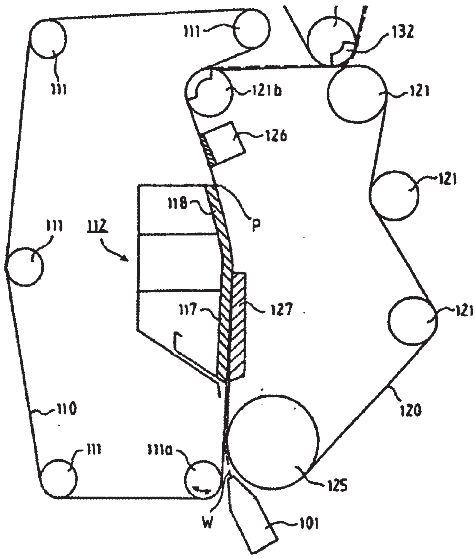

Figure 42 Roll-blade former according to Valmet patent [166]. Item “127” includes the loadable blades against inner wire. This is basically the SpeedFormer MB design.

However, serious developments on the pilot machine in Jyväskylä did not start until 1993, and in 1994 the first Speed Former MB unit was installed as a rebuild of a fine paper fourdrinier machine [167]. In comparison with fourdrinier operation, the new forming unit gave better formation, two-sidedness and sheet bending stiffness.

New installations were designed with a vertical fabric arrangement in the MB unit; see Figure 42. Like in the corresponding Voith design, the suction shoes were mounted against the outer fabric, with the inherent requirement of adjustment of the front position of the first suction shoe according to the prevailing dewatering situation.

In the latest Valmet forming section design, the “OptiFormer”, the loadable blade unit is located as close to the forming roll as possible; see Figure 43. This arrangement is claimed to minimize the time for reflocculation in the centre layer of the web, and thus maximize the formation potential.

Pilot plant tests have shown the OptiFormer arrangement to give better sheet formation than SpeedFormer MB. One major difference between the earlier SpeedFormer MB and the new OptiFormer is, however, that in the latter case, the loadable blades act against the outer wire, while they in the

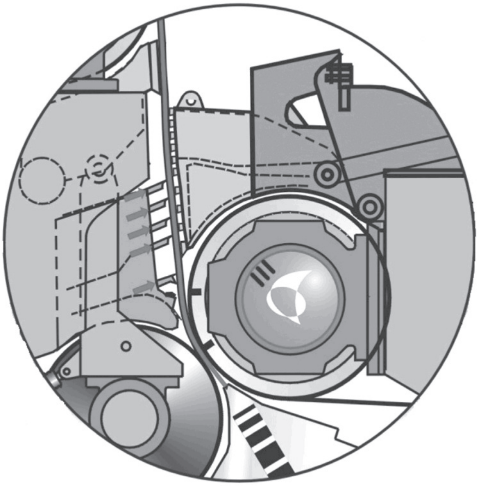

Figure 43 Forming roll followed by suction shoe against the inner wire and loadable blades against the outer wire in the Valmet Optiformer [168].

former case were acting against the inner wire. Thus the fixed blades, like in the STFI-Former (Fig 37), are now acting against the inner wire, the entering position of which is always defined by the roll periphery, independently of the separation between the two wires. Therefore no adjustment of the position of the first fixed blade is needed, when running conditions are changed. This is most probably the main reason why better formation is obtained on the OptiFormer.

Beloit developments

The traditional design of the Beloit Bel Baie machines included initial dewatering over a forming shoe consisting of nine blades. In 1995 Bel Baie IV design was presented, in which the initial dewatering takes place over three wide (ca 150 mm) blades with large radius of curvature [169]. This introduces a gentler initial dewatering in comparison with the sharp pulses over the traditionally narrow (ca 15 mm) Bel Baie blades. It can be seen as a replacement of initial roll forming, with the drawback of only one-sided dewatering as well as considerable friction against the contacting wire.

A top wire unit for rebuild of fourdrinier printing paper machines, consisting of curved, inverted suction boxes on top and pneumatically loadable blades below the wires was described in 1995 [170].

A further development of the Bel Baie IV unit is reported in 1997 [171]. An initial for Finally, in 1998, the Bel Baie RCB (Roll and Counter Blades) was developed [172], a roll-blade former of similar design as those by STFI, Voith and Valmet. According to Crouse, the roll-blade former at the Rockton pilot plant was successful in manufacturing all qualities from printing paper to linerboard [173].

However, this introduction was too late, and no order was taken before the company went out of business early 2000. During the 1980s three new newsprint machines were installed in Sweden, all three Bel Baie blade former designs. The new printing paper machines installed in Sweden during the 1990s were of the roll-blade type. The inability of Beloit to deliver a competitive forming section during the 1990s was possibly one reason for their unsuccessful business operations during the last decade.

Mitsubishi, a prior Beloit licensee, has introduced a new blade holder, with on-line control of the blade angle against the wires [174]. Some angular opening between blade surface and contacting wire on the upstream side is shown to have a positive effect on paper formation.

5.2 Multi-ply board forming

Board products have traditionally been formed from separate plies, successively couched together [175]. The ply forming can be performed using separate fourdrinier wires.

Pressure formers are still used in different configurations, and are often installed at machine rebuilds [176].

Twin-wire forming of the individual plies is applied increasingly. The Dörries principle described above has widespread use as the Voith D-former, as well as the corresponding Valmet Symformer MB design. Beloit has developed the Inverform technique [1] by the introduction of adjustable counter blades facing the inverted suction shoe [170].

Recently, also, separate twin-wire roll-blade forming units for board plies have been applied [177,178]; see Figure 44. Several of these units can be applied to add individually formed plies on top of the base ply. In principle the same former design is also applied to form the base ply [179].

6 WEB FORMING

6.1 Random sheets

The sheet formation number F_{Random} (coefficient of variation) for a sample with identical, randomly distributed fibres is determined by the square root

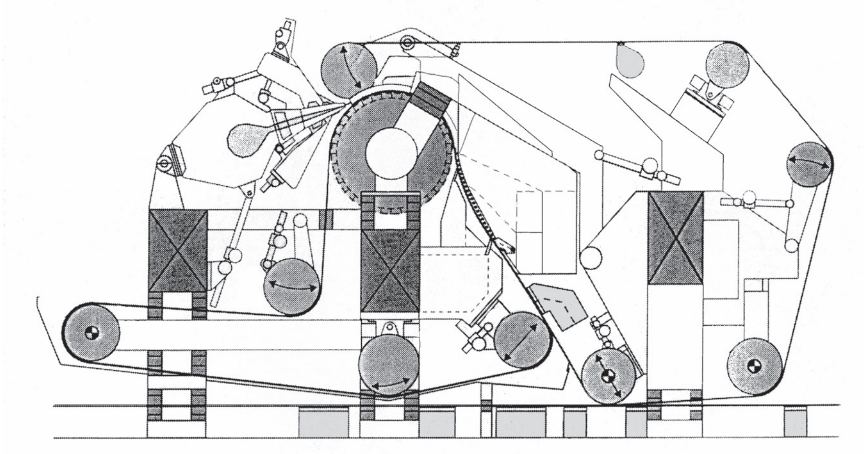

Figure 44 Top-ply roll-blade board forming design; the Voith DuoformerTop [177].

of the inverse mean number of fibres at a point in the plane of a paper sheet; see Equation 5:

$$F_{Random} = \sqrt{\frac{w_{Fibre}}{w_{Sheet}}} \tag{5}$$

where w_{fibre} is fibre and w_{sheet} is sheet grammage respectively [180].

This equation follows from a Poisson distribution of the number of fibres at any specified point in the sheet plane.

Several conclusions can be drawn from this simple equation:

- Formation number is independent of degree of fibre orientation anisotropy.
- Formation number is independent of fibre length or width.

However, if the complete formation wavelength spectrum is considered, longer fibres will mean a shift towards longer wavelengths and a more oriented sheet will give a shift towards longer wavelengths for the spectrum in the orientation direction and the opposite in the perpendicular direction.

In practice, formation is not evaluated from zero to infinite wavelength, and especially the lower limit is considerable, relative to e.g., fibre width. Therefore, when influence is found on formation levels of random sheets by fibre length or fibre orientation, this is often due to geometrical limitations of the evaluation method [20,181,182,183,184].

Sometimes the effect of fibre orientation on paper formation is evaluated. According to the above, no such general relationship exists. However, some process changes will affect both formation and orientation, but not in a unique way.

Dodson et al. attempted to model paper formation as a result of a random distribution of flocs in the fibre suspension, entering the wire section [185]. Random distributions of stars [186] and discs [187,188,189] have been suggested, but it has been pointed out that the results indicate unrealistic floc grammage levels [190].

6.2 Self-healing effects

It was suggested by Wrist during the 1960s that fibre distribution in a real paper could be more even than that of a random sheet [1]. The reason would be that there is an inherent **self-healing effect** in the dewatering process. If a hole is present in the web on the wire during the dewatering phase, the local dewatering resistance will be low, and excess fibre suspension will be dewatered at that position. Thus extra fibres will be deposited, and the overall basis weight will be evened out. Norman et al. later studied this by analytic evaluation of the formation spectrum of a random sheet and comparison with real sheets using beta radiography evaluation of well-formed laboratory sheets [1]. The results confirmed that the real sheet is more even than the random sheet in the small and medium floc size range. At larger floc sizes, the real sheet is, however, more uneven, due to fibre flocculation effects, by definition not present in the random sheet.

Sampson et al. introduced the term "hydrodynamic smoothing *s*", where *s* varies from 0 to 1 with increasing self-healing effects [191]. For laboratory handsheets formed at a range of grammage and crowding factor, *s* was found to be positive in all cases, confirming that the self-healing effect exists. Formation values at low grammage with 1 mm^2 resolution were high in comparison with random fibre distribution, indicating a locally uneven drainage resistance in the forming wire with its stabilising backing.

Norman et al. [192] confirmed that the real sheet is more even than the random sheet at wavelengths smaller than about 10 mm using up-to-date radiography analysis equipment [8], and comparing with computer simulated random sheets.

Normalised formation numbers for handsheets formed at constant concentration was shown to improve with grammage up to ca 60g/m^2, above which forming concentration had to be increased due to the limiting height of the forming vat; see Figure 45. This improvement would be a result of the self-healing effect.

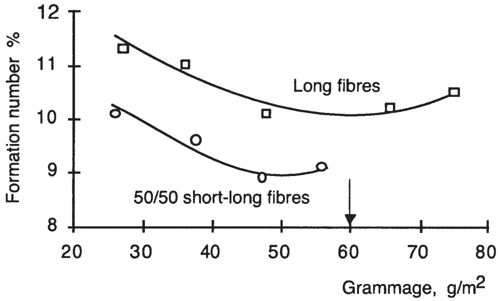

Figure 45 Normalised formation number as a function of grammage for laboratory sheets; increased forming concentration above arrow [192].

Tensile strength index increased up to 60 g/m^2; see Figure 46. Although some of the strength increase is caused by a decreasing relative influence of the less bonded sheet surfaces, the self-healing effect is thought to be a main effect.

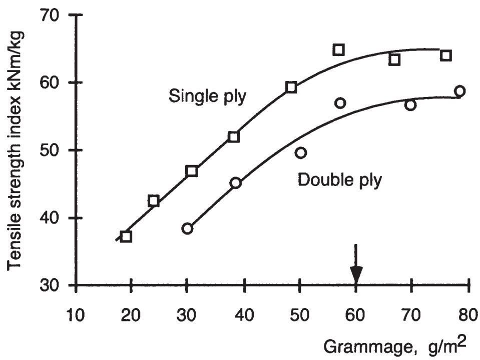

Figure 46 Tensile strength index for single- and double-layered sheets. Laboratory sheets of long fibre pulp; increased forming concentration above arrow [192].

Self-healing was further demonstrated by the comparison of one solid 60 g/m^2 sheet and one 60 g/m^2 sheet made from two 30 g/m^2 sheets couched together. The solid sheet was significantly stronger. This indicates that paper made with one-sided dewatering, due to the larger self-healing effect has a higher strength potential than the corresponding twin-wire formed sheet, which consists of two separately dewatered halves.

It was demonstrated that the normalised formation number of Formette Dynamique formed laboratory sheets improves with increased grammage. In this case, forming concentration will not increase at high grammages. It was further verified that the formation numbers are equal in MD and CD for anisotropic laboratory sheets, as predicted by equation (5); see Figure 47.

Lucisano and Norman [193] tried to avoid the self-healing effects in standard handsheet forming by extreme reduction of the dewatering velocity (4 h dewatering time). To avoid fibre flocculation and fibre settlement from gravity, the water was made viscous and the fibres naturally buoyant by the addition of sugar (60% by weight). 20 g/m^{2}sheets were formed, and compared to the corresponding sheets with normal drainage in pure water. To avoid periodic, wire generated drainage resistance effects, a flat, porous polymer plate was replacing the wire. The formation wavelength spectrum of the quasi-random sheet was close to that of a random sheet. The crossover point was at 0.5 mm, with the quasi-random sheet slightly lower at short and higher at large wavelengths. It was found that the "quasi-random" sheets had significantly lower tensile properties than the conventional sheet.

The formation improving self-healing effect was further demonstrated by free gravity draining of the suspension with sugar solution, whereby the shorter drainage time, 20 minutes in comparison to 4 hours, generated a ca 50% lower formation spectral density over the whole wavelength range.

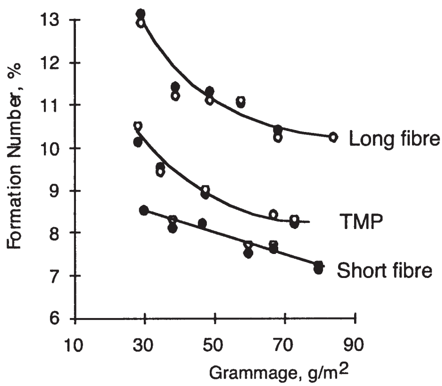

Figure 47 Normalised formation numbers measured in MD (filled symbols) and CD (unfilled symbols) as a function of grammage for anisotropic Formette Dynamique laboratory sheets of short- and long-fibre chemical pulps and TMP respectively [192].

6.3 Formation improving mechanisms

It is of vital importance that the fibre distribution in the web is as uniform as possible so that the best formation is attained. Traditionally, according to Parker [1], there were three main ways of improving the fibre distribution on the wire:

- dewatering;
- oriented shear; and
- turbulence.

It is now suggested that **four** effects are important, to improve sheet formation; see Figure 48.

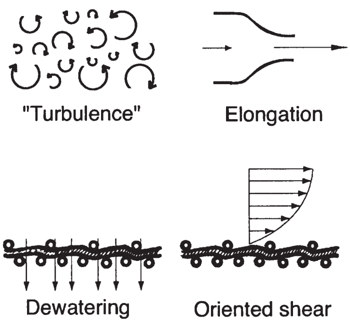

Figure 48 Principles for improving the evenness of fibre distribution in web: "turbulence" elongational flow, dewatering and oriented shear [3].

1. Turbulence in the traditional sense can probably not be present in a fibre suspension, as discussed in section *Headboxes*. To have turbulence present also during the dewatering phase would have a dominating, negative effect on the evenness of fibre deposition. It is therefore motivated to move turbulence effects to the headbox, and make sure that they have decayed when the jet reaches the wire/s.
2. Elongational flow is developed by the acceleration in the headbox nozzle, and an improvement in paper formation can be obtained using a high nozzle contraction ratio (see Figures 71–72). Possibly, formation improving extensional flow could also be generated by the flow in the headbox tube bank and by the pressure pulses in twin-wire blade forming.
3. Dewatering has a self-healing effect on local variations in grammage, as described above.

4. Oriented shear has a well-established positive effect on formation, although there is also an example where this is not the case (see Figure 72). To avoid floc rotation in a shear field, it might be important that the flocs are fixed to the surface of the forming web by the drainage forces, to improve the floc-breaking efficiency of a shear field. "Activity" on a Fourdrinier wire could be considered as shear, rather than "turbulence" effects.

6.4 Fibre deposition on wire

The geometry of the forming fabric is of vital importance for the surface structure of the sheet formed, and thus also for the dewatering capacity.

An overview of forming fabrics is given by Kilpeläinen et al. [194].

Johnson [195] studied the effect of jet impingement in a twin-wire blade former. It is pointed out that the wire on which the jet is landed has a dominating effect on the wire mark in the final paper product.

Fejér discusses the influence of fabric design on formation and paper structure with Fourdrinier and twin-wire forming [196].

Adanur [197] studied the effects of wire design on sheet properties in laboratory forming. Drainage index, fibre support index and number of yarns (MD × CD) were used as fabric parameters. Considerable influence on paper properties was reported, but to what extent this was caused by different retention levels is unknown (pulp type not reported).

Hampson [198] points out that fabric surface aperture size has to be chosen with consideration of the fibre length distribution. High fabric density at the top surface avoids channel blocking in the interior of the fabric and sheet sealing. This promotes high dewatering rates during the early phases.

Kilpeläinen et al. [199] compared different fabric designs in twin-wire forming of newsprint at speeds up to 2000 m/min. Triple layered fabrics gave 3% higher retention than double layered, but slightly lower dewatering rates. However, both fabric designs could handle the increased amounts of water brought into the former at higher speeds. Changes in fines distribution were small.

It is pointed out that the interweave pattern between the layers in a triple-layer fabric is critical, if internal wear is to be minimized [200,201].

Herzig and Johnson [202] designed a closed water flow loop in which the desired amount of fibres can be injected and a web collected on an inserted fabric, at dewatering rates similar to those during initial forming. Figure 49 shows the fibre deposition at four grammage levels. It is obvious that the fabric structure has a big influence on the surface layer of the paper. Not until a grammage of 10g/m^2 does the fibre mat reasonably cover the knuckles.

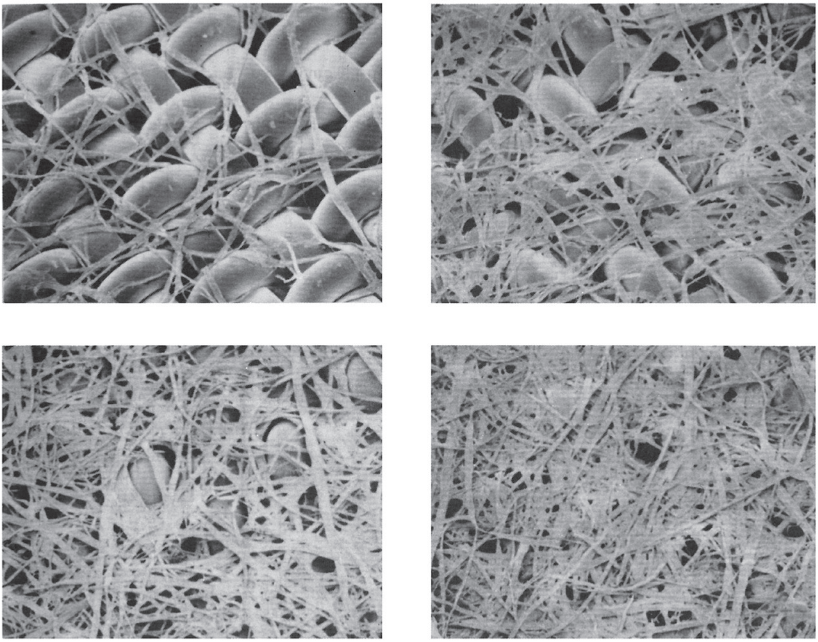

Figure 49 Fibre mat development for groundwood on a triple-layer fabric; 0.2, 4, 7 and 10 g/m² respectively [202].

They calculated the mat pressure drop using the equation

$$\Delta P_{mat} = \Delta P_{total} - \Delta P_{fabric} \tag{6}$$

where the fabric pressure drop is determined separately. According to the fibre distributions described above, there is however a high correlation between fabric openings and fibre locations, during the early stages of dewatering,. This means that a low grammage web, separated from the fabric would have a very low flow resistance, due to considerable openings in the positions where the knuckles were detached. The combination of web and fabric, therefore, give a much higher pressure drop than the sum of those of the two individual components. This was earlier discussed by Meyer [203].

Dewatering resistance as a function of velocity v is generally modelled using both the linear, viscous coefficient a and the second-order turbulent induced dynamic coefficient b, see Equation 7.

$$\frac{\Delta P}{L} = av + bv^2 \tag{7}$$

Danby et al. made several studies of the influence of the forming fabric on print quality. Initially, the different geometries of single, double and triple layer fabrics on print evenness were demonstrated [204]. Periodic marking in split sheet surfaces was evaluated. It correlated highly with respective fabric surfaces and print marking [205,206]. With consideration of the fibre length distribution, a correct choice of fabric mesh pattern (opening size and orientation) had a large effect on retention level. A computer model was also developed to predict print quality from the image of the surface layer of paper samples after sheet splitting [207].

A similar flow loop as that of Herzig and Johnson was used by Jong et al. [208]. The specific flow resistance of sheets of different grammage, formed by LWC pulp, was measured. It could be noted among their results that in the case "Closed loop Screen B", a very high flow resistance was recorded at 20-30 g/m^2, which dropped drastically at further fibre addition; see Figure 50. This might indicate "sheet sealing".

If no flow resistance were imposed by further fibre addition, the resistance curve would follow the added broken curve. In reality, the extra fibres do contribute to sheet resistance, but only to a degree corresponding to the distance from the broken curve.

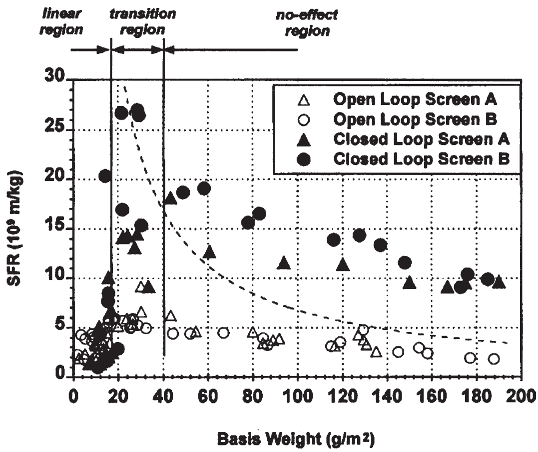

Figure 50 Effect of basis weight BW on mat flow resistance SFR for a LWC pulp (Figure 7 in [208]). Added broken curve follows the equation SFR = k/BW.

Fabric design may also be very important regarding rewetting. When the actual web build-up is finalised, web dryness is increased over vacuum boxes and couch roll. If water after this still remains in the fabric structure, a substantial part of this water is likely to be sucked back into the paper web, before and/or after its transfer to the pickup felt. Web rewetting by a single layer forming fabric was studied by McDonald [209] on a pilot machine. Samples for dryness evaluation were collected after the couch, in a grammage range of 25–88 g/m^2 using newsprint furnish. Rewetting was evaluated using the Sweet method and gave a rewet value of 55 g/m^2. This is a significant amount of rewetting, especially for a low grammage product.

Simulation of initial fibre retention by the forming fabric has been made using software developed to model the forming fabric in 3D, given the yarn and weave parameters [210,211]. The geometric probability of initial retention for a fibre is calculated based on its given length and orientation.

6.5 Wet web resistance

Sayegh and Gonzalez [212] studied the compressibility of fibre mats during drainage. A constant-rate drainage apparatus was used, and it was found that the drainage resistance increased considerably with time at a constant water flow rate. A Maxwell model was used to simulate the results. The time scale used was from a few seconds and upwards, a too long time to be of value in applications at papermaking conditions.

Vomhoff and Schmidt studied the effect of static compression on the dryness of wet webs [213]. After ordinary filtration dewatering with low filtration pressure, the wet web concentration will be in the order of 3–4%. As seen from Figure 51, web concentration will increase to above 10% with the application of a pressure of 10 kPa, a typical dewatering pressure in e.g., twin-wire roll forming. Due to the dynamic effects, it is however still unknown how much of this compression will take place in reality during a roll dewatering phase (≈ 25 ms) or a blade pressure pulse (≈ 1ms) respectively.

Jong [214] studied the compression of thick wet mats with pressures up to ca 10 kPa.

Sampson and Bridle [215] studied the flow pattern in a web using CFD. By assuming a porosity gradient in the thickness direction, he demonstrated a direction dependent flow resistance.

Sampson and Kropholler [216] modified a batch-drainage tester by introducing an electronic balance and a data acquisition system. The apparatus yielded a full batch-drainage curve, representing dewatering on the forming table to the dry line. Wet-pad concentration was evaluated to be in the range 2.5–3% for hardwood and 3–3.5% for softwood. These values were extremely

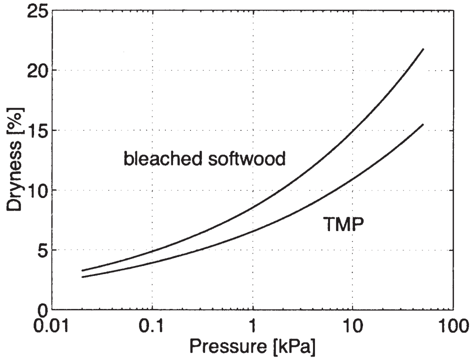

Figure 51 Web concentration as a function of static compression pressure [213].

insensitive to degree of beating and beater type. A model was presented for the build-up of a fibre mat from a fibre suspension based on the response determined in the above drainage device [217].

Mantar et al. [218] used a constant pressure drainage tester to study dewatering of fibre suspensions of chemical and mechanical pulps using 17 kPa dewatering pressure. Dewatering rate was evaluated by measurement of the drained volume. Influence of grammage (up to ca 400 g/m^2), suspension concentration (0.1–0.9%) and fines was included.

Ramarao and Kumar [219] modelled gravity drainage of pulp suspensions. During gravity drainage, pressure, concentration and filtration resistance will pass through a maximum with respect to time.

The model can be used to study drainage in conventional laboratory devices such as hand sheet formers and freeness testers.

Wildfong et al. [220] studied filtration mechanisms of sheet forming. Constant pressure filtration was generated by opening a valve to a vacuum chamber with a pressure of –6 kPa. Dewatering rate was evaluated using optical triangulation of the slurry surface. Realistic suspensions were taken as headbox samples from newsprint, LWC and fine paper operations, but since the retention values obtained were as high as 80–90%, fines content in the webs formed were over-represented. Industrial like conditions (slice opening) were used for initial slurry height. Although considerably more realistic than other dewatering experiments reported, a slow initial dewatering (acceleration from standstill) may be the most important deviation from industrial conditions with a sudden jet to fabric impact. As related above, the initial dewatering velocity may have an important influence on the build-up of the first fibre layers on the fabric surface openings. The viscous resistance coefficient *a* (Equation 7) was evaluated from the experiments. Before this, fabric pressure drop was evaluated separately and subtracted from the total pressure drop. An example of the evaluated resistance coefficient is shown in Figure 52.

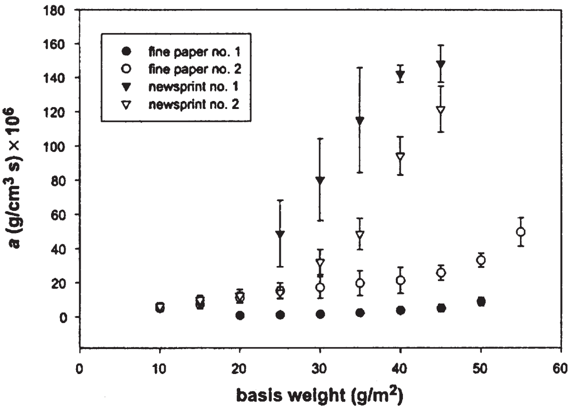

Figure 52 Viscous resistance coefficient values *a* for different fibre suspensions [220].

In a separate investigation they studied the effect on dewatering resistance of fine material and compression, which were found to be the two most important parameters influencing specific filtration resistance at increasing grammage [221].

Green et al. [222] suggested a design for a permeability cell, in which dewatering resistance can be measured with controlled shear imposed upon a dewatering event, to simulate forming conditions. A prototype not including the shear device has been tested with three different pulps and different forming fabrics [223]. The main principle is to use a fibre suspension of headbox consistency and an initial channel height similar to the headbox slice opening. A moving cylinder generates dewatering, and is accelerated and decelerated during a test sequence.

The main difference from the real dewatering situation is the gradual increase in dewatering velocity in the initial phase, compared to the high velocity jet impact on a forming fabric.

7 DEWATERING PROCESSES

7.1 Jet impingement

The jet impingement on a forming fabric is a critical part of the paper forming process, and has been studied experimentally and by modelling.

Shands [122] studied mix jump at jet impingement using linear wave theory, and experimentally using laboratory flow models and pilot paper machine trials. The experiments confirmed the theoretically suggested mechanism that mix jump can result from wave amplification caused by the acceleration changes that are produced as the mix jet lands on the wire. The effects of headbox generated turbulence, free jet length, jet speed and curvature were studied experimentally (see Figure 25).

A forming board arrangement with a radiused lead blade that can be used to control mix jump at high machine speeds was also described.

Audenis [224] modelled the impingement of a plane inviscid liquid jet on a forming fabric at different jet incidence angles. The deformability and the porosity were considered separately. The present method extends previous works in that part of the fluid is allowed to flow out of the computational domain along the fabric and a more realistic boundary condition has been applied at the porous fabric in terms of a permeability law.

Jong [214] made a numerical and an experimental analysis of jet impingement on one wire and in a twin-wire nip. Measurements were made on the Paprican pilot machine. There was a free wedge zone against one wire, also in the twin wire case before contact with the forming roll took place. Reasonable results were obtained, with roughly twice the amount of dewatering evaluated numerically in comparison with experiments.

Dalpke, Green and Kerekes [225] modelled the impact of a jet onto a flat wire using CFD software. Their main aim was to study the entrance region of a twin-wire roll former, but the initial investigation treated the landing of a jet on a flat wire. One viscous and one inertial term were used to characterise wire flow resistance. In the main part of the calculations, fibre mat resistance was neglected. Jet angle and velocity were important parameters. It was found that the main part of dewatering took place within a distance equal to the jet thickness, and that the pressure event further downstream was little influenced by the different variables settings.

7.2 Fourdrinier dewatering

Loewen and Butler [226] applied infrared laser light reflection and correlation techniques to evaluate mix surface flow velocity in a Fourdrinier section. At

450 m/min a jet excess speed of 7% was reduced to zero within 7 m (ca 1 s). It was also possible to evaluate MD and CD velocity components at jet exit.

CD velocities agreed with fibre orientation misalignment angles of the paper produced. Loewen [227] also discussed fibre orientation anisotropy and misalignment in relation to jet-to-wire speed difference and headbox edge flow adjustments.

Farnood et al. [228] used a laser velocity sensor to evaluate MD mix speed and table activity and a gamma radiation gauge to evaluate drainage profile. They studied effects of slip velocity, mix concentration and table activity on paper formation. They suggested that such equipment could be applied for on-line control of formation.

Kiviranta [229] made several studies of table activity in the Fourdrinier section, and its effect on paper formation. Initially a photo clinometric method to quantify mix surface irregularity was developed [230]. It was based on a low angle sideways incident stroboscope flash, and a recording CCD camera mounted over the wire section. Three main parameters were found to be important in characterising activity: surface roughness, correlation length and scale.

The factors affecting stock surface structure and paper formation for the middle ply of folding boxboard was studied on a pilot machine [231]. The same pilot machine was used to study the effects of mix concentration and gravity foil parameters on fine paper formation [232] and on linerboard formation [233]. These results were later also summarized [234].

The new method was tested on an industrial fine paper machine [235]. It was found that table activity should be kept low in the initial dewatering stages. A too severe activity decreased retention, which in turn automatically increased retention aid addition, generating a higher degree of fibre flocculation.

Kiviranta and Dodson [53] used the pilot machine data by Kiviranta described above, and included the Crowding factor N to replace the fibre concentration. This improved the possibilities to predict formation levels. An increase of N by 10 units corresponded to roughly 10% increase of local grammage variations, which also corresponded to the range of influence on formation by change of foils angles. The regression equations developed could describe the effect of the parameters considered within a rather wide range of operating conditions.

Foulger [236] investigated the submerged drainage concept of dewatering. The new submerged drainage box replaces the conventional low vacuum box. The main difference is that air is avoided by the use of a water filled box under gentle vacuum. An increased dewatering capacity in the low mix concentration range, 1–2%, was reported, combined with a significant increase in the retention level.

Zu and Chen [237] made a theoretical model of the vacuum generation by gravity foils and step foils. Equations were developed based on lubrication theory. For gravity foils, peak vacuum occurs at the tail of the foil, while step foils show the opposite behaviour, with peak vacuum occurring near the front tip of the foil, just after the step change. Comparisons of simulations and experiments demonstrated the validity of the proposed equations.

A new type of foil element with an undulating upper surface has been introduced [238,239]. Water is successively removed and returned, which reduces the risk for "sheet sealing", and with positive effects on retention level. The design also makes it possible to generate constant mix activity, independently of the actual dewatering rate. Sodergren and Neun [240] applied classical fluid dynamic techniques to model the interaction between the drainage surface and the slurry. Pilot trials were used to validate the fluid model. While the forming fabric does contribute to the foil surface pressure profile, the most significant input is from the shape of the foil surface.

An often-used method of modernisation of Fourdrinier machines was a rebuild into a hybrid machine, by the installation of a top-wire unit at the end of a wire section. This could be the Voith D-unit [1] or the Valmet MB-unit [241,178], both including loadable blades below the wires. Also Beloit introduced loadable blades beneath a top wire [170]. See further under twin-wire dewatering.

7.3 Blade dewatering

Bando et al. [242] measured blade pressure pulses using the capillary probe technique developed by Beloit [1]. They mainly looked at the maximum pressure peaks using 5, 9 and 18 blades respectively in a typical "Bel Baie shoe". Parameters varied were wire bending stiffness (slight decrease of peak pressure at increasing stiffness), pulp freeness (peak decrease at higher freeness) and machine speed (slight peak increase at increased speed). It should be remembered that since the pressure peaks are generated by local outer wire deflections over the blades, changes in the dewatering rate at each blade will influence local wire separation and thus pressure pulse events.

Bando et al. [244,243] also modelled the blade pressure pulses and studied the effects on dewatering. They designed a filtration apparatus, in which dewatering could be pulsated in a time of ca 15 s. In comparison with constant dewatering rate, the pulses gave higher web concentration and higher filtration resistance. The modelled pressure pulses agreed satisfactorily with those measured with a capillary probe; see Figure 53.

They also measured the outward and inward dewatering respectively and compared these with the flows based on simulated pressure profile; see Figure 54.

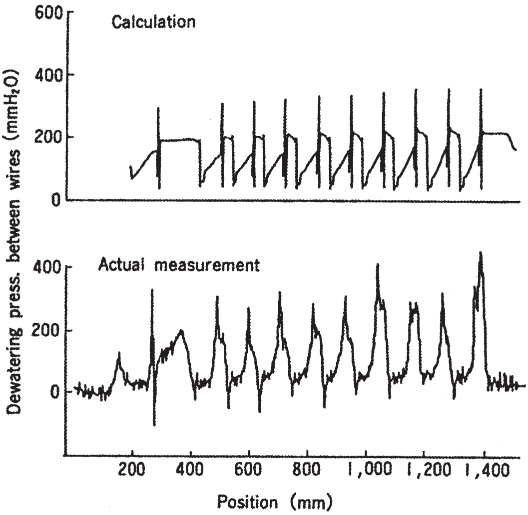

Figure 53 Comparison of pressure profile obtained by calculation and actual measurement. 9 blades, radius of curvature 5 m, speed 700 m/min and basis weight 64 g/m^2 [243].

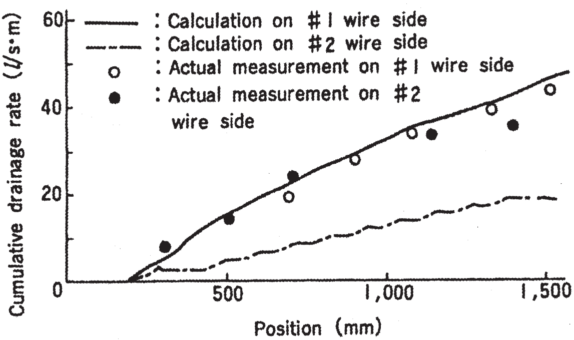

Figure 54 Comparison of drainage rate between calculation and experiment; data as in Figure 53 [243] outer wire deflections over the blades, changes in the dewatering rate at each blade would influence wire separation and thus pressure pulse events.

Since the actual inward flow was much higher than simulated, they concluded that the inner web resistance was low. This could be a result of washing out effects by the blades, similar to that on a fourdrinier machine.

Bando et al. [39] also studied the effect of pressure pulses on orientation anisotropy.

At increased jet to wire speed difference, they found that changes in anisotropy only took place in the middle half of the sheet. They calculated local flow velocity between the wires (see Figure 55), and evaluated cumulative shear factor (m^2/s) by integrating the absolute difference between wire and mix speeds along the forming section. Fibre orientation anisotropy in the middle layer increased with cumulative shear factor, but the effect of high amplitude pulses was relatively much higher than that of lower pulses.

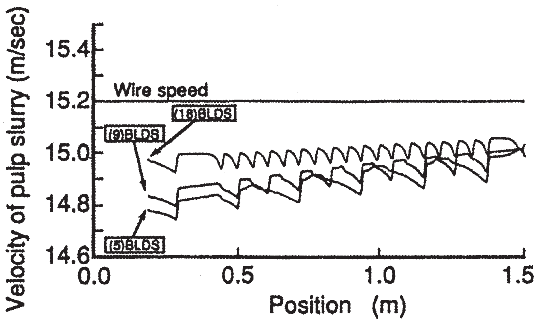

Figure 55 Velocity profile of pulp slurry between top and bottom wires as a function of distance from jet impingement position for 5, 9 and 18 blades respectively [39].

The shape of blade pressure pulses was also studied by Zhao and Kerekes [245]. A mathematical model was developed, assuming inviscid flow, a thin blade, zero wire bending stiffness and constant permeability; see Figure 56 (left). They also made experiments on the Paprican pilot machine, and measured the pressure events using tappings along a flat blade, with wire deflection over the back end; see Figure 56 (right).

Zhao and Kerekes [246] also tried to model the formation improvement generated by blade pulses. They compared formation values (NUI) in roll and roll-blade forming using a range of blade pulse amplitudes. They finally correlated the formation improvement NUI with the calculated total mix displacement due to the blade pulses and claimed a positive correlation.

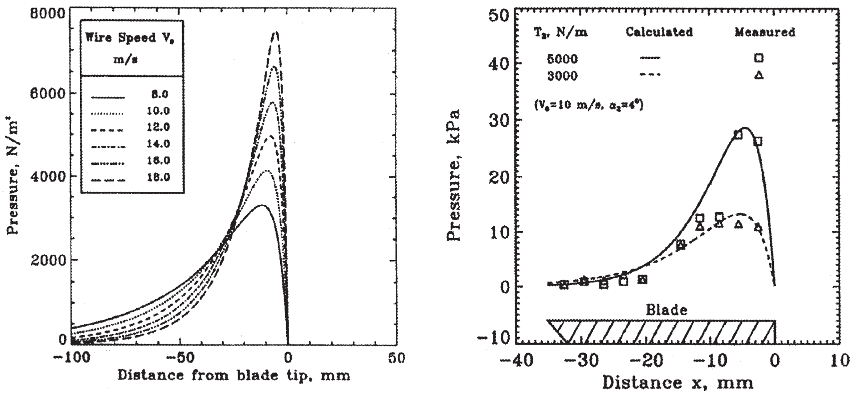

Figure 56 Left: Calculated pressure pulses at different wire speeds along a flat blade with wire deflection over downstream end. Right: Comparison between calculated and measured pressure pulses [245].

However, the spread in the data was much too high to motivate such conclusions. It would be useful to characterise also formation scale, if conclusions about the sheet forming mechanisms are to be drawn.

Nigam and Bark [247] considered the two-dimensional flow field between two wires deflected over a curved blade. The case with impermeable wires and irrotational flow was analytically solved; see an example in Figure 57.

Zahrai et al. [248] studied different aspects of twin-wire forming. Initially a two-dimensional model was applied using a thin blade, and effects of permeability and wire bending stiffness were considered [249,250]. Local suction pulses downstream of a blade were predicted. Analytical calculations were compared with experimental results from the EuroFEX machine using different blade shapes [251]; see Figure 58.

Green [252] reinvented the fact that the blade force (integrated blade pressure) is proportional to the outer wire deflection angle over a blade.

Green et al. modelled different aspects of blade related pressure events and studied:

- two-dimensional simulation of pressure pulses in blade formers [253], (like Zahrai, see above) they found a downstream vacuum pulse;
- influence of wire stiffness, inner and outer wire tensions and blade width [254];
- numeric analysis of blade pulses, in comparison with earlier analytical

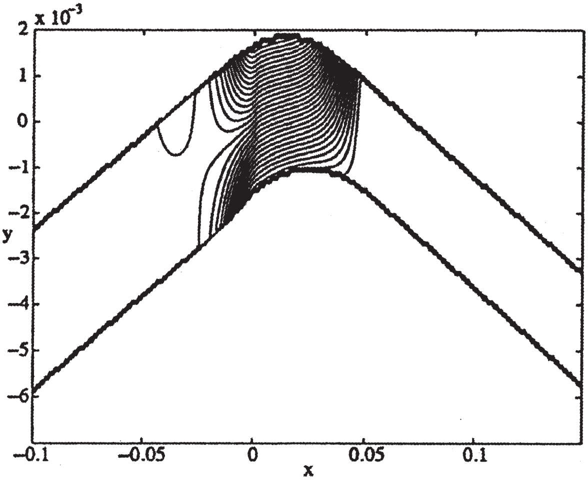

Figure 57 Streamlines for the velocity field between two wires deflecting over a curved blade (tip length 50 mm). No deflection of inner wire on ingoing and outgoing side. Scales in m [247].

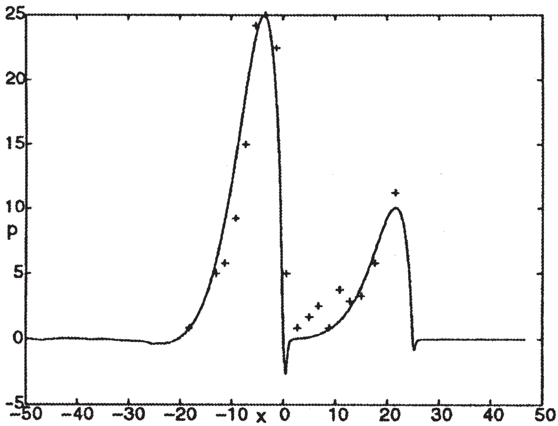

Figure 58 Fluid pressure over a 50 mm-wide triangular blade. Wire deflections at front edge: 0 deg, top: 2,3 deg and back edge: 0.85 deg. Modeling (curve) and measurements (crosses). Values on x-axis in mm and on y-axis in kPa [251].

solutions [255], the possibility to introduce decreasing permeability along the dewatering zone was beneficial;

- the extension of the hydrodynamic pressure pulse generated at doctoring of water layer [256];
- the effect of non-Darcy's law web permeability on the hydrodynamics of blade dewatering [257].

Shands and Wildfong [258] modelled the blade pressure pulses in a blade plus counter blade arrangement. An example is given in Figure 59.

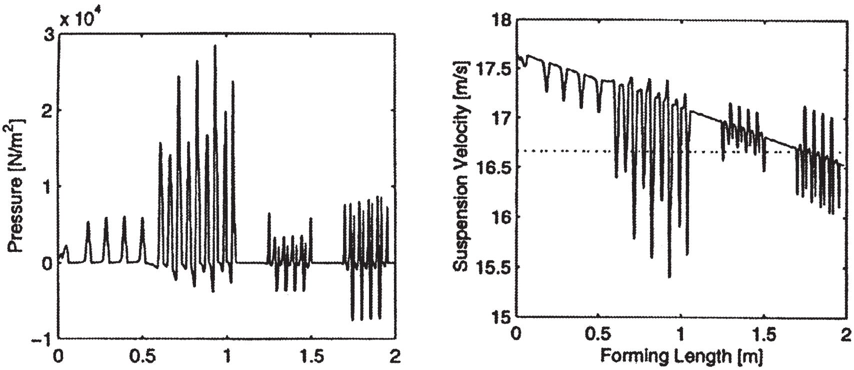

Figure 59 Modelled blade pressure peaks (left) and local mix velocities (right) in a blade arrangement with 5 initial blades followed by 4 loadable blades and 5 stationary blades. Wire tensions 6 kN/m and blade loads 0.5 kN/m [258].

Suction shoes

It was suggested by Odell, Pakarinen and Luontama [259] that when a twin wire sandwich passes over a suction shoe, the wires will be bent into the shoe openings by the suction forces; see Figure 60. The hypothetical result would be an increased outer wire deflection around blade back and front edges, which in turn would create increased pressure pulse amplitudes between the wires.

Green [260,261] made an effort to model the mechanisms of suction shoe dewatering, starting from a wire geometry as shown in Figure 61.

Roshanzamir, Green and Kerekes [262] attempted to model the suction shoe event with a two-dimensional simulation, based on the 1-D method earlier tried by Green. The argument that good agreement with the 1-D

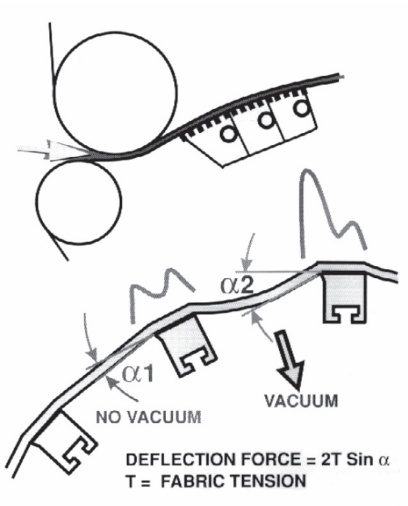

Figure 60 Hypothetical wire deformation due to suction forces [259].

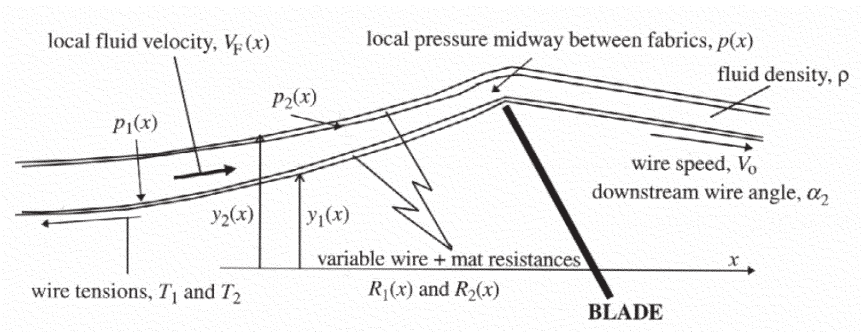

Figure 61 Hypothetical paths for two wires travelling along a suction shoe opening [261].

method lends credence also to the 2-D method does not seem convincing. Also in this case a considerable suction is predicted inside the outer web. The modelled geometry of the wire runs in the different cases treated is, however, not reported.

However, the physical model behind Figures 60 and 61 is incorrect since the force bringing down the outer wire into the opening is negligible. The wire will, therefore, travel along a mainly straight path between two adjacent suction shoe blades.

When there is still free mix between the inner and outer webs, the web on the inner wire will absorb the main part of the suction pressure, and the inner wire would bend. The free mix would then support a vacuum high enough to loosen the web from the outer wire. At a later stage, there will be one solid web between the wires, which would loosen from the outer wire due to an inside vacuum.

Suction application in the blade section of a twin-wire former will have a major effect, previously not reported, on the generation of blade pressure pulses.

In a blade arrangement with fixed blades on one side and loadable blades on the opposite side, a pressure pulses is created in front of a loaded blade. (Also about half the effect will occur at the two surrounding blades on the opposite side, but this will not be further discussed now.) The basic reasons for this mechanism is that when a loadable blade moves the contacting wire closer to the opposing wire, the space for mix between the wires is reduced. To still maintain the same rate of mix flow, a high-pressure zone will develop upstream of the blade, and that pressure zone will locally move away the opposite wire, so that the cross sectional area is mainly restored.

If now suction is applied beyond the opposite wire, the low pressure will help to locally displace the opposite wire, and thus increase the cross sectional area for mix flow. At some suction pressure level, the displacement of the opposite wire will be sufficient to let the mix pass without the help of the blade generated pressure pulse between the wires mentioned above. The blade pressure pulse will thus disappear. The applied blade load will instead be completely balanced by the local deflection of the contacting wire, which will then increase in comparison with the deflection without suction (and then increase the pressure pulses at the two surrounding blades on the opposite side).

7.4 Roll dewatering

Martinez [263] studied the roll-dewatering phase in roll-blade forming on the EuroFEX pilot machine. An example of dewatering pressure event is shown in Figure 62.

A pressure sensor at the end of a thin flexible cord is initially released into the jet (A), then into the twin-wire nip (B), and finally into the zone where the wires leave the roll, generating a suction pulse (C). It is evident that the pressure level does not reach the nominal level T/R until the final stages of roll dewatering.

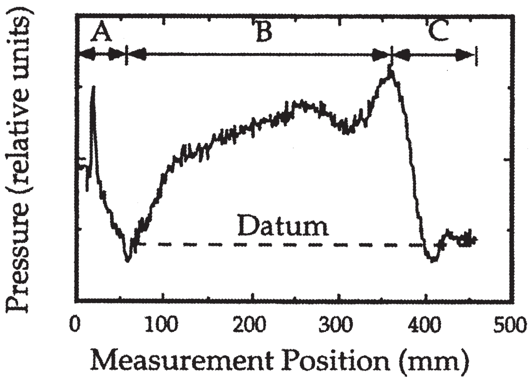

Figure 62 Pressure event in roll dewatering during roll-blade forming (trial N in Figure 63). Roll diameter 1635 mm, wire wrapping 30 deg, wire tension 8 kN/m, machine speed 800 m/min. Recorded on the EuroFEX machine in co-operation with Valmet [263].

The pressure event during the initial part of roll forming has not yet been modelled theoretically, and the local pressure minimum just before the final maximum is also so far unexplained (see further below).

Martinez developed a physical model to predict the dewatering through the two wires in twin-wire roll forming. A series of force and mass balances were applied to the web, and expressions were derived for web thickness and solidity based on fibre and process conditions. Using the measured pressure event, dewatering rates were estimated with Darcy's law. A series of experiments on the EuroFEX machines were performed, and one test was used to calibrate the parameters. The numerical solution predicted flow rates within 10%; see Figure 63.

Boxer applied modelling techniques to a roll-blade former. He modified the method by Martinez for roll dewatering, by replacing the numerical solution method by an analytical one [264]. It is claimed that with the new method, knowledge of the actual pressure event during dewatering is not required for the solving of the dewatering flow rates [265].

Zahrai, Martinez and Dahlkild [266] presented a physical model to estimate the thickness of the web in twin-wire formers with nearly constant drainage pressure. Web thickness was found to be proportional to the square root of forming distance. The constant of proportionality was related to parameters such as compressibility and permeability of the web, headbox consistency and machine speed.

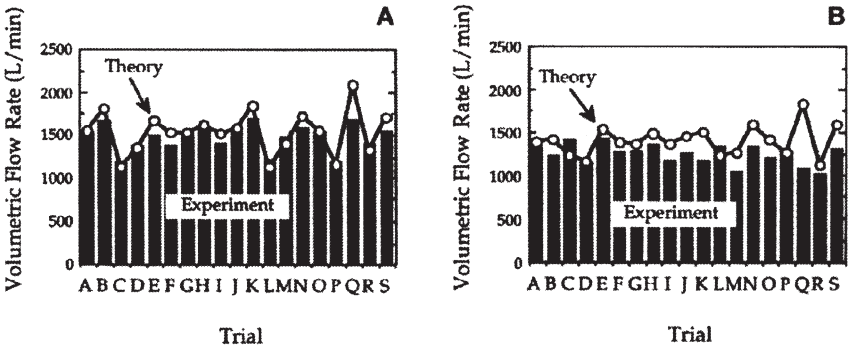

Figure 63 Comparison of the estimated to the predicted dewatering rates from both the inner (A) and outer (B) fabric [263].

Zahrai, Bark and Martinez [267] modelled the dewatering from a curved converging channel with moving walls, of which the outer one was permeable. A numerical solution was obtained with increasing wall excess speeds relative to the suspension for two fibre suspension models: one power law version and one more "fluid-like". It was shown that with increasing speed difference, the fluid-like model resulted in an increased fibre concentration of the web at the interface to the suspension, which was not the case using the power law model.

Turnbull et al. [268] developed a 1-D model for a Crescent former (roll former with one-sided dewatering) to study dewatering events, and specifically the influence of longitudinal disturbances. Despite heavy damping, the model showed significant amplification of disturbances near resonant frequency. The model predicts that 2% disturbance in jet velocity then may result in nearly 7% variation in basis weight. The wavelength for such variations approximately equals the forming roll radius.

Chen et al. [269] modelled the CD mat thickness disturbances on a Crescent former using a two-dimensional dynamic model with viscosity. The study examined the CD variations due to the influence of major classes of steady disturbances, and the coupled MD and CD variations due to dynamic process disturbances in the fluid jet. Among many results, those from unsteady disturbances show that the coupled MD and CD variations are magnified near the fundamental natural frequency of a translating wire for long wavelength disturbances.

Jong [214] made some roll forming modelling attempts and compared the results with measurements on the Paprican pilot machine. One main conclusion was that the model should be further developed before good predictions of dewatering could be expected.

In a recent overview of twin-wire forming, Malashenko [270] discussed a typical roll pressure event in a roll-blade former and commented “Prior to exit, there is an ever present and unexplained reversal in pressure . . .”. It could be pointed out that such a local minimum is also present at the end of the B-section in Figure 62.

Malashenko also stressed the importance of relative motion between wires and connected web shear to different wire tensions and running radius over rolls; see Figure 64.

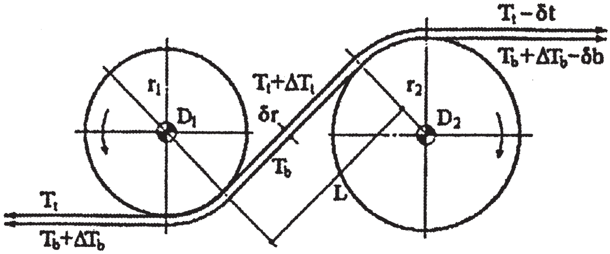

Figure 64 Differential fabric displacement and web shear in twin-wire “S” path, [270].

Wildfong et al. [271] modelled drainage during roll forming, and validated results using pilot paper machine data. Stock drainage data were evaluated according to methods described above [220,221]. Roll dewatering pressure was assumed constant, and the vacuum in the forming roll was neglected. Prediction accuracy of drainage flow was within 15% of experimental values.

A pilot plant study of roll dewatering of reslushed newsprint was made by Gooding et al. [272]. They found that dewatering comprised two main parts, one momentum driven and one tension-driven. Dewatering rates were obtained by scooping with a special collection device, and further by flow balances based on wire position estimations based on a probe recording mechanical bending of the probe assembly. No separate measurement was made of dewatering to the roll side, and the concluded values resulted in some peculiarities. Normal fabric tensions were applied, but since the roll diameter was only about half that of a modern industrial installation, the dewatering pressures were twice the normal levels. Recorded retention levels were high; for a fine fabric over 85% was obtained. Pressure events were recorded using an air purged capillary tube introduced through the headbox, and stopped at different positions along the forming zone, the same technique as that used by Beloit and Mitsubishi [242]. Pressure recordings reveal some uncertainty about the probe tip location; sometimes it seems to have been located inside the forming web.

7.5 Vacuum dewatering

Neun [273] studied vacuum box dewatering on an experimental paper machine. Different vacuum levels and vacuum slot dimensions were used, and web dryness was tested on blow samples. For a given vacuum level he found that solids content C of the web as a function of time t could be described by the equation:

$$C = b + m \tanh(ct) \tag{8}$$

where b, m and c are constants.

Figure 65 shows an example of experimental data and application of Equation 8.

He also demonstrated how a segmented dewatering curve for a set of consecutive vacuum boxes could be designed:

Follow the bottom curve in Figure 65 for the desired time. Then move left at constant solids content until the middle curve is reached. Follow the

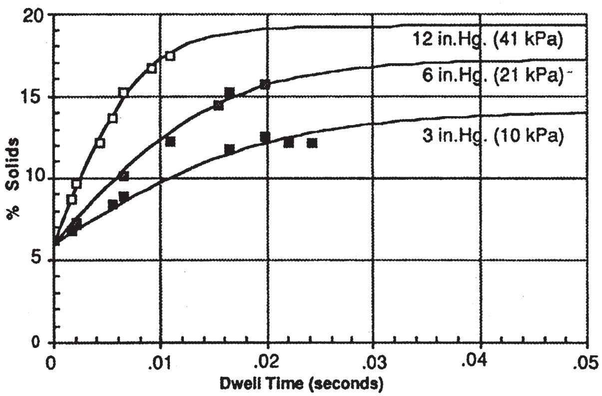

Figure 65 Web solids as a function of dwell time for flat box at three vacuum levels. The lines are drawn using Equation 8 [273].

middle curve for the relevant time period, and then move left to the third curve, etc.

By application of this principle, he demonstrated considerable potential in reductions of drag forces (fabric wear) and vacuum energy consumption through improved strategies of vacuum application, replacing traditional settings.

Neun and Fielding [274] studied vacuum box dewatering by field measurements. They concluded that corresponding laboratory results were reasonable absolute predictors. Increased grammage had an effect on slowing down dewatering rather than on achievable dryness. Furnish had a large effect, and higher temperature improved dryness.

Neun also evaluated the parameters m and c (Equation 8) for newsprint, OCC and Kraft furnish at different vacuum levels [275,276,277].

Räisänen [278,279] studied flat box vacuum dewatering using the "Moving Belt Drainage Tester", MBDT (see description below). Using this equipment, the same type of vacuum pulses are applied both during forming and vacuum dewatering.

The process was considered to be basically a wet pressing event, and the solid content C as a function of time t was described based on a first order viscoelastic model

$$C = C_0 + b\left(1 - e^{-\frac{t}{r}}\right) + dt \tag{9}$$

The linear term was added to account for the effect on water removal of the through-flow of air. The effect of different furnish parameters were studied [280] and the laboratory evaluations were successfully compared with the results for a pilot [281] and a commercial [282] paper machine respectively.

If, in fact, wet pressing is the dominating effect for water removal on vacuum boxes, this part of the process should preferably be treated together with the press section. Traditionally this has however not been the case, and therefore this part is here still included in the forming section.

The MBDT was later also used by Mitchell and Johnston [283] to study vacuum dewatering.

Shands and Hardwick [284] studied flat box vacuum dewatering on a pilot machine for newsprint at commercial speeds. Dryness increase was found to be mainly proportional to "vacuum impulse", i.e., vacuum level multiplied by dwell time. Also airflow requirements and drive loads were found to be proportional to vacuum impulse.

Jones [285] developed a dynamic simulation model for flat box vacuum dewatering using the experimental results by Neun (mentioned above). The model is based on flow through compressible porous media. What appear to explain the limitation of the flat box are the forces required to remove water from the smaller pores of the sheet. Dewatering stops at the point at which the surface tension forces in the pores exceed the applied vacuum. This can explain why solids content levels off regardless of dwell time but increases with increasing vacuum and temperature. Increased grammage slows drainage but does not reduce maximum solids content.

8 LABORATORY FORMING

Since fundamental research within the forming process performed on industrial paper machines is generally too expensive and too restricted regarding process design, means have been developed to perform such research in the laboratory. Different kinds of laboratory sheet formers have therefore been developed as well as new pilot machines for web forming.

8.1 Sheet forming

The main drawbacks with a standard hand sheet former are low forming concentration, slow dynamics, no white water recirculation, isotropic fibre orientation in the paper sheet and unrealistic fines distribution in the Z-direction. The aim has therefore often been to increase forming concentration, to make it possible to control fibre orientation anisotropy and to rearrange dewatering to be closer to a real situation. White water recirculation is however usually still missing.

Nazhad and Kerekes [286] modified a standard hand sheet former by applying agitation before drainage of a mix with headbox concentration. This means that mix height before drainage is ca 10 mm. Mixing was performed using a plastic plate with rather closely spaced 10 mm diameter holes. The plate was initially placed in contact with the upper surface of the mix and then withdrawn vertically. Depending on the desired degree of uniformity of the final sheet, 1–15 mixing actions could be performed. It is pointed out that the retention of fine material is not simulated in this procedure, and that the method therefore is only useful for determining the formation potential of the long fibre component of the mix.

Using the equipment above, Nazhad et al. [287] demonstrated that both paper formation and strength deteriorated when forming concentration increased from 0.017% to 0.5% using TMP fibres of different size fractions. Northern softwood was confirmed to give higher strength values than southern pine. The strength for all samples decreased when grammage was reduced to ca 30 g/m^2.

The BetzDearborn Pulsed Drainage Device (BPDD) was developed in the late 1980s [288]. The mix is deflocculated in a separate mixing chamber, and then released onto the forming wire. A rotating foil below the wire will agitate the mix during the drainage. Vacuum is applied below the wire, and the dewatering rate is recorded (with a short delay) by measurement of the water level at the bottom of the white water collection chamber; see Figure 66.

The BPDD equipment was later modified by Sutman [289] especially to improve its predicting capabilities regarding dewatering times. By decreasing the mix volume by a factor of four and aiming at a relevant grammage, a mix

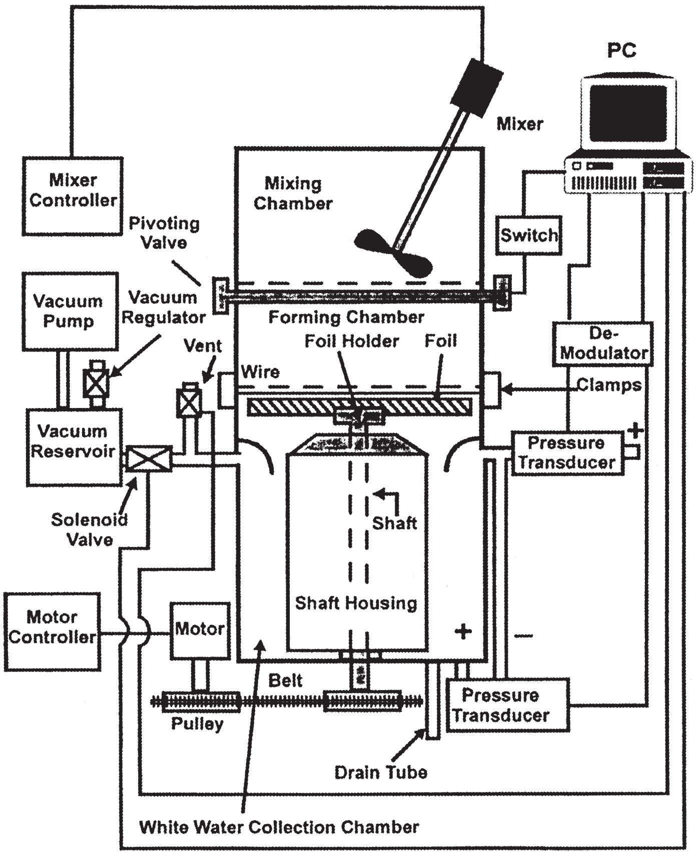

Figure 66 The BetzDearborn Pulsed Drainage Device [289].

concentration close to that in an industrial application was utilised. A coarse stainless steel screen replaced the wire, the foil speed below the screen was increased and a moderate vacuum was applied at the beginning of a test. The basic idea was to introduce more thickening dewatering, replacing the earlier filtration dewatering.

The modified device gives dewatering times close to those in reality, while the earlier design had given one order of magnitude too long times. The vacuum during dewatering is recorded, and it is suggested that the peak to equilibrium vacuum ratio would be an indicator of sheet formation, which seems to be an oversimplification.

The Moving Belt Drainage Tester (MBDT) [290] is another device developed to study dewatering under process-like conditions, especially the final vacuum dewatering stage (see above); see Figure 67. The basic principle of the MBDT is in principle similar to that of the BPDD. However, the

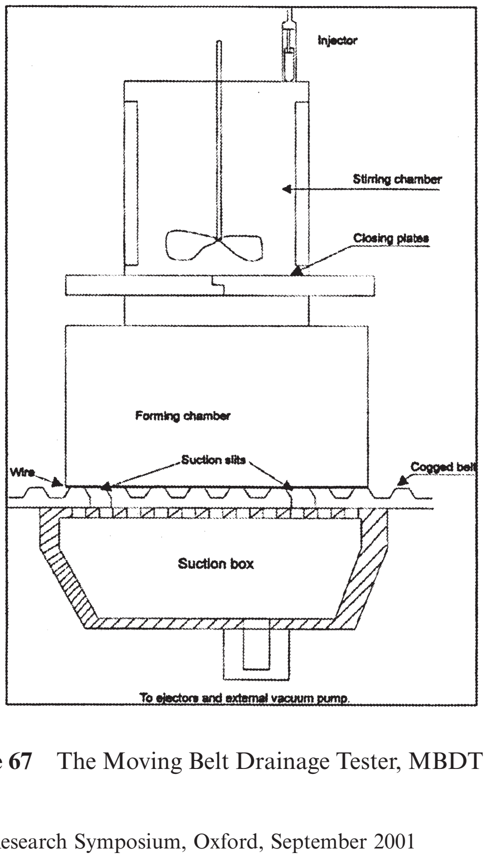

Figure 67 The Moving Belt Drainage Tester, MBDT [290].

agitation during dewatering is performed with a cogged, endless belt, which is run below the wire. The geometry of the cogged belt and its running speed will control the mode of agitation. It has been applied for the study of wire section dewatering, including the use of retention aids [291,280].

Xu and Parker [292] developed the MBDF former, a variety of the above former. Instead of dewatering studies, the main aim was to study forming effects on sheet properties. At increased forming concentration formation deteriorated, and the accompanying effect on paper mechanical properties was low for short fibre pulps and significant for long fibre pulp.

Helmer et al. [293,294] have developed a system for the forming of anisotropic hand sheets. The mix is delivered from a headbox, and flows across a wire-covered vacuum box; see Figure 68. The sheets produced are of considerable size, 260 × 320 mm^2. Typical running data would be slice opening 10 mm, mix concentration 0.5%, and jet velocity 30 m/min. A typical tensile stiffness index anisotropy obtained would be ca 1.8.

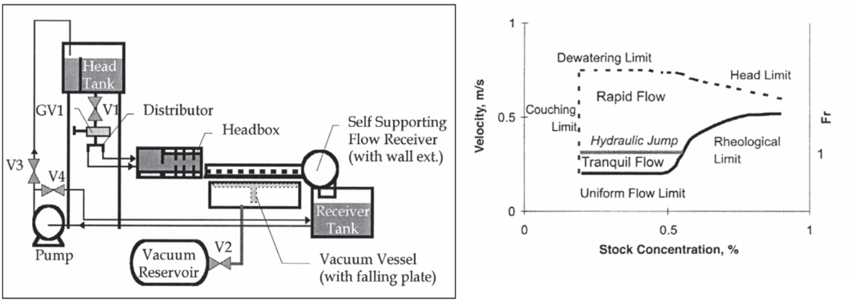

Figure 68 The University of Melbourne stationary wire laboratory former [293] (Left) and operation limits at constant depth and vacuum [294] (Right).

For the channel flow on top of the wire, the Froude number *Fr* has significance, with

$$Fr = \frac{v^2}{gd} \tag{10}$$

with v flow velocity, g gravity factor and d mix height.

The application of the new former has so far concentrated on paper formation and anisotropy – other paper properties have not been reported.

Sivén and Manner [295] designed a high-speed retention tester, the HSR-Tester, based on a moving headbox and stationary twin-wire arrangement. Inside the inner wire, drainage foils are mounted on a radius defining the inner wire radius, and the set-up is rotated at ca 5 r/s. Outside of the inner wire, the likewise stationary outer wire is tensioned. In between, the headbox is placed, and when a sheet forming event is started it is retracted at ca 90 m/min along a half-circle formed track, leaving the mix mainly stationary to be drained through the two wires with the foil pulses agitation from inside. The quality of the paper regarding formation and mechanical properties are not reported so far. Its main aim is to study retention as a function of retention aids addition [296].

Hammock and Garnier have developed a laboratory apparatus simulating industrial twin-wire forming [297]; see Figure 69. The headbox width is 160 mm. The forming roll (diameter not specified) surface has 2×2 mm^2 grooves separated by 1 mm-wide ridges, to allow also inwards dewatering. After the roll fixed blades on both sides and vacuum boxes bring final sheet dryness up to 8–10%, which allows sheet sampling. The mix is pumped from a 400 L reservoir, and bypassed back to the reservoir via a three-way valve before and after the trial. Trial time is within the range 5–50 s. In a typical trial slice opening was 4 mm, wire speed 320 m/min and mix consumption 140 L.

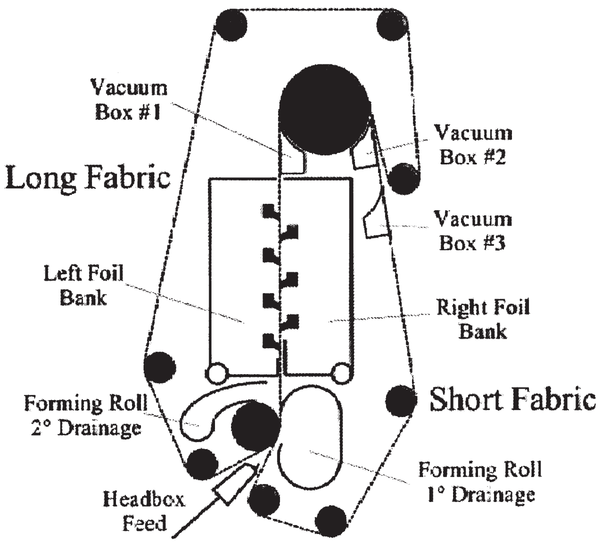

Figure 69 McGill roll-blade twin-wire laboratory sheet former [297].

It should be pointed out that in most laboratory devices described and forming experiments reported, except for those in industrial systems and in the EuroFEX system, a fibre suspension with the same composition as that of the furnish is used. This means that it is not representative for a realistic headbox mix, in which components with low retention are over-represented due to the recirculation from the short and long circulations.

8.2 Pilot machines

An overview of paper pilot plants was presented in 1997 [298].

During the 1990s, the three dominating paper machine manufacturers all started new pilot machines, mainly for printing paper development. A main reason in all cases was to increase machine speed, since the speed potential of the industrial machines started to surpass the pilot machines during the early 1990s. The machines were more complete than earlier versions by including larger parts of the drying sections.

A new Voith machine was started in December 1990 in Heidenheim [154] and after one year it was redesigned into a roll-adjustable blade twin-wire version. Maximum speed was 2200 m/min and width 1 m.

Beloit started a new pilot machine Rockton in 1994 [299], with a maximum speed of 2400 m/min and 1 m width. During its last working years the wire section was run in the roll-adjustable blade version.

Valmet started a pilot machine Jyväskylä in 1996 [300]. Design speed 2500 m/min and width 1 m. The wire section was of the roll-blade/adjustable blade design.

Paprican built a new machine (with some reuse of existing components), which was started in Pointe Claire in 1999 [301]. Headbox width 0.5 m, design speed 1600 m/min and the machine is balanced for 2500 m/min. The wire section is designed as a roll-adjustable blade unit. The white water system is closed by the addition of a sand filter, in which material from the excess white water is collected but not recycled. The stock system is designed for recirculation of the furnish.

The EuroFEX machine at STFI, Stockholm, was started up already in 1982. It was balanced for 3000 m/min, design speed was 2400 m/min and width 0.3 m. In 1991 the wire section was complemented to also include the first ever roll-adjustable blade section [153]. The comparatively narrow machine width was chosen to make a full day running without furnish recirculation possible. This would not have been realistic with a wider machine, considering the level of stock consumption. Continuous recovery of fines and filler from the excess white water with a disc filter is enforced during all runs.

The EuroFEX plant is today the only laboratory plant in which industrial running conditions can be simulated if chemical additions and/or multi-ply forming are involved, due to continuous fresh stock addition as well as continuous recovery of material from excess white water. The difference from a pilot plant without these two design features was recently demonstrated by Nalco Chemical Co [302]; see Figure 70. They made similar test runs in the EuroFEX and the Beloit pilot plants. It is clear from these tests that in the EuroFEX plant the white water chemistry levels out between the different test points and that the levels recorded are higher.

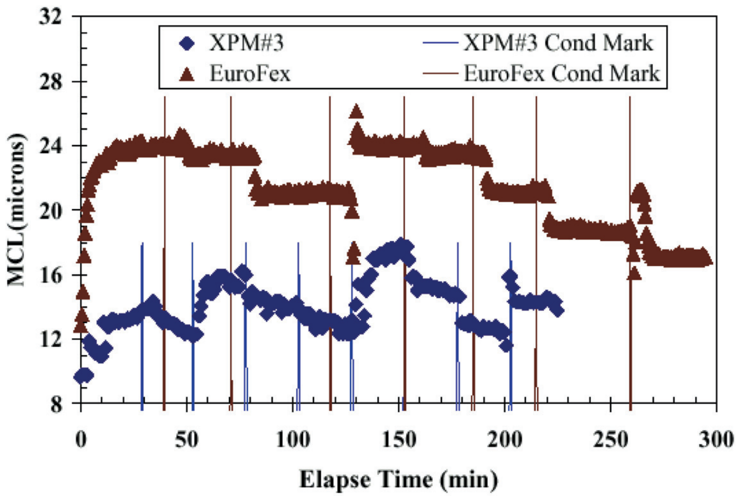

Figure 70 "Comparison of the SLM/FBRM mean chord length traces obtained for XPM3 (Beloit) and EuroFEX pilot paper machines. The marks on the figure indicate changes in retention chemistry or dose." Figure 12 from [302].

9 FORMING, STRUCTURE AND PROPERTIES

Initially the generally spread misunderstanding that formation improvements also mean paper strength improvements should be commented upon. A correct statement is instead that under some circumstances, both strength and formation will be changed in the same direction.

- The most obvious way of improving both formation and paper strength is to reduce forming concentration, assuming that current drainage limitations are not superseded.
- An often-used method to worsen formation in hand sheet forming is to impose a delay time before drainage. Formation as well as strength will then deteriorate.

On the contrary, there are several occasions where the opposite situation will be true, i.e., formation improvements will not be accompanied by strength improvements:

- Excessive addition of retention aid can improve formation, but paper strength will be unchanged.
- Manipulation of the activity on a fourdrinier wire may improve formation, but this will normally be associated with a reduction in paper strength.
- An industrial method to improve formation in twin-wire forming is to introduce blade pressure pulses. However, in this case paper strength will deteriorate [117].

A "general rule" was formulated by Fredlund [303] as a summary to a range of EuroFEX pilot plant experiments:

Strength potential in forming lies in the quality of the headbox jet. Manipulations at later stages can improve formation but not paper strength.

9.1 Single-layer forming

In 1992, Holik made an overview of the state-of-the-art technology within forming at Sulzer Escher Wyss [304,305].

Ohlsson [306] studied twin-wire forming of mechanical pulp containing printing papers on the EuroFEX machine. It was found that formation improved with decreasing slice opening, and not until around 5 mm, formation started to deteriorate due to the high forming concentration. It should be remembered that the small slice opening resulted in a high nozzle contraction, with its positive effects on paper formation. This was however not appreciated at that time.

Albinsson, Swerin and Öberg [307] studied the effect of blade dewatering in the EuroFEX machine on formation and filler retention. It was found that with a suitable retention aid strategy (addition components, dosage time strategy), increased mechanical blade action due to increased outer wire tension could be used to improve formation without reducing the retention level.

Swerin and Mähler [308] studied the effect of fibre suspension properties on final sheet formation in twin wire roll-blade forming on the EuroFEX machine. When flocculants (cationic polyacrylamide and bentonite clay) were added, higher shear (mix-to-wire speed difference) during dewatering was needed to produce a less flocculated paper. At minimum speed difference, formation number, filler retention and drainage (given as the amount drained over the forming roll) all showed maximum values.

Nilsson [309] studied different aspects of twin-wire roll forming. He found that a positive velocity difference between mix and wires would align fibres in the negative MD (when viewed in a sample cross sectioned in MD), and vice versa for a negative velocity difference. A tape splitting test on a paper sample easily confirms this. A tape is attached in the MD on a paper surface. When it is peeled off in the negative MD, few fibres will be pulled out, when the fibre orientation is in the negative MD. With the opposite fibre orientation in the sample, an increasing amount of fibres will be pulled out; see also [310]. Nilsson further studied the effect on paper formation of the mix to wire velocity difference. He found that the traditional formation optimum at a certain velocity difference between mix and wires moved towards increased velocity differences for increased floc strength in the mix (Crowding factor, chemical additives etc.).

Nordström and Norman [117] studied paper properties using a TMP furnish in roll and roll-blade forming respectively, using different degrees of headbox nozzle contraction. The effects on fibre orientation anisotropy were discussed above. The effects on small-scale and large-scale formation are shown in Figures 71 and 72.

At low and medium headbox nozzle contraction ratio (traditional for hydraulic headboxes), small-scale as well as large-scale formation behaved in the traditional way.

This means that optimum formation was obtained at a certain positive and negative mix-to-wire speed difference respectively [1].

Large-scale formation optimum using a high nozzle contraction ratio was obtained in a wide range around zero mix-to-wire speed difference (if the low value at –60 m/min speed difference is disregarded), and the formation values were the same as the optimum at low and medium contraction; see Figure 71. The addition of blade pressure pulses (in combination with reduced roll dewatering) improved large-scale formation in a wide speed difference range.

Small-scale formation optimum using a high nozzle contraction was obtained at zero mix-to-wire speed difference, and the formation value was significantly lower than that at low and medium contraction ratio; see Figure 72. This indicates that the fibre flocculation structure in the jet is improved at high contraction, which is a result of floc stretching and breakage in the elongational flow in the headbox nozzle (as also discussed in a previous section). However, even a small increase of mix-to-wire speed difference during

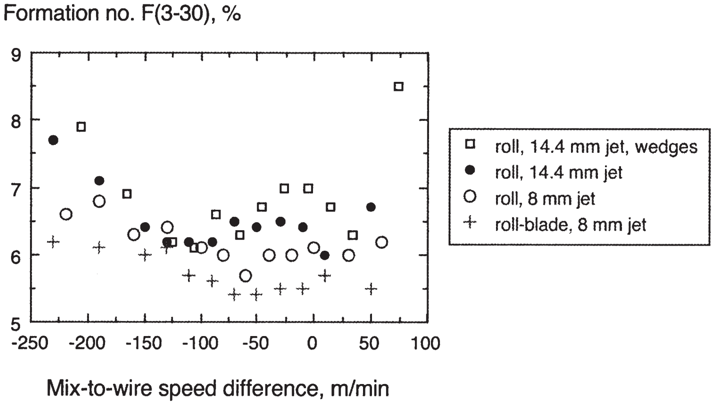

Figure 71 Large-scale formation as a function of mix-to-wire speed difference in roll and roll-blade twin-wire forming on the FEX machine. "Square" – high nozzle contraction, "filled circle" – medium contraction, "unfilled circle" – high contraction, "+ marks" – high contraction and blade pulses after the roll [117].

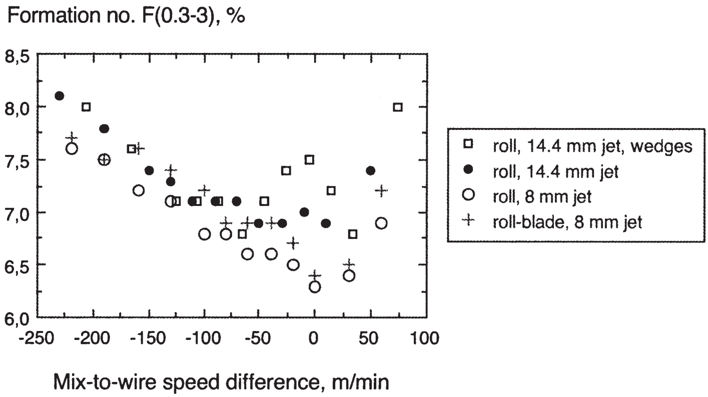

Figure 72 Small-scale formation as a function of mix-to-wire speed difference and headbox nozzle contraction in roll and roll-blade twin-wire forming, data as in Figure 71 [117].

dewatering generates a deteriorated small-scale formation. This is surprising, since all previous investigations have shown a formation improvement with some degree of shear during dewatering. The reason could be that the degree of small-scale flocculation in the jet after strong elongation in the headbox nozzle is so low that all shear during dewatering only can increase grammage variations. The addition of blade pressure pulses after roll dewatering slightly worsens small-scale formation in the whole speed difference range investigated. Retention level and paper mechanical properties were either maintained or impaired (especially Z-toughness) for roll-blade forming in comparison with pure roll forming.

Nordström and Norman [311] further found that the separation distance between the blades in roll-blade forming of TMP could be reduced from 116 mm to 46 mm without any negative effects on paper properties.

Nordström and Norman [312] studied the effect of jet quality on paper properties in roll-blade forming of TMP. The high quality jet was produced with high nozzle contraction, resulting in a paper tensile stiffness MD/CD ratio of 4 at minimum mix-to-wire shear (thus generated by the orientation anisotropy in the jet), and a more flocculated jet from a low contraction nozzle, with a MD/CD ratio of ca 1.5. The detrimental effect on formation of jet flocculation was reduced by introducing low level blade pulses after initial roll forming, and also some increase in final paper tensile stiffness MD/CD ratio was obtained. The lower Z-toughness for roll-blade dewatering compared to pure roll dewatering was only to a minor degree influenced by jet quality and blade force level.

Nordström and Norman [313] studied the influence of the proportion of roll dewatering in roll-blade dewatering by changing the roll-covering angle of the initial roll forming. It was found that the improvement in the large-scale formation was best exploited with a sufficiently large proportion of roll dewatering. The deterioration with lower degree of roll dewatering might be caused by negative effects on the thin wet webs at the separation of the wires from the roll surface as discussed above.

Odell [259,314] discussed Valmet roll-blade forming technology in relation to different sheet structure properties, such as formation/retention, layered orientation and material distribution in the Z-direction. In Figure 73 an example is given of the influence of suction shoe vacuum in a roll-blade former on filler distribution in the Z-direction.

Verkasalo, Odell and Korhonen [241] described the development of LWC base paper from fourdrinier over hybrid formers to roll-blade twin-wire formers.

Erkkilä, Pakarinen and Odell [43] quantified fibre orientation profiles in the Z-direction using the tape-stripping method described above, with

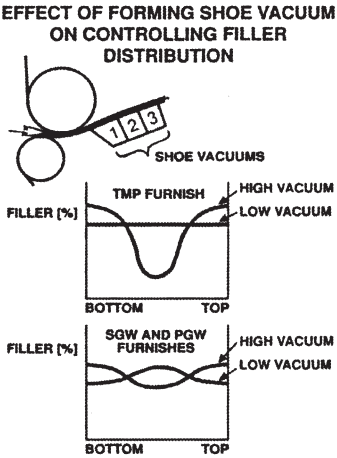

Figure 73 Effect of suction shoe vacuum on controlling filler distribution [259].

different forming principles and jet-to-wire speed ratios; see Figure 74. They motivated the different profile shapes by different dewatering rates and different speed differences between web and mix:

- the low degree of anisotropy towards the wire surfaces is due to the fast drainage in those areas, which leaves little time for fibres to orient due to shear;
- the lower degree of anisotropy at the centre with two-sided dewatering is due to reduced shear velocities due to viscous damping;

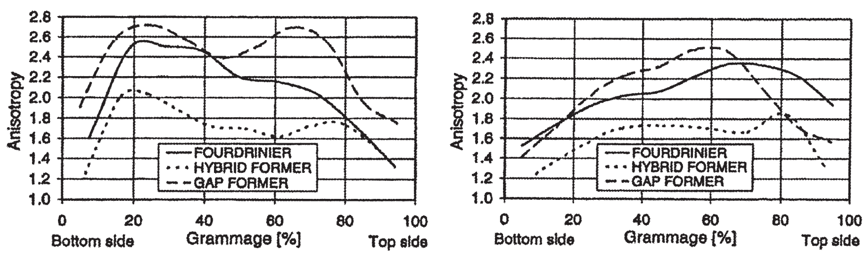

Figure 74 Layered orientation anisotropy during "rush" (left) and drag (right) forming conditions for three forming principles [43].

• the asymmetry of fourdrinier sheets is due to the unsymmetrical shear effects along the dewatering section.

The local anisotropy minimum in the centre of a gap dewatered sheet could alternatively be an effect of space limitations for fibre rotation at this stage, as well as a natural, geometric accumulation in the centre of fibre flocs.

Jansson [44] studied the effect of headbox nozzle contraction ratio on fibre orientation anisotropy for roll forming at minimum shear conditions during dewatering; see Figure 75. According to this figure, anisotropy is low at sheet edges even when orientation around sheet centre is high. One reason for this has later been shown by Asplund [120] to be the lower degree of fibre orientation anisotropy in the headbox nozzle boundary layers (see Figure 22). Another reason could be the effects of local micro flow disturbances at jet-to-wire contact.

Erkkilä, Pakarinen and Odell [315] made further studies of the layered structure of twin-wire formed paper. It is initially proposed that the role of turbulence is extremely important when the suspension enters the forming section. Elimination of turbulence might produce frozen flow with the absence of relative motion between fibres, leading to flocculation and poor formation. In contrast, small-scale turbulence in the flow is supposed to create constant deflocculating action in the stock.

These views on fibre suspension turbulence are debatable (see also in section *Headboxes*). It is true that the traditional model for turbulence decay in a fluid will tell that the large eddies are broken down into smaller units, and this process gradually continues until the final viscous dissipation into heat in

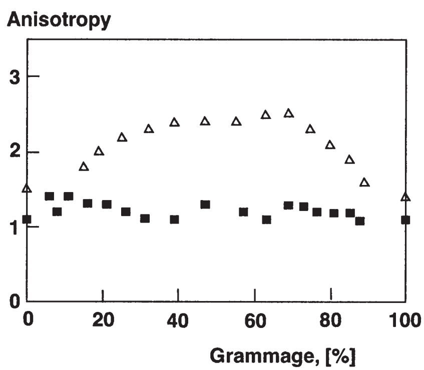

Figure 75 Fibre orientation anisotropy with different headbox nozzle contraction ratios for roll formed paper at zero mix-to-wire speed differences; squares – low contraction, triangles – high contraction [44].

the micro-scale. However, the situation in a fibre suspension is drastically different. Bennington [60] claims that a large part of the dissipation takes place directly between the fibres. Small-scale turbulence is also efficiently damped by the presence of the fibres. A smaller part of the fluid energy will then be transformed into the micro-scale range. Thus mainly more large-scale turbulence will survive, and this large-scale turbulence, if present during the dewatering phase, is highly detrimental to paper formation.

There is no known experimental evidence that turbulence present during dewatering has a positive effect on paper formation. The basic idea should instead be to affect the fibre suspension inside the head box, so that the fibre flocs are as weak as possible and can be easily broken apart by the shear allowable during dewatering.

Turbulence should be avoided at all stages of forming, since it is the main source for reflocculation.

Using the tape stripping method, Erkkilä et al. analysed the different layers for **four** different parameters; see Figures 76 and 77.

1. Anisotropy;
   the definition of "anisotropy" in this work, Equation 11, differs from that in Equation 2; see Figure 8.

$$\text{“}Anisotropy\text{”} = 1 - a/b \approx 1 - CD/MD \tag{11}$$

2. Standard deviation of anisotropy; calculated on 3.3×3.3 mm^2 measurement areas.
3. Floc index.
4. Orientation angle.

It is clear from Figure 76 that "anisotropy" is considerably lower at minimum mix-to-wire speed difference than with a negative speed difference. The aligning effects from some shear considerably suppress local anisotropy variations during dewatering

Fibre orientation misalignment traditionally changes from positive to negative angle when going from negative to positive speed differential. The misalignments shown in Figure 77 therefore would indicate that minimum shear occurs slightly below jet/wire ratio1.04, rather than at 1.02.

From Figure 77 it is evident that flocculation at minimum mix-to-wire shear during dewatering is substantially higher, especially at web centre. One reason for the ever-present better formation close to the wires could be that dewatering will initially move the free fibres to these positions. The more flocculated state of mix would then be left to dewater in the later stages, at

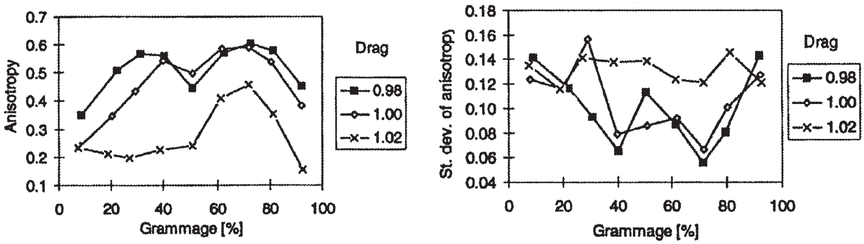

Figure 76 Layered orientation structure for roll-blade forming at 1200 m/min, LWC 50 g/m^2. “Anisotropy” (Left) and Standard deviation of “anisotropy” (Right). Jet/wire ratio on the low side; 1.02 corresponds to minimum shear during dewatering [315].

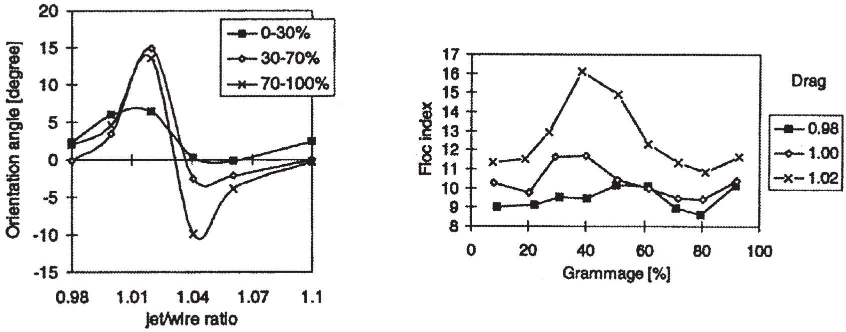

Figure 77 Layered floc index (left) and misalignment angle (right), three different thickness ranges from sheet bottom to top; different jet/wire ratios, data as in Figure 76 [315].

web centre. This could explain why shear during dewatering mainly has a positive effect in the late dewatering phases – this is simply when the flocs are to be dewatered.

The results reported by Erkkilä et al. also include rush conditions, but space does not allow its presentation at this time.

The effect of differences in vacuum levels in forming roll surface and forming shoes was also studied, but had only limited influence on sheet structure.

The mounting of vanes inside a headbox nozzle is well known to have a decreasing effect on fibre orientation anisotropy in the final paper product. As shown above in Figure 22, vane insertion reduces fibre orientation anisotropy in the headbox jet.

Erkkilä et al. [315] studied the effects on the paper of headbox vanes and roll-bade forming; see Figure 78.

It is obvious that there is no influence of vane length itself (with the actual dimensions), only of end shape. However, the turbulent eddies generated by the blunt vane end probably lasted all the way to the dewatering stage. The reducing effect of turbulence on anisotropy and the negative effect on floc index are clearly demonstrated.

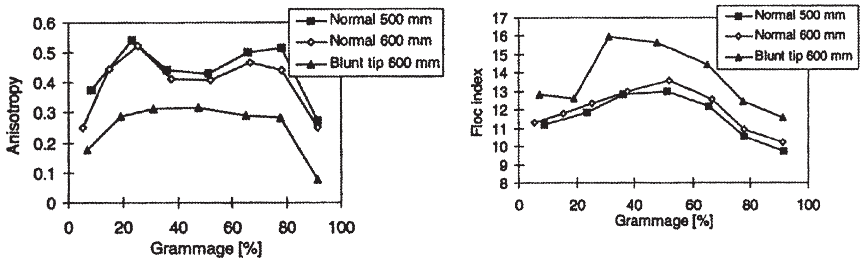

Figure 78 The effect of different vanes on layered "anisotropy" (Left) and floc index (Right). The 500 and 600 mm vanes end 220 and 120 mm respectively, before slice opening [315].

Figure 79 shows a fibre orientation vector map, where anisotropy magnitude is represented by individual line length and orientation by line angle. The high degree of local variations is clearly demonstrated.

Lloyd and Chalmers [45] applied sheet splitting using the tape-method and optical fibre orientation analysis to characterise the structure of anisotropic

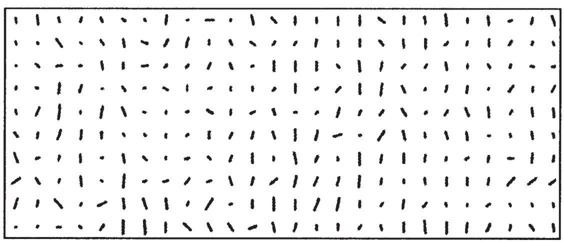

Figure 79 Fibre orientation map for layer next to sheet top using blunt tip vanes; data as in Figure 78 [315].

laboratory sheets. It was also demonstrated that variations in the Z-direction of fibre orientation misalignment and its variability correlated with the occurrence of cockle on machine made paper.

Räisänen and Paananen discussed the influence of furnish properties on linerboard quality using hybrid and roll-blade forming principles [178].

Mohlin [316] performed pulp evaluation using the EuroFEX system. Comparison with standard pulp evaluation techniques demonstrated that different ranking orders could be obtained in the two cases.

Mohlin [317] also studied the influence of fibre dimensions on formation and strength properties using the pilot machine EuroFEX. 100% chemical pulp and also LWC-type furnishes were tested. Small-scale formation was improved by decreasing fibre coarseness and increasing fines content and large-scale formation was also influenced by fibre flocculation. The ratio between the two formation numbers was suggested to be a measure of floc formation, and decreased with decreasing crowding factor. There was no general correlation between formation and strength. About the same strength was obtained on the fourdrinier and in the twin-wire roll-adjustable blade former, in spite of their very different formation properties. Fibre flocculation had a larger effect on burst strength than on tensile strength.

Odell and Pakarinen [318] made a recent overview, aiming at fibre orientation related defects on different scales, and the effects on curl, and local dimensional instabilities.

An interesting application of layered orientation information as that described above is to construct a 3-D orientation map of the paper cross-section; see Figure 80. Local orientation and orientation variability are interpreted as effective shear and turbulence present during dewatering.

However, it should be pointed out that some of the structure characteristics in the final paper might originate from upstream conditions in the headbox.

9.2 Multi-layer forming

Traditionally, multi-layer forming of tissue products has been applied industrially already since the 1970s. Some recent headbox flow investigations are included under *Headboxes*. However, probably due to the secrecy within the tissue area, no results from recent tissue applications can be found in literature.

Already during the 1970s, a three-layer headbox was installed on a new 10 m wide Bel Baie twin-wire linerboard machine; Page and Hergert [319]. 25% mixed waste was placed in the centre layer and it was claimed that the reduction in burst value was only 6% in comparison to a 20% loss using single layer

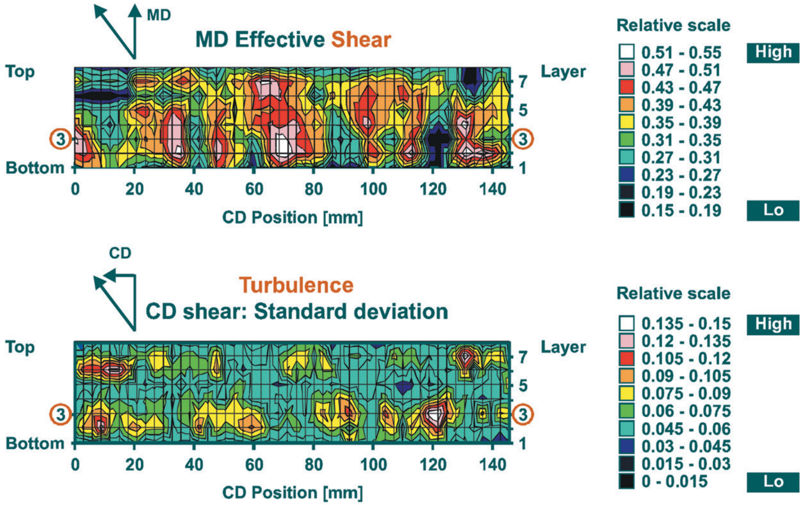

Figure 80 CD cross-section of a paper sample. Local MD orientation anisotropy (Top) and variability in CD anisotropy (Bottom), [318].

forming on a fourdrinier machine. Page and Hergert also discuss the advantages for paper mechanical properties using different layering in alternative cases.

During the 1990s several installations of 2-layer headboxes on linerboard machines have been made. This makes it possible to manufacture white-top liner with only one forming unit.

During the last decade much work has been performed to improve the quality of 3-layered printing papers (see section *Headboxes*). One main problem in comparison with 2-layer linerboard forming is the low grammage of the surface layers; brighter surface layers cannot optically cover a darker centre layer. The centre layer brightness therefore should not deviate too much from that of the surfaces.

Häggblom-Ahnger [320] made several pilot-plant trials to study three-layer forming of printing papers. Häggblom-Ahnger and Eklund [321] studied the effects of a CTMP middle layer in a 3-layer copy paper. Positive effects on mechanical properties were found, but the surface layer cover was not even enough.

In a study of the location of softwood fibres (30%) in a three-layer office paper bending stiffness was found to increase with a central placement;

Häggblom-Ahnger [322]. At the same time surface smoothness and formation improved. For runnability purposes, the amount of softwood fibres could be reduced with central placement.

Filler distribution in the Z-direction can be controlled using selective addition in three-layer forming [323,314]. There is also a large control potential through selective retention aid addition in the different layers.

An overview of layering possibilities was made by Lloyd [324].

9.3 Multi-ply forming

Current methods for single-ply forming and combinations into multi-ply products are summarised in *Wire section designs*. There is no relevant literature available from the last decade, on the multi-ply aspects of board properties.

ACKNOWLEDGEMENTS

Dr Hannes Vomhoff is thanked for valuable views on the original manuscript and Tekn-Lic student Greger Asplund for skilful help with many of the illustrations.

REFERENCES

1. Norman, B., "Overview of the physics of forming", in 9th Fundamental Research Symposium, Cambridge, pp. 3: 73–149 (1989).
2. Lindström, T., "Overview of the chemistry of forming", in 9th Fundamental Research Symposium, Cambridge, pp. 311–412 (1989).
3. Norman, B., "Web forming", Papermaking Part 1, Stock Preparation and Wet End in *Papermaking Science and Technology*, Fapet OY, Helsinki, **8**(6): pp. 191–250 (2000).
4. Beghello, L., et al., "A device for measuring fiber floc sizes in highly turbulent fibre suspensions", *Nord. Pulp Pap. Res. J.*, **11**(4): pp. 254–259 (1996).
5. Keller, S., Luner, P., and Pawlak, J., "Characterization of the spatial variability of paper formation using a continuous wavelet transform", in International Paper Physics Conference, San Diego, pp. 357–368 (1999).
6. Keller, S., Lewalle, J. and Luner, P., "Analysis of paper variability using the continuous wavelet transform", *Paperi ja Puu*, **81**(6): pp. 440–446 (1999).
7. Söderberg, D., "A comparison between the flow from a paper machine headbox and a low Reynolds number water jet", in Tappi Engineering Conference, Anaheim, pp. 1155–1172 (1999).

8. Johansson, P. Å. and Norman, B., "Methods for evaluating formation, print unevenness and gloss variations developed at STFI", in Tappi Process and Product Quality Conference, Cincinnati, p. 140 (1996).
9. Cresson, T., Tomimasu, H. and Luner, P., "Characterisation of paper formation. Part 1: Sensing of paper formation", *Tappi J.*, **73**(7): pp. 153–159 (1990).
10. Cresson, T. and Luner, P., "The characterization of paper formation – Part 2: The texture analysis of paper formation", *Tappi J.*, **73**(12): pp. 175–185 (1990).
11. Cresson, T. and Luner, P., "The characterization of paper formation – Part 3: The use of texture maps to describe formation", *Tappi J.*, **74**(2): pp. 167–175 (1991).
12. Cresson, T. and Luner, P., "Description of the spatial grey level dependence method algorithm", *Tappi J.*, **73**(12): pp. 220–222 (1990).
13. Dodson, C., "A rational approach to formation analysis and spreadsheet schema for data interpretation", *Tappi J.*, **76**(5): pp. 153–156 (1993).
14. Ambertec, "Beta formation tester", Ambertec OY, Espoo, Finland. (1990).
15. Waterhouse, J., "Effect of papermaking variables on formation", *Tappi J.*, **76**(1): pp. 129–134 (1993).
16. Tomimasu, H., et al., "Comparison of four paper imaging techniques: b-radiography, electrography, light transmission and soft X-radiography", *Tappi J.*, **74**(7): pp. 165–176 (1991).
17. Keller, S., "Paper formation measurement by electron beam transmission imaging and analysis using wavelet transforms", SUNY, Syracuse, PhD Thesis (1996).
18. Dodson, C., "A universal law of formation", (Research Note). *J. Pulp Pap. Sci.*, **16**(4): pp. 136–137 (1990).
19. Lloyd, M., "Turbulent layer mixing during stratified forming of woodfree paper", Pulp and Paper Chemistry and Technology, KTH, Stockholm, Licentiate thesis (1997).
20. Deng, M. and Dodson, C., "Paper: An engineered stochastic structure", Tappi Press, Atlanta (1994).
21. Trepanier, R., Jordan, B. and Nguyen, N., "Specific perimmeter: a statistic for assessing formation and print quality by image analysis", *Tappi J.*, **81**(10): pp. 191–196 (1998).
22. I'Anson, S., "Identification of periodic marks in paper and board by image analysis using two-dimensional fast Fourier transforms. Part 1: The basics", *Tappi J.*, **78**(3): pp. 113–119 (1995).
23. I'Anson, S., "Identification of periodic marks in paper and board by image analysis using two-dimensional fast Fourier transforms. Part 2: Forming and press section marks", *Tappi J.*, **78**(7): pp. 97–106 (1995).
24. Wahjudi, U., Duffy, G. and Kibblewhite, P., "Effect of grammage and concentration on paper sheet formation of pinus radiata kraft pulps", in Appita Annual Conference, pp. 671–678 (2000).
25. Bernié, J.-P. and Douglas, M., "Local grammage distribution and formation of paper by light transmission image analysis", *Tappi J.*, **79**(1): pp. 193–202 (1996).
26. Bouydain, M., Colom, J. and P. J, "Using wavelets to determine paper formation by light transmission image analysis", *Tappi J.*, **82**(7): pp. 153–158 (1999).

27. Daunais, R. and Garner, R., "The NUI formation tester – an evaluation, modification and comparison with other techniques", in Inernational Paper Physics Conference, Mont Gabriel, p. 43 (1987).
28. Kallmes, O. and Ayer, J., "Light scanning system provides qualitative formation measurement", in International Paper Physics Conference, Mont Gabriel, p. 209 (1987).
29. Popil, R. and Jordan, B., "The wavelength dependence of transmitted light formation measurement", in International Paper Physics Conference, pp. 61–69 (1995).
30. Lloyd, M. and Norman, B., "Effect of headbox slice geometry during the stratified forming of woodfree paper", *Nord. Pulp Paper Res. J.*, **12**(4): pp. 252–259 (1997).
31. Moineau, D., Bloch, J-F. and Eymin, G., "On-line 2D formation sensor: A new tool to evaluate the quality of paper formation", in International Paper Physics Seminar, Grenoble, pp. 29–38 (2000).
32. Hiertner, M., "Basis weight varies faster than on-line systems can measure", in Control Systems '98, Porvoo, p. 307 (1998).
33. Ferguson, H., "Full sheet image system becomes control reality", *Pulp & Paper*, **71**(10): p. 75 (1997).
34. Mathias, T., "Paper industry's first full sheet imaging system", in 52nd Appita Annual Conference, pp. 429–433 (1998).
35. Hagart-Alexander, C., "Wet end measurement system for MD and CD quality monitoring and control", in 86th Annual Meeting, PAPTAC, Monteral, pp. 231–233 (2000).
36. Niskanan, K., Kajanto, I. and Pakarinen, P., "Fibre orientation", *Paper Physics, Papermaking Science and Technology*, Fapet OY, Helsinki, **16**(1.4): pp. 37–50 (1998).
37. Titus, M., "Ultrasonic technology – measurements of paper's orientation and elastic properties", *Tappi J.*, **77**(1): pp. 127–130 (1994).
38. Nomura, T., "Introduction of new SST-3000 and development of sonic sheet tester uses". *Japan Tappi J.*, **48**(1): pp. 215–219 (1994).
39. Bando, T., et al., "Drainage mechanism on a twin-wire former. Part 3: Dependence of the structural anisotropy of paper sheet on the pulsating drainage", *Japan Tappi*, **49**(49): pp. 841–848 (1995).
40. Masuda, K., Hasuike, M. and Bando T., "Characterization on 3-D geometric arrangement of fibres in a paper sheet", in ISF, Yokohama, p. 243 (1994).
41. Hasuike, M., Kawasaki, T. and Murakami, K., "Evaluation method of 3-D geometric structure of paper sheet", *J. Pulp Pap. Sci.*, **18**(3): pp. J114–120 (1992).
42. Hasuike, M., Masuda, K and Bando, T., "Characterization of three-dimensional sheet structure", Mitsubishi Heavy Industries, *Technical Review*, **32**(3), 127–131 (1995).
43. Erkkilä, A.-L., Pakarinen, P. and Odell, M., "Sheet forming studies using layered orientation analysis", *Pulp Paper Canada*, **99**(1): pp. 81–85 (1998).
44. Jansson, M., "Fibre orientation anisotropy – variations in the z-direction", (in Swedish). Pulp and Paper Chemistry and Technology, KTH, Stockholm, MSc Thesis (1998).

45. Lloyd, M. and Chalmers, I., "Use of image orientation analysis technique to investigate sheet structural problems during forming", in APPITA, Melbourne, pp. 495–502 (2000).
46. Scharcanski, J. and Dodson, C., "Local spatial anisotropy and its variability", *J. Pulp Pap. Sci.*, **25**(11): pp. 393–397 (1999).
47. Thorpe, J., "Exploring fiber orientation within copy paper", in International Paper Physics Conference, San Diego, pp. 447–457 (1999).
48. Xu, L., Parker, I. and Filonenko, Y., "A new technique for determining fibre orientation distribution through paper", in International Paper Physics Conference, San Diego, pp. 421–427 (1999).
49. Kao, S. and Mason, S., "Dispersion of particles by shear", *Nature*, **253**(February 20): pp. 619–621 (1975).
50. Norman, B. et al., "Hydrodynamics of papermaking fibres in water suspension", in Fibre-Water Interactions in Paper-Making, Oxford, pp. 195–250 (1977).
51. Steen, M., "Modeling fiber flocculation in turbulent flow: a numerical study", *Tappi J.*, **74**(9): pp. 175–181 (1991).
52. Kerekes, R. and Schell, C., "Characterization of Fibre Flocculation Regimes by a Crowding Factor", *J. Pulp Pap. Sci.*, **18**(1): pp. J32–38 (1992).
53. Kiviranta, A. and Dodson, C., "Evaluating fourdrinier formation performance", *J. Pulp Pap. Sci.*, **21**(11): pp. J379–384 (1995).
54. Kerekes, R. "Perspective on fibre flocculation in papermaking", in International Paper Physics Conference, Niagara, pp. 23–31 (1995).
55. Andersson, S., "Netwok disruption and turbulence in fibre suspensions", Dep of Chemical Engineering and Design, CTH, Gothenburg, PhD Thesis (1998).
56. Wikström, T., "Flow of pulp suspensions at low shear rates", Dep of Chemical Engineering Design, CTH, Gothenburg, Licentiate Thesis (1998).
57. Wikström, T. and R. A, "Yield stress of pulp suspensions", *Nord. Pulp Paper Res. J.*, **13**(3): pp. 243–250 (1998).
58. Andersson, S. and Rasmuson, A., "The network strength of non-flocculated fibre suspensions", *Nord. Pulp Paper Res. J.*, **14**(1): pp. 61–70 (1999).
59. Andersson, S., Nordstrand, T. and Rasmuson, A., "The Influence of Some Fibre and Suspension Properties on Pulp Fibre Friction", *J. Pulp Pap. Sci.*, **26**(2): pp. 67–71 (2000).
60. Bennington, C. and Mmbaga, J., "Liquid phase turbulence in pulp fibre suspensions", in Fundamental Research Symposium, Oxford (2001).
61. Schmid, C. and Kingenberg, D., "Mechanical flocculation in flowing fiber suspensions", *Phys. Rev. Letters*, **84**(2): pp. 290–293 (2000).
62. Huhtanen, J.-P., "Non-Newtonian Flows in Paper making", Energy and Process Engineering, Tampere University of Technology, Tampere, Techn.lic. Thesis (1998).
63. Ross, R. and Klingenberg, D., "Simulation of flowing wood fibre suspensions", *J. Pulp Pap. Sci.*, **24**(12): p. 388 (1998).
64. Schmid, C., Switzer, L. and Klingenberg, D., "Simulation of fiber flocculation: Effects of fiber properties and interfiber friction", *J. Rheol.*, **44**, pp. 781–809 (2000).

65. Schmid, C. and Klingenberg, D., "Properties of fiber flocs with frictional and attractive interfiber forces". *J. Coll. Int. Sci.*, **226**, pp. 136–144 (2000).
66. Shah, P., et al., "The role of turbulent elongational stresses on deflocculation in paper sheet formation", *Tappi J.*, **83**(4): pp. 8 pages (2000).
67. Kaji, H., Monma, K. and Katsura, T., "Fractal analysis of flocculation in pulp suspension", in International Paper Physics Conference, Hawaii, pp. 291–297 (1991).
68. Kallmes, O., Kallmes, P. and Bishop, B., "Monitoring flocculation in the paper machine", *Tappi J.*, **77**(7): pp. 194–198 (1994).
69. Zhao, R. and Kerekes, R., "The effect of suspending liquid viscosity on fiber flocculation", *Tappi J.*, **76**(2): pp. 183–188 (1993).
70. Paul, T., Duffy, G. and Chen, D., "New insights into the flow of pulp suspensions", in 54th Appita Annual Conference, Melbourne, pp. 645–654 (2000).
71. Giri, M., Simonsen, J. and Rochefort, W., "Dispersion of pulp slurries using carboxymethylcellulose", *Tappi J.*, **83**(10): pp. 14 pages (2000).
72. Kerekes, R. and Schell, C., "Effects of fibre length and coarseness on pulp flocculation", *Tappi J.*, **78**(2): pp. 133–139 (1995).
73. Beghello, L., "The tendency of fibers to build flocs", Laboratory of Paper Chemistry, Åbo Akademi University, Åbo, PhD Thesis (1998).
74. Raghem-Moayed, A. and Kuhn, D., "Turbulent flocculation measurement", *J. Pulp Pap. Sci.*, **26**(4): pp. 163–165 (2000).
75. Raghem-Moayed, A., "Characterisation of fibre suspension flows at papermaking consistencies", Dept of Chemical Engineering and Applied Chemistry, University of Toronto, Toronto, PhD Thesis (1999).
76. Wågberg, L. and Nordqvist, T., "Detection of polymer induced flocculation of cellulosic fibres by image analysis", *Nord. Pulp Pap. Res. J.*, **14**(3): pp. 247–255 (1999).
77. Pierre, C., "A new sensor for the measurement of fibre flocculation in the stock. A tool for the sheet formation control", in COST E14, Lisbon (2000).
78. Swerin, A., "Flocculation and fibre network strength in papermaking suspansions flocculated by retention aid systems", Division of Paper Technology, KTH, Stockholm, PhD Thesis (1995).
79. Tuomisaari, M., Gullichsen J. and Hietaniemi, J., "Floc disruption in medium-consistency fiber suspensions", in International Paper Physics Conference, Hawai, pp. 609–612 (1991).
80. Hietaniemi, J. and Gullichsen, J., "Floc disruption in medium consistency fibre suspensions: Empirical results and their interpretation", in International Paper Physics Conference, Niagara-on-the-Lake, pp. P29–38 (1995).
81. Cichoracki, T., Gullichsen, J. and Paulapuro, H., "High consistency forming: A new concept", *Tappi J.*, **84**(3): pp. 8 pages (2001).
82. Björkman, U., "Flow of flocculated fibres". Stockholm: Paper Technology, KTH. 283. (1999).
83. Helmer, R., Covey, G. and Lai, L., "Approach flow stock mixing", in 52nd Appita Annual Conference, pp. 223–228 (1998).

84. Ringnér, J. and Rasmuson, A., "Characterization of fibre suspensions using X-ray computed tomography and image analysis", *Nord. Pulp Pap. Res. J.*, **15**(4): pp. 319–325 (2000).
85. Kellomäki, M. et al., "Fiber flocculation measurement in pipe flow by digital image analysis", in International Paper Physics Conference, San Diego, pp. 461–463 (1999).
86. Karema, H. et al., "Transient fluidisation of fibre suspension in straight channel flow", in International Paper Physics Conference, San Diego, pp. 369–379 (1999).
87. Li, T.-Q., et al., "Velocity measurements of fiber suspensions in pipe flow by the magnetic resonance imaging method", *Tappi J.*, **77**(3): pp. 145 (1994).
88. Li, T.-Q. and Ödberg, L., "Flow of pulp suspension through an abrupt contraction studied by flow encoded nuclear magnetic resistance imaging". *Nord. Pulp Paper Res. J.*, **10**(2): pp. 133 (1995).
89. Li, T.-Q. et al., "Pipe flow behaviour of hardwood pulp suspensions studied by NMRI", *J. Pulp Pap. Sci.*, **21**(12): pp. J408–414 (1995).
90. Li, T.-Q. and Ödberg, L., "Studies of flocculation in cellulose fibre suspansions by NMR imaging", *J Pulp Pap. Sci.*, **23**(8): pp. J401 (1997).
91. Houvila, J. et al., "The Valmet Headbox Family-A New Level of Customer Orientation", in XII Paper Technology Days, Turku, pp. 128–139 (2000).
92. Pantaleo, S., "Headboxes – Past, Present and Future", in CPPA Annual Meeting, Montreal, pp. A131–139 (2000).
93. Schultz, H.-J. "The use of standard units for headbox design", in 4th International Conference: New available techniques and current trends, Bologna, pp. 6–45 (1992).
94. Schultz, H.-J., "Der BTF-Universalverteiler. ein verbindenes Trennelement zwichen kontasntem Teil und Stoffauflauf", Wochenbl f. Papierfabr. (11/12): pp. 461–465 (1992).
95. Knoller, H., Foulger, M. and Parisian, J., "A new dilution control system for existing headboxes", in 86th Annual Meeting, PAPTAC, Montreal, pp. 17–21 (2000).
96. Begemann, U., "Module Jet, das neue Stoffauflaufkonzept mit Stoffdickte-Querprofilregelung", *Das Papier*, **47**(10A): pp. V149 (1993).
97. Begemann, U., "The new headbox concept with CD consistency control", in Annual Meeting, Technical Section CPPA, Montreal, pp. A305–310 (1995).
98. Heinzmann, H., "Faserorientierung – Querprofil", *Wochenbl f. Papierfabr.*, (4): pp. 121–126 (1995).
99. Pantaleo, S., "A new headbox design featuring consistency profiling decoupled from fiber orientation response", *Tappi J.*, **78**(11): pp. 89 (1995).
100. Pantaleo, S., "Basis weight profiling experience of the concept IV-MH headbox", in Annual Meeting, Technical Section CPPA, Monteal, pp. B193–199 (1996).
101. Nyberg, P. and Malashenko, A., "Dilution control headbox – choises, threats and solutions", in 83rd CPPA Annual Meeting, Montreal, pp. 17 (1997).
102. Wurster, H. and Weitkämper, K., "Stoffdichteabhängige Querprofilregelung – Betriebserfahrungen", *Das Papier*, **49**(10A): pp. V99–102 (1995).

103. Wyse, R. et al., "Consistency profiling – A new technique for CD basis weight control", in Annual Meeting, Technical Section CPPA, Montreal, pp. A267–273 (1995).
104. Heaven, M. et al., "Recent Experiences with Consistency Profile Control Installations", in 84th Annual Meeting, Technical Section CPPA, Montreal, pp. 261 (1998).
105. Smits, M. "Results from a consistency profiling headbox and a method of analysing the CD profile performance", in 52nd Appita Annual Conference, pp. 397–401 (1998).
106. Pantaleo, S. "A headbox design minimizing MD fiber orientation streaks while maintaining high resolution basis weight control", in 85th Annual Meeting, PAPTAC, Montreal, pp. 113–119 (1999).
107. Collins, D., R. Leclerc and J. Perrault. "Operation of a moduljet dilution headbox on Dolbeau PM5", in 85th Annual Meeting, PAPTAC, Montreal, pp. 101–106 (1999).
108. Lee, J. and Pantaleo, S., "Headbox Flow Analysis", *J. Pulp Pap. Sci.*, **25**(12): pp. 437–441 (1999).
109. Hämäläinen, J. and P. Tarvainen. "CFD-based shape and control optimization applied to a paper machine headbox", in 86th Annual Meeting, PAPTAC, Montreal, pp. 99–102 (2000).
110. Fortier, L. "A new family of high turbulence headboxes", in 76th Annual Meeting, PAPTAC, Montreal, pp. 197–201 (1990).
111. Haptmann, E., Vyse, R. and Mardon, J., "The wake effect as applied to modern hydraulic headboxes, Parts 1 & 2", *Pulp Paper Can.*, **91**(9: 10): pp. T357–364 and T369–377 (1990).
112. Shariati, M. et al., "Numerical and experimental models of flow in the converging section of a headbox", in Tappi Papermakers Conference, Vancouver, pp. 685–693 (2000).
113. Aidun, C., "Opportunities to improve CD strength and to reduce fibre consumption in boardmaking", in PIRA International Conference: Scientific and Technical Advances in Boardmaking, Heathrow (1999).
114. Aidun, C., "Methods and apparatus to enhance paper and board forming qualities", IPST patent, US 6 153 057 (2000).
115. Nordström, B., "Effects of headbox design and dewatering conditions on twin-wire forming of TMP", Pulp and Paper Chemistry and Technology, KTH, Stockholm, PhD Thesis (1995).
116. Nordström, B. and Norman, B., "Influence on sheet anisotropy, formation, Z-toughness and tensile stiffness of reduced feed area to a headbox nozzle", *Nord. Pulp Pap. Res. J.*, **9**(1): p. 53 (1994).
117. Nordström, B. and Norman, B., "Effects of roll-blade and roll forming on formation, retention, mecanical properties and anisotropy – A preliminary comparison", *J. Pulp Pap. Sci.*, **21**(7): pp. J223–229 (1995).
118. Ullmar, M., "On fiber alignment mechanisms in a headbox nozzle", Pulp and Paper Chemistry and Technology, KTH, Stockholm, Tekn Lic Thesis (1998).

119. Ullmar, M. and Norman, B., "Observation of fiber orientation in a headbox nozzle at low consistency", in Tappi Engineering Conference, Nashville, pp. 2: 865 (1997).
120. Asplund, G., "Fibre orientation anisotropy at different levels in a headbox jet", (in Swedish) Division of Paper Technology, KTH, Stockholm, Masters Thesis (1999).
121. Chuang, S., "Microturbulence generation in a papermacine headbox", in Tappi Engineering Conference, pp. 205–213 (1982).
122. Shands, J., "Mechanics of stock jump at jet impingement", *J. Pulp Pap. Sci.*, **17**(3): pp. J92–J99 (1991).
123. Farrington, T., "A numerical investigation of three tissue machine headboxes", in AIChE Proceedings, Forest Products Symposium, pp. 177–188 (1991).
124. Hua, L. et al., "Flow distribution in a hydraulic headbox", in Tappi Engineering Conference, Annaheim, pp. 1123–1133 (1999).
125. Bandhakavi, V. and Aidun, C., "Analysis of turbulent flow in the converging zone of a headbox", in Tappi Engineering Conference, Anaheim, pp. 1135–1154 (1999).
126. Parsheh, M. and Dahlkild, A., "Modelling the flow around elastic guiding vanes in the converging zone of a headbox", in Tappi Engineering/Process and Product Quality Conference, Anaheim, pp. 1433–1452 (1999).
127. Parsheh, M., "Flow in contractions with applications to headboxes", Dep of Machanics, Kungl. Tekniska Högskolan, Stockholm (2001).
128. Baker, J., Beuther, P. and Farrington, T., "Impact of three dimensional headbox flows on tissue layer purity", in AIChE Symposium Series, Advances in Pulp and Papermaking, pp. 132–142 (1995).
129. Lloyd, M. and Norman, B., "Layer mixing during three-layer stratified forming: The role of vane length and mix-wire speed difference", *Tappi J.*, **81**(11): pp. 194–208 (1998).
130. Lloyd, M. and Norman, B., "Use of stepped vanes to alter headbox turbulence levels during stratified forming of woodfree paper", *Appita*, **52**(2): pp. 98–104 (1999).
131. Parsheh, M. and Dahlkild, A., "Numerical modelling of mixing in stratified headbox jet", in Tappi Engineering Conference, Nashville, pp. 1159–1173 (1997).
132. Li, A., Neill, E. and Rogers, T., "Fundamental studies of mixing in a stratified headbox jet", in Annual Meeting, PAPTAC, Montreal, pp. A53–56 (2000).
133. Li, A., Rogers, T. and Shands, J., "Mixing intensity analysis of a 2-layer stratified headbox jet", *Tappi J.*, **83**(12): pp. 16 pages (2000).
134. Norman, B., "Hydrodynamic developments in twin-wire forming – an overview. *Paperi ja Puu*, **78**(6–7): p. 376 (1996).
135. Matsson, J. and Alfredsson, H., "Curvature- and rotation-induced instabilities in channel flow", *J. Fluid Mech.*, **210**, pp. 537–563 (1990).
136. Alfredsson, H. and Matsubara, M., "Streaky structures in transition", in Transitional Boundary Layers in Aeronautics, (ed.) H. v. Ingen, Elsevier, pp. 374–386 (1996).

137. Söderberg, D. and Alfredsson, H., "Experimental and theoretical investigations of plane liquid jets", *Eur. J. Mech. B/Fluids*, **17**(5): pp. 689–737 (1998).
138. Söderberg, D. and Alfredsson, H., "Experiments concerning the creation of streaky structures inside a planar water jet", in Tappi Engineering Conference, Nashville, pp. 1205–1222 (1997).
139. Söremark, C., Johansson, G. and Kiviranta, A., "Characterization and elimination of fibre orientation streaks", in Tappi Engineering Conference, pp. 97–104 (1994).
140. Aidun, C. and Kovacs, A., "Hydrodynamics of the forming section: the origin of non uniform fibre orientation", *Tappi J.*, **78**(11): pp. 97–106 (1995).
141. Schlupp, K., Karrila, S. and Paulapuro, H., "An experimental study of a high speed slice jet", in Annual Meeting, Technical Section CPPA, Monteal, pp. B199–205 (1995).
142. Schlupp, K., "Characteristics of a headbox slice jet at elevated speed", Department of Forest Products Technology, HUT, Helsinki, Licentiate Thesis (2000).
143. Lindqvist, A., "Structures in the flow from paper machine headboxes", Division of Fluid Mechanics, Luleå University of Technology, Luleå, Licentiate Thesis (1996).
144. Li, A., Neill, E. and Rogers, T., "Jet trajectory from a converging nozzle", in Tappi Engineering Conference, Nashville, pp. 1197–1204 (1997).
145. Aidun, C., "Hydrodynamis of streaks on the forming table", *Tappi J.*, **80**(8): pp. 155–162 (1997).
146. Aidun, C., "Quantitative evaluation of the forming jet delivered from four different hydraulic headboxes using high speed digital imaging", *Tappi J.*, **81**(4): pp. 172–179 (1998).
147. Ono, K. et al., "Forming jet surface velocity profile measurements with high speed digital imaging", *Tappi J.*, **84**(3): pp. 13 pages (2001).
148. Söderberg, D. and Alfredsson, H., "Experiments concerning the origin of streaky structures inside a plane water jet", *J. Pulp Pap. Sci.*, **26**(11): pp. 395–400 (2000).
149. Baker, D. and Reimer, K., "Twin-wire gap forming: Leading edge technology for newsprint in the 90s", *Pulp Paper Canada*, **93**(6): pp. T170–175 (1992).
150. Banning, J., "Vorrichtung zum Führen der Siebe einer Doppelsiebpartie einer Papier-oder Kartongmaskin", Dörries patent, DE 35 03 242 (1986).
151. Norman, B., "Pilot plant machines and the future", in Pira Conference: New technologies in multiply and multilayer structures, Bristol, pp. Forum panel presentations (1991).
152. Norman, B. et al., "The STFI-former for roll/blade dewatering", in 4th International Conference New Available Techniques and Current Trends, Bologna, pp. 114–121 (1992).
153. Nordström, B. and Norman, B., "Development of the STFI former". *Nord. Pulp Pap. Res. J.*, **9**(3): p. 176 (1994).
154. Voith, "PM 2000-neue Versuchspapiermaschine bei Voith", *Wochenbl f.Papierfabr.*, **119**(3): p. 98 (1991).

155. Zippel, F., "Formation und retention bei Doppelsieb-Formern", *Wochenbl f. Papierfabr*., (18): pp. 802–808 (1990).
156. Bück, R. et al., "Twin-wire paper-web former", Voith patent, WO 91/02842 (1991).
157. Schmidt-Rohr, V. and Kohl, B., "Der Duoformer CFD – eine Neuentwicklung auf dem Gebiet Blattbildungssysteme", *Wochenbl. f. Papierfab*. (11/12): pp. 455–460 (1992).
158. Schmidt-Rohr, V., "Betriebserfahrungen mit dem Roll-Gap-Former (Duoformer CFD) bei grafischen Papieren", *Wochenbl. f. Papierfabr.* (11): pp. 441–446 (1994).
159. Egelhof, D. and Bubik, A., "Der Einfluss des Maschinenbaus auf die Blattbildung", *Wochenbl f. Papierfabr*., (4): pp. 111–117 (1994).
160. Moser, H., "Forming technology today and tomorrow", in 6th International Conference on New Available Techniques, Stockholm, pp. 450–453 (1999).
161. Palm, C. and Cedra, I., "Inbetriebnahme und erste Erfahrungen mit einer Online-SC-Papiermachine", ipw Science and Technology **?**(11): pp. T191–T194 (2000).
162. Moser, H., "DuoFormer TQv", in 86th Annual Meeting, PAPTAC, Monteal, pp. 255–256 (2000).
163. Moser, H. et al., "DouFormer TQv – a new twin wire former", *Together* (10): pp. 17–21 (2000).
164. Moser, H., "State of the art forming technology", in 87th Annual Meeting PAPTAC, Monteal, pp. C121–126 (2001).
165. Mohrhardt, G. et al., "Wet end, method for the production of a fibrous material web", Voith patent, WO 9828489, prior. Dec. (1996, 1998).
166. Partanen, H., "Web forming method and apparatus", Valmet patent, EP 0397430, Prior. May (1989, 1994).
167. Ahonen, P. et al., "Former development for an environmetally concious paper mill", in 1st EcoPaperTech Conference, Helsinki, pp. 341–351 (1995).
168. Verkasalo, L. and Kinnunen, J., "Experiences of new forming technology", in 6th International Conference on New Available Techniques, Stockholm, pp. 471–477 (1999).
169. Clarke, R., "The evolution of Beloit forming technology", *Pulp Paper Can*., **96**(8), pp. T281–285 (1995).
170. Shands, J., Irwin, J. and Wildfong, V., "An examination of two former rebuild options for fourdrinier machines producing light weight coated grades", in Tappi Engineering Conference, pp. 801–806 (1995).
171. Walcher, G., "Improved newsprint operation with a Bel Baie IV", in Annual Meeting, Technical Section CPPA, Montreal, pp. A109–113 (1997).
172. Lockie, M., "Filling in the gaps with new forming technology", *Pulp & Paper Int*., (February): pp. 45–47 (1998).
173. Crouse, J., "Personal communication, Beloit" (1998).
174. Iwata, H., Goto, D. and Matumoto, M., "Application of novel dewatering element for high speed former", in 2000 Pan Pacific Conference, pp. 75–82 (2000).

175. Attwood, B. and Moore, G., "An introduction to the theory and practice of multiply forming", Leatherhead: PIRA. 179. (1994).
176. Attwood, B. and Loy, K., "Pressure forming developments in multi-ply paperboard forming", *Tappi J.*, **76**(10): pp. 160–164 (1993).
177. Halmschlager, G., "Duoformer Top – a new former for the production of top plies of packaging grades", in Tappi Engineering Conference, Nashville, pp. 1239–1243 (1997).
178. Räisänen, K. and Paananen, J., "Forming process requirements set by a furnish type in linerboard production", in 6th International Conference on New Available Techniques, Stockholm, pp. 454–457 (1999).
179. Halmschlager, G., "Douformer Base – compact concept for increased board and packaging paper production", in 6th International Conference on New Available Techniques, Stockholm, pp. 460–464 (1999).
180. Norman, B., "Fibre coarseness (weight per unit length) should be replaced by fibre grammage (weight per unit area)", *Nord. Pulp Paper Res. J.*, **13**(2): p. 166 (1998).
181. Dodson, C., "The effect of fibre length distribution on formation (Research note)", *J. Pulp Pap. Sci.*, **18**(2): pp. J74–J76 (1992).
182. Dodson, C. and Fekih, K., "The effect of fibre orientation on paper formation", *J. Pulp Pap. Sci.*, **17**(6): pp. J203–J206 (1991).
183. Dodson, C., "Flocculation and orientation effects on paper formation statistics", *Tappi J.*, **75**(1): pp. 167–171 (1992).
184. Kuhn, D. and Dodson, C., "Measurement of fibre orientation effects on formation", in 78th Annual Meeting, Technical Section CPPA, Montreal, pp. A283–A286 (1992).
185. Dodson, C. and Serafino, L., "Flocculation, dispersion and dynamic scenarios for formation", *Nord. Pulp Paper Res. J.*, **8**(2): pp. 264–272 (1993).
186. Deng, M. and Dodson, C., "Random star patterns and paper formation", *Tappi J.*, **77**(3): pp. 195–199 (1994).
187. Farnood, R., Dodson, C., and Loewen, S., "Modeling flocculation. Part I: Random disc model", *J. Pulp Pap. Sci.*, **21**(10): pp. J348–355 (1995).
188. Farnood, R. and Dodson, C., "The similarity law of formation", in International Paper Physics Conference, Niagara-on-the-Lake, pp. 5–12 (1995).
189. Farnood, R. et al., "Modelling flocculation: A gallery of simulated flocculated papers", *Nord. Pulp Paper Res. J.*, **12**(2): pp. 86–89 (1997).
190. Norman, B., "Letter to the editor", *Nord. Pulp Paper Res J.*, **12**(3): p. 210 (1997).
191. Sampson, W. et al., "Hydrodynamic Smoothing in the Sheet Forming Process", *J. Pulp Pap. Sci.*, **21**(12): pp. J422–426 (1995).
192. Norman, B. et al., "The effect of localised dewatering on paper formation", in International Paper Physics Conference, Niagara-on-the-Lake, pp. 55–59 (1995).
193. Lucisano, M. and Norman, B., "The forming and properties of quasi-random laboratory paper sheets", in International Paper Physics Conference, San Diego, pp. 331–340 (1999).

194. Kilpeläinen, R. et al., "Stock Preparation and Wet End. Part 1: forming fabrics", in Papermaking Science and Technology, Fapet OY, Helsinki **8**(7): pp. 251–283 (2000).
195. Johnson, D., "Effects of jet impingement on Bal Baie machines", *Pulp Paper Canada*, **95**(5): pp. 12–15 (1992).
196. Fejér, M., "Der Einfluss des Blattbildungsmediums Sieb auf die Formation", *Wochenbl. f. Papierfab*., (20): pp. 839–846 (1993).
197. Adanur, S., "Effects of forming fabric structural parameters on sheet properties, *Tappi J*., **77**(10): pp. 187–195 (1994).
198. Hampson, P., "Fibre length and fabric aperture", in 52nd Appita Annual Conference, pp. 377–382 (1998).
199. Heinola, M. et al., "The influence of forming fabrics on the retention and drainage on gap formers", in Annual Meeting, Technical Section CPPA, Montreal, pp. A59–64 (1996).
200. Cole, S., "Huytexx – a new breed of forming fabric", in 87th Annual Meeting, PAPTAC, Montreal, pp. A5–7 (2001).
201. Keen, P. and Cole, S., "Unique forming fabric structures deliver added value", in 87th Annual Meeting PAPTAC, Montreal, pp. A57–60 (2001).
202. Herzig, R. and Johnson, D., "Investigation of thin fiber mats formed at high velocity", *Tappi J*., **82**(1): pp. 226–230 (1999).
203. Meyer, H., "The effect of wire screens on forming fiber mats", *Tappi J*., **52**(9): pp. 1716–1723 (1969).
204. Danby, R., "The impact of forming fabric structures on print quality", in CPPA Annual Meeting, Montreal, pp. 33–38 (1993).
205. Danby, R., "Forming fabric design definition and selection – The means to machine and fiber efficiency", in 85th Annual Meeting, PAPTAC, Montreal (1999).
206. Danby, R. and Plouffe, P., "Print quality improvements through forming fabric design changes", *Pulp Paper Can*., **101**(9): pp. 66–69 (2000).
207. Dudley, W. et al., "Engineered approach and unique forming fabric design provide mill with dramatic paper & print improvements", in Tappi Engineering Conference, Atlanta, pp. 9 pages (2000).
208. Jong, J. H., Baines, W. D. and Currie, I. G., "Experimental Characteristics of Forming Fabrics and Fibre Mats", *J. Pulp Pap. Sci*., **25**(3): pp. 95–99 (1999).
209. McDonald, D., "Web rewetting by forming fabrics", in Tappi Engineering Conference, Anaheim, pp. 597–599 (1999).
210. Barratte, C. et al., "Simulation of initial fibre retention by forming fabric", in 54th Appita Annual Conference, Melbourne, pp. 415–420 (2000).
211. Keen, P., "Bringing virtual reality to forming fabric design", Paper Technology (December): pp. 47–50 (1999).
212. Sayegh, N. and Gonzales, T., "Compressibility of Fibre Mats During Drainage", *J. Pulp. Pap. Sci*., **21**(7): pp. J255–261 (1995).
213. Vomhoff, H. and Schmidt, A., "The steady-state compressibility of saturated finre webs at low pressure", *Nord. Pulp Pap. Res. J*., **12**(4): pp. 267–269 (1997).

214. Jong, J., "Characteristics of jet impingement, drainage and compression in a forming roll of a twin-wire machine", Department of Mechanical and Industrial Engineering, University of Toronto, Toronto, PhD Thesis (1998).
215. Sampson, W. and Bridle, I., "Simulation of the directional dependence od flow through fibre mats", *Nord. Pulp Paper Res. J.*, **10**(2): pp. 145–149 (1995).
216. Sampson, W. and Kropholler, H., "Batch-drainage curves for pulp characterization. Part 1: Experimental", *Tappi J.*, **78**(12): pp. 145–151 (1995).
217. Sampson, W. and Kropholler, H., "Batch-drainage curves for pulp characterization. Part 2: Modeling", *Tappi J.*, **79**(1): pp. 151–160 (1996).
218. Mantar, E., Co, A. and Genco, J.M., "Drainage Characteristics of Pulp Slurries", *J. Pulp Pap. Sci.*, **21**(2): pp. J44–J50 (1995).
219. Ramarao, B. and Kumar, P., "A Model for the Gravity Drainage of Papermaking Suspensions", *Nord. Pulp Paper Res. J.*, **11**(2): p. 86 (1996).
220. Wildfong, V. et al., "Filtration Mechanics of Sheet Forming. Part I: Apparatus for Determination of Constant-Pressure Filtration Resistance", *J. Pulp Pap. Sci.*, **26**(7): pp. 250–254 (2000).
221. Wildfong, V. et al., "Filtration Mechanics of Sheet Forming. Part II: Influence of Fine Material and Compression", *J. Pulp Pap. Sci.*, **26**(8): pp. 280–283 (2000).
222. Hung, L., Leung, W. and Green, S., "Pulp fibre mat permeability measurements under simulated forming conditions", in Tappi Engineering Conference, Atlanta, pp. 5 pages (2000).
223. Duplantis, W. and Green, S., "Measurements of fibre mat permeability with a new device", in 87th Annual Meeting PAPTAC, Montreal, pp. B7–12 (2001).
224. Audenis, G., "On the impingement of a plane liquid jet on the wires of a paper machine", Dep. of Mechanics, KTH, Stockholm, Licentiate Thesis (1999).
225. Dalpke, B., Green, S. and Kerekes, R., "Modelling of jet impingement in twin-wire paper-machines: Impingement on one fabric", *Tappi J.*, **84**(2): pp. 19 pages (2000).
226. Loewen, S. and Buttler, A., "Laser speed measurement of forming section flow properties", *Pulp Paper Can.*, **93**(12): pp. 161–164 (1992).
227. Loewen, S., "Fibre orientation optimization", *Pulp Paper Can.*, **98**(10): pp. T391–396 (1997).
228. Farnood, R., Loewen, S. and Dodson, C., "Machine direction profiles of stock speed and table activity", in Annual Meeting, Technical Section CPPA, Montreal, pp. B241–245 (1997).
229. Kiviranta, A., "Table activity on the fourdrinier: Its characterization and its effect on formation", Laboratory of Paper Technology, HUT, Helsinki, PhD Thesis (1993).
230. Kiviranta, A. et al., "Measurement of table activity on a Fourdrinier paper machine", *J. Pulp Pap. Sci.*, **19**(6): p. J234 (1993).
231. Kiviranta, A. "Characterization and optimization of Fourdrinier table activity on the middle ply of a folding boxboard machine", *Paperi ja Puu*, **74**(8): pp. 640–649 (1992).
232. Kiviranta, A. and Paulapuro, H., "The role of table activity in the manufacture

of fine paper", in 4th New Available Techniques and Current Trends Conference, Bologna, pp. 46–72 (1992).
233. Kiviranta, A. and Paulapuro, H., "Characterization and optimization of Fourdrinier table activity in linerboard manufacture", *Paperi ja Puu*, **74**(9): pp. 728–737 (1992).
234. Kiviranta, A. and Paulapuro, H., "The role of fourdrinier table activity in the manufacture of various paper and board grades", *Tappi J.*, **75**(4): pp. 172–186 (1992).
235. Ahonen, P., Kiviranta, A. and Kaipila, J., "Effect of Fourdrinier table layout on the wet-end performance of a fine paper machine", *Paperi ja Puu*, **74**(10): pp. 802–806 (1992).
236. Foulger, M., "Submerged drainage: A new concept of dewatering", in Annual Meeting, Technical Section CPPA, Montreal, pp. A65–A68 (1995).
237. Zu, J. and Chen, J., "A theoretical study of vacuum force on gravity foils and step foils", *Tappi J.*, **82**(11): pp. 93–98 (1999).
238. Evans, D. and Fielding, S., "VID formation system", in 54th Appita Annual Conference, Melbourne, pp. 437–442 (2000).
239. Palm, D. and Sodergren, O., "VID dormation system", in 87th Annual Meeting PAPTAC, Montreal, pp. A185–190 (2001).
240. Sodergren, O. and Neun, J., "Developments in activity generation on Fourdriniers", *Tappi J.*, **83**(10): pp. 10 pages (2000).
241. Verkasalo, L., Odell, M. and Korhonen, H., "Forming of LWC base papers", in Tappi Engineering Conference, Nashville, pp. 1231–1238 (1997).
242. Bando, T., Iwata, H. and Nagano, A., "Drainage mechanism on a twin-wire former. Part 1: Factors affecting on the drainage phenomena", *Japan Tappi*, **48**(7): pp. 948–954 (1994).
243. Bando, T., Adachi, T. and Iwata, H., "Drainage mechanism on a twin-wire former. Part 2: Computer simulation on pulsating drainage", *Japan Tappi*, **48**(11): pp. 1493–1498 (1994).
244. Iwata, H. et al., "Development of Mitsubishi new former for papermaking machine". Mitsubishi Heavy Industries, Technical Review, Technical Review, Vol. 30, No. 2, 123–128 (1993).
245. Zhao, R. and Kerekes, R., "Pressure distribution between forming fabrics in blade gap formers: Thin blades", *J. Pulp Pap. Sci.*, **21**(3): pp. 97–103 (1995).
246. Zhao, R. and Kerekes, R., "The effect of consistency on pressure pulses in blade gap formers", *Paperi Ja Puu*, **78**(1/2): pp. 36–38 (1996).
247. Nigam, M. and Bark, F., "An analytical method to calculate the flow past a blade in twin-wire formers", Dep of Mechanics, KTH, Stockholm, 1997: 7 (1997).
248. Zahrai, S., "On the fluid mechanics of twin-wire formers", Dep of Mechanics, KTH, Stockholm, PhD Thesis (1997).
249. Zahrai, S. and Bark, F., "On the fluid mechanics of twin wire blade forming in paper machines", *Nord. Pulp Pap. Res. J.*, **10**(4): pp. 245–252 (1995).
250. Zahrai, S. and Bark, F., "Analytical and numerical approaches to solve the

model equations for the flow of pulp in blade forming process", in *AIChE Symposium Series*, Pulping, Papermaking and Chemical Preparation, pp. 68–73 (1996).

251. Zahrai, S., Bark, F. and Norman, B., "An analysis of blade dewatering in a twin-wire paper machine", *J. Pulp Pap. Sci.*, **23**(9): pp. J452–459 (1997).
252. Green, S., "Analytical and computational modeling of twin-wire blade forming", *J. Pulp Pap. Sci.*, **23**(7): pp. J353–358 (1997).
253. Roshanzamir, A., Green, S. and Kerekes, R., "Two-Dimensional Simulation of Pressure Pulses in Blade Gap Formers", *J. Pulp Pap. Sci.*, **24**(11): pp. 364–368 (1998).
254. Green, S., Zhao, R. and Kerekes, R., "Pressure Distribution Between Forming Fabrics in Blade Gap Formers: Blades of Finite Width and Fabrics of Finite Stiffness", *J. Pulp Pap. Sci.*, **24**(2): pp. 60–66 (1998).
255. Green, S. and Kerekes, R., "Numerical analysis of pressure pulses induced by blades in gap formers", *Tappi J.*, **81**(4): pp. 180–187 (1998).
256. Roshanzamir, A. et al., "Hydrodynamic Pressure Generated by Doctoring in Bade Gap Formers", in Tappi Engineering Conference, pp. 1181–1189 (1999).
257. Roshanzamir, A., Green, S. and Kerekes, R., "The Effect of Non-Darcy's Law Drainage on the Hydrodynamics of Blade Gap Formers", in Tappi Papermakers Conference, Vancouver, pp. 701–708 (2000).
258. Shands, J. and Wildfong, V., "A twin wire former rebuild option for improved formation and drainage", in Tappi Engineering Conference, pp. 53–69 (1998).
259. Odell, M., Pakarinen, P. and Luontama, M., "Customizing roll and blade forming to control paper structure", in Valmet Paper Machine Days, Jyväskylä, pp. 21–42 (1996).
260. Green, S., "Modeling suction shoes in twin-wire blade forming: Theory", *Tappi J.*, **82**(9): pp. 136–142 (1999).
261. Green, S., "Modelling Suction Shoes in Twin-Wire Forming: Results", *J. Pulp Pap. Sci.*, **26**(2): pp. 53–58 (2000).
262. Roshanzamir, A., Green, S. and Kerekes, R., "Two-Dimensional Simulation of Suction Shoes in Gap Formers", *J. Pulp Pap. Sci.*, **26**(4): pp. 158–162 (2000).
263. Martinez, M., "Characterizing the dewatering rate in roll gap formers", *J. Pulp Pap. Sci.*, **24**(1): pp. 7–13 (1998).
264. Boxer, T., "Quantitative modelling of an industrial roll-blade gap former", Department of Paper Science, UMIST, Manchester, PhD Thesis (1999).
265. Boxer, T., Dodson, C. and Sampson, W., "Analytic solution to the Martinez dewatering equations for roll gap formers", *J Pulp Pap. Sci.*, **26**(11): pp. 391–394 (2000).
266. Zahrai, S., Martinez, M. and Dahlkild, A., "Estimating the thickness of the web during twin-wire forming", *J. Pulp Pap. Sci.*, **24**(2): pp. 67–72 (1998).
267. Zahrai, S., Bark, F. and Martinez, M., "A numerical study of cake formation in 2-D cross-flow filtration", *J. Pulp Pap. Sci.*, **24**(9): pp. 281–285 (1998).
268. Turnbull, P. et al., "One-dimensional dynamic model of a paper forming process", *Tappi J.*, **80**(1): pp. 245–252 (1997).

269. Chen, E., Schultz, W. and Perkins, N., "A two-dimensional viscous model of a wet paper forming process", in Tappi Engineering Conference, pp. 21 (1998).
270. Malashenko, A. and Karlsson, M., "Twin Wire Forming – An Overview", in Annual Meeting PAPTAC, Montreal, pp. A189–201 (2000).
271. Wildfong, V. et al., "Drainage during roll forming – Model validation using pilot papermachine data", in Tappi Engineering Conference, Atlanta, pp. 11 pages (2000).
272. Gooding, R., McDonald, D. and Rompré A., "Measurement of drainage around a forming roll", in 87th Annual Meeting, PAPTAC, Montreal, pp. A125–138 (2001).
273. Neun, J., "Performance of high vacuum dewatering elements in the forming section", *Tappi J.*, **77**(9): pp. 133–138 (1994).
274. Neun, J. and Fielding, S. "High vacuum dewatering optimization", in Tappi Papermakers Conference, pp. 307–312 (1994).
275. Neun, J., "High vacuum dewatering of brown paper grades", in Tappi Papermakers Conference, pp. 259–265 (1995).
276. Neun, J., "High-vacuum dewatering of newsprint", *Tappi J.*, **79**(9): pp. 153–157, (1996).
277. Gagnon, J. and Neun, J., "High vacuum dewatering on fourdriniers and formers", in Annual Meeting, Technical Section CPPA, Montreal (1996).
278. Räisenen, K., "Water removal by flat boxes and a couch roll on a paper machine wire section", Laboratory of Paper Technology, HUT, Helsinki, PhD Thesis (1998).
279. Räisänen, K., "High-vacuum dewatering on a paper machine wire section – a literature review", *Paperi ja Puu* (*Papper och Trä*), **78**(3): pp. 113–120 (1996).
280. Räisänen, K., Paulapuro, H. and Karrila, S., "The effects of retention aids, drainage conditions and pretreatment of slurry on high-vacuum dewatering; a laboratory study", *Tappi J.*, **78**(4): pp. 140–147 (1995).
281. Räisänen, K., Karrila, S. and Maijala, A., "Effect of vacuum level and suction time on vacuum assisted drainage of a paper machine wire section", *Appita J.*, **48**(4), pp. 269–274 (1995).
282. Räisänen, K., Karilla, S. and Maijala, A., "Vacuum dewatering optimization with different furnishes", *Paperi ja Puu* (*Papper och Trä*), **78**(8): pp. 461–467 (1996).
283. Mitchell, C. and Johnston, R., "Pulsating suction during vacuum dewatering and its effect on the rate and extent of water removal", in 54th Appita Annual Conference, Melbourne, pp. 443–447 (2000).
284. Shands, J. and Hardwick, C., "Dewatering on a high vacuum flat box", in 86th Annual Meeting, PAPTAC, Montreal, pp. A113–117 (2000).
285. Jones, G., "Dynamic simulation of dewatering in high vacuum flat boxes", in Tappi Engineering Conference, Anaheim, pp. 197–209 (1999).
286. Nazhad, M. and Kerekes, R., "Producing handsheets at headbox consistency", in Annual Meeting, PAPTAC, Montreal, pp. A203–208 (1999).

287. Nazhad, M. et al., "The influence of formation on tensile strength of paper made from mechanical pulps", *Tappi J.*, **83**(12): pp. 9 pages (2000).
288. Lin, J. and Schuster, M., "Predicting drainage retention and formation development on high alkaline paper machines", in Tappi Papermakers Conference, pp. 253–266 (1992).
289. Sutman, F., "Development and validation of a new drainage testing methodology", in Tappi Papermakers Conference (1999).
290. Karrila, S., Räisänen, K. and Paulapuro, H., "The moving belt drainage tester (MBDT)", in Tappi Papermakers Conference, Nashville, pp. 275–299 (1992).
291. Räisenen, K., Karrila, S. and Paulapuro, H., "Wire section siulation with the moving belt drainage tester (MBDT)", in Tappi Papermakers Conference, Atlanta, pp. 103–113 (1993).
292. Xu, L. and Parker, I., "Simulating the forming process with the moving belt drainage former", in 53rd Appita Annual Conference, Rotorua, pp. 169–173 (1999).
293. Helmer, R. et al., "Preliminary development of a laboratory former for oriented sheets", in *Appita J*, pp. 465–470. (2000).
294. Helmer, R. et al., "Flow phenomena and paper forming", *Appita J.*, **54**(1): pp. 54–60 (2001).
295. Sivén, S. and Manner, H., "High speed retention tester", in 86th Annual Meeting, PAPTAC, Montreal, pp. A37–41 (2000).
296. Sivén, S. and Manner, H., "Multicomponent retention systems in twin wire forming", in Apita Annual Meeting, pp. 215–220 (2000).
297. Hammock, C. and Garnier, G., "The laboratory twin-former. Part 1: Design and performance", *Tappi J.*, **83**(10): pp. 13 pages (2000).
298. Lockie, M., "Getting competitive through pilot plant trials", *Pulp Paper Int.*, (August): pp. 28–33 (1997).
299. Hynnek, M. and Shands, J., "Beloit Corporation's new pilot paper machine", in Annual Meeting, Technical Section CPPA, Montreal, pp. A51–53 (1996).
300. Valmet, "Valmet's new tool in printing paper R& D", *Paperi ja Puu*, **78**(4): pp. 139, (1996).
301. Crotogino, R. et al., "Paprican's new pilot paper machine", in CPPA Annual Meeting, pp. A121–A127 (1999).
302. Gerli, A., Keised, B. and Strand, M., "The use of a flocculation sensor as a predictive tool for paper machine retention program performance", *Tappi J.*, **83**(10): pp. 16 pages (2000).
303. Fredlund, M., "Unpublished summary of FEX investigations" (1996).
304. Holik, H., "Blattbildung – Grundlage für Papierqualität, Teil 1", *Wochenbl f. Papierfabr.*, (10): pp. 375–380 (1992).
305. Holik, H., "Blattbildung – Grundlage für Papierqualität, Teil 2", *Wochenblatt f. Papierfabr.* (11/12): pp. 443–454 (1992).
306. Ohlsson, K., "Influence of raw material and forming process on quality of woodcontaining printing papers", (in Swedish). Dep Pulp and Paper Chemistry and Technology, KTH, Stockholm, Licentiate Thesis (1993).

307. Albinsson, C.-J., Swerin, A. and Ödberg, L., “Formation and retention during twin-wire blade forming of a fine paper stock”, *Tappi J.*, **78**(4): pp. 121–128 (1995).
308. Swerin, A. and Mähler, A., “Formation, retention and drainage of a fine paper stock during twin-wire roll-blade forming. Implications of fibre network strength”, *Nord. Pulp Paper Res. J.*, **11**(1): pp. 36–42 (1996).
309. Nilsson, B., “Fibre orientation effects in twin wire forming”, (in Swedish). Dep. Paper Technology, KTH, Stockholm, Licentiate Thesis (1993).
310. Eguchi, A. et al., “Flow characteristics in a headbox and fiber orientation of paper. Part 2: Verification by the experimental paper machine”, *Japan Tappi*, **47**(7): pp. 887–889 (1993).
311. Nordström, B. and Norman, B., “Effects on formation, retention and mechanical properties of forming blade distance in a twin-wire roll-blade former”, *Appita J.*, **48**(1): pp. 19–24 (1995).
312. Nordström, B. and Norman, B., “Effects of headbox jet quality and blade pulse force on formation, retention and mechanical properties during roll-blade forming with curved blades”, *Nord. Pulp Pap. Res. J.*, **10**(1): pp. 33–40 (1995).
313. Nordström, B. and Norman, B., “Effect on paper properties and retention of the proportion of roll dewatering during twin-wire roll-blade forming of TMP”, *J. Pulp Pap. Sci.*, **22**(8): p. J283 (1996).
314. Odell, M., “Paper structure engineering”, in 53rd Appita Annual Conference, Rotorua, pp. 155–160 (1999).
315. Erkkilä, A.-L., Pakarinen, P. and Odell, M., “The effect of forming mechanisms on layered fiber structure in roll and blade gap forming”, in Tappi Papermakers Conference, pp. 389–400 (1999).
316. Mohlin, U.-B., “Pulp evaluation for modern papermaking”, in 6th International Conference on New Available Techniques, Stockholm, pp. 343–350 (1999).
317. Mohlin, U.-B., “Fibre dimensions-formation and strength”, in International Paper Physics Seminar, Grenoble, pp. 5–14 (2000).
318. Odell, M. and Pakarinen, P., “The complete fibre orientation control and effects on diverse paper properties”, in Tappi Papermakers Conference, Cincinatti, pp. 27 pages (2001).
319. Page, R. and Hergert, R., “Enhancement of Paper Properties and Fibre Economics Through Web Stratification”, *Appita J.*, **42**(1): pp. 33–41 (1989).
320. Häggblom-Ahnger, U., “Three-ply office paper”, Laboratory of Paper Chemistry, Åbo Akedemi University, Åbo, PhD Thesis (1998).
321. Häggblom-Ahnger, U. and Eklund, D., “The role of the middle ply in multilayered copy paper”, *Appita Journal*, **51**(3): pp. 199–204 (1998).
322. Häggblom-Ahnger, U., “Optimum location of softwood sulphate pulp in three-ply office paper”, *Tappi J.*, **82**(6): pp. 181–187 (1999).
323. Häggblom-Ahnger, U., “Layering of office paper”, *Paper and Tiber*, **80**(7): pp. 508–513 (1998).
324. Lloyd, M., “Stratified (multilayer) forming – a technology for the new millenium? in 53rd Appita Annual Conference, Rotorua, pp. 161–168 (1999).

Transcription of Discussion

OVERVIEW OF FORMING LITERATURE, 1990–2000

Bo Norman and Daniel Söderberg
Royal Institute of Technology

Bill Sampson Department of Paper Science, UMIST

In your review you mention that there are some sort of grey areas, different conditions can give different influence on formation and strength, and I wondered with your high contraction nozzle where you observe better formation at zero jet to wire speed difference, whether there was any influence on strength in that region?

Bo Norman

Well our basic finding is that if you do these improvements in the head box such that you have an improved jet coming out then you will get better strength. If you introduce some of these shear influences in dewatering you will lose strength. So when stock is coming onto the wire section it is too late to make any strength improvements; these have to be upstream in the head box. We think that is one conclusion.

Jean-Claude Roux EFPG

You have presented what you believe to be the best forming twin wire machines with adjustable blades and with fixed blades. What are your feelings; can you extend this philosophy to hybrid forming machines?

Bo Norman

I think that the hybrid former is a retro-fit for older machines. I do not think that you would fit this technology to new machines. For an optimum machine you should not combine Fourdrinier dewatering forming and twin wire dewatering, that will not be the best option.

Discussion

Jean-Claude Roux

Why do we do it like that?

Bo Norman

We want to dewater paper under minimum shear. If you start dewatering on a Fourdrinier wire and you add a top wire the suspension will enter into a pressure zone that will decelerate the suspension which will inevitably cause shear. This should be avoided in the final, perfect paper machine but we have a long way to go so with today's machines, of course for rebuilds on a Fourdrinier machine you will often have a positive formation effect when introducing these top wires.

Jean-Claude Roux

You mean we lose orientation profile at the beginning of the hybrid former, and it is not possible to achieve it later in the process?

Bo Norman

Yes, the best alternative is however to add stationary and adjustable blades in the top wire unit, to be able to control and minimize shear effects.